

615-148

MVM '73 TV SUBSYSTEM

CALIBRATION REPORT

July 1975

Authors:

M. Benesh

M. Merrill

Edited By:

S. LaVoie

N. Evans

EDITOR'S NOTE

In editing this document to a size economically feasible for publication, a great deal of the authors' original material was combined or omitted. Effort was made also to reference standard testing procedures to previous documents for explanation.

As the TV subsystems actually flown on MVM '73 were the Flight-2 A and B cameras, the graphs and charts are generally the results of the testing of these two cameras. Only in the case of anomalies in test findings, or unavailable results for the Flight-2 subsystems were the Flight-1 data illustrated.

Every effort has been made to produce a calibration document of general interest to all concerned. The original data have been filed and can be made available upon notification of G. E. Danielson.

ACKNOWLEDGEMENTS

Calibration of the Mariner Venus-Mercury '73 Photoscience System was the result of well-organized teamwork. The efforts of those who participated in these activities were greatly appreciated by all concerned.

The authors wish to express special appreciation to F. Vesceles and E. Danielson for continued organizational, scientific, and moral support, and to L. Snyder for sharing his invaluable MM '71 experience; to the Calibration Team - R. Barker, W. Cunningham, L. Douglass H. Enmark, L. Hovland, J. Ryder, R. Steinkraus, D. Thiessen, and R. Toombs, who were instrumental in obtaining these data; to the Engineering Team of N. Emmer, G. Frascchetti, C. LaBaw, K. LaBau, W. Magruder, D. Perrenoud, and J. Voeltz, under the direction of M. Herring, for their unfailing technical assistance; and to IPL personnel under the direction of D. Lynn for their support and the processing of calibration data - F. Akers, D. Atwood, D. Haas, J. Lorre, and A. Schwartz.

TABLE OF CONTENTS

	<u>PAGE</u>
1. <u>INTRODUCTION</u>	1
2. <u>COMPONENT-LEVEL CALIBRATION</u>	1
2.1. OPTICS	2
2.1.1. <u>Spectral Transmittance</u>	2
2.1.2. <u>T-Stop Number</u>	7
2.1.3. <u>Polarization</u>	11
2.2. FILTERS	15
2.2.1. <u>Spectral Transmittance</u>	17
2.2.2. <u>Polarization Axis</u>	17
2.3. SHUTTERS	21
2.3.1. <u>Characteristics</u>	21
2.3.2. <u>Exposure Table and Shading</u>	21
2.4. VIDICONS	22
2.4.1. <u>Spectral Response</u>	22
2.4.2. <u>Reseau Map</u>	22
3. <u>SUBSYSTEM-LEVEL CALIBRATION</u>	26
3.1. LIGHT SOURCES	26
3.1.1. <u>Spectral Characteristics</u>	26
3.1.2. <u>Determination of Source Radiance</u>	30
3.1.3. <u>Error Estimation</u>	35

	<u>PAGE</u>
3.2. RADIOMETRY	35
3.2.1. <u>Shutter Performance</u>	38
3.2.1.1. Reciprocity	38
3.2.1.2. Offset	38
3.2.2. <u>Light Leak</u>	42
3.2.3. <u>Residual Image and Hysteresis</u>	45
3.2.4. <u>Vidicon Shading</u>	49
3.2.5. <u>Filter Response</u>	54
3.2.5.1. Bench Test Light Transfer	54
3.2.5.2. Relative Filter Factors	54
3.2.6. <u>Veiling Glare</u>	61
3.3. GEOMETRY	64
3.3.1. <u>Optical Orientation</u>	64
3.3.1.1. Narrow-Angle Optics	64
3.3.1.2. Wide-Angle Optics	66
3.3.1.3. Opto-Mechanical Alignment	69
3.3.2. <u>Geometric Calibration</u>	74
3.3.2.1. Object Space Reseau Locations	74
3.3.2.2. Apparent Aspect Ratio	74
3.3.2.3. Nominal Field of View	80

TABLE OF CONTENTS

(Cont'd.)

	<u>PAGE</u>
3.4. MODULATION TRANSFER FUNCTION	80
3.5. NOISE ANALYSIS	82
3.5.1. <u>Power Spectra</u>	82
3.5.2. <u>Coherent vs. Random Noise</u>	82
4. <u>SYSTEM-LEVEL CALIBRATION</u>	82
4.1. THERMAL VACUUM TESTING	82
4.1.1. <u>Light Transfer</u>	86
4.1.2. <u>Modulation Transfer Function</u>	86
5. <u>REFERENCES</u>	96

FIGURES

1. MVM TELEVISION CAMERAS	3
2. BUS ELECTRONICS AND AUXILIARY ELECTRONICS SUBASSEMBLY	4
3. SPECTRAL TRANSMITTANCE TEST CONFIGURATION	5
4. TYPICAL SPECTRAL TRANSMITTANCE TEST SETUP	6
5. SPECTRAL TRANSMITTANCE	8
6. T-STOP NUMBER DETERMINATION	10
7. T-STOP NUMBER MEASUREMENT SETUP	13

FIGURES
(Cont'd.)

	<u>PAGE</u>
8. SETUP FOR POLARIZATION AXIS ORIENTATION	14
9. POLARIZATION INDUCED BY NAO, FLIGHT 2-A	16
10. SPECTRAL TRANSMITTANCE (CLEAR, ORANGE, BLUE)	18
11. SPECTRAL TRANSMITTANCE (MUV, UV, UVP)	19
12. DIRECTION OF POLARIZATION AXIS ON VIDICON FACEPLATE	20
13. EXPOSURE SHADING	24
14. RELATIVE SPECTRAL RESPONSE	25
15. VIDICON RESEAU GRID, FLIGHT 1-A, 63 RESEAU PATTERN	27
16. VIDICON RESEAU GRID, FLIGHT 1-B, 2-A, 2-B, 111 RESEAU PATTERN	27
17. LIGHT CANNON SHOWING VEEDER ROOT IRIS CONTROL AND PLEXIGLASS DIFFUSER	31
18. 2" LIGHT CANNON COUPLED TO CELESTRON COLLIMATORS	32
19. FIELD FLATNESS OF 12 INCH LIGHT CANNON	33
20. RELATIVE SPECTRAL RADIANCE OF 12 INCH LIGHT CANNON	34
21. IRIS CALIBRATION CURVE - 12 INCH LIGHT CANNON	36
22. 12 INCH LIGHT CANNON RADIANCE ERROR CURVE	37
23. LIGHT TRANSFER CURVES LOW AND HIGH LEVEL LIGHT	39
24. RECIPROCITY, FLIGHT 2-A	40
25. RECIPROCITY, FLIGHT 2-B	41
26. LIGHT LEAK CALIBRATION PROCEDURE	44

FIGURES
(Cont'd.)

	<u>PAGE</u>
27. RESIDUAL IMAGE TEST CYCLES	48
28. HYSTERESIS ANALYSIS FLIGHT 2--A BENCH 2	50
29. HYSTERESIS ANALYSIS FLIGHT 2-B BENCH 2	51
30. VIDICON SHADING FLIGHT 2-A	55
31. VIDICON SHADING FLIGHT 2-B	56
32. FLAT FIELD LIGHT TRANSFER SEQUENCES	57
33. FABRY ANALYSIS	58
34. SELECTED REGION LIGHT TRANSFER CURVE, WAF	59
35. VEILING GLARE TEST SETUP	62
36. GEOMETRY OF A PHOTOGRAPHIC SYSTEM	65
37. NAO FOCAL LENGTH MEASUREMENT	67
38. OPTO-MECHANICAL ALIGNMENT ON ASKANIA BENCH	70
39. GEODETIC INTERSECTION OF THE OPTO-MECHANICAL ALIGNMENT OF CAMERA B	71
40. OPTO-MECHANICAL ALIGNMENT, FLIGHT 2-A	72
41. OPTO-MECHANICAL ALIGNMENT, FLIGHT 2-B	73
42. MEAN ASPECT RATIO VS. PICTURE AREA	78
43. FORMAT DIMENSIONS	79
44. MODULATION TRANSFER FUNCTION (MTF)	81
45. POWER SPECTRA SAMPLE AREAS	83

FIGURES
(Cont'd.)

	<u>PAGE</u>
46. POWER SPECTRUM	84
47. TYPICAL NOISE LEVELS	85
48. 10' ION VACUUM CHAMBER	87
49. ASSEMBLY JUST PRIOR TO CLOSING 10' ION CHAMBER	88
50. OPTICAL TRANSMISSION	89
51. FLAT FIELD LIGHT TRANSFER CORRECTED FOR WINDOW LOSSES AND SHUTTER OFFSET, FLIGHT 2-A	90
52. FLAT FIELD LIGHT TRANSFER CORRECTED FOR WINDOW LOSSES AND SHUTTER OFFSET, FLIGHT 2-B	91
53. RESPONSE AS A FUNCTION OF TEMPERATURE AT CONSTANT EXPOSURES, FLIGHT 2-A	92
54. RESPONSE AS A FUNCTION OF TEMPERATURE AT CONSTANT EXPOSURES, FLIGHT 2-B	93
55. FLAT FIELD LIGHT TRANSFER WITH VIDICON SHADING, FLIGHT 2-B	94
56. FLAT FIELD LIGHT TRANSFER WITH VIDICON SHADING, FLIGHT 2-A	95

TABLES

1. T-STOP NUMBER AND ABSOLUTE TRANSMITTANCE	12
2. SHUTTER EXPOSURE TIMES AND REPEATABILITY	23
3. FLIGHT 2-A VIDICON RESEAU LOCATIONS	28

TABLES
(Cont'd.)

	<u>PAGE</u>
4. FLIGHT 2-B VIDICON RESEAU LOCATIONS	29
5. SHUTTER OFFSET CORRECTIONS	43
6. SUMMARY OF LIGHT LEAK TESTS	46, 47
7. HYSTERESIS ANALYSIS	52
8. RESIDUAL IMAGE	53
9. RELATIVE FILTER FACTORS	60
10. VEILING GLARE TEST SETUP	63
11. FOCAL LENGTH AND FIELD OF VIEW	68
12. NOMINAL RESEAU LOCATIONS, FLIGHT 2-A	75
13. NOMINAL RESEAU LOCATIONS, FLIGHT 2-B	76
14. DIMENSIONS OF IMAGES	77

1. INTRODUCTION

This report compiles the results of calibrations and tests performed on the Flight-1 and Flight-2 Mariner Venus-Mercury '73 Television Subsystems. Previous JPL experience (summarized in Reference 2) was heavily drawn upon by the MVM '73 Calibration Team, as the design of this subsystem was similar to that of the MM '71. It is hoped that this calibration manual, summarizing methods, equipment, and results, can be used as a convenient reference for future spaceflight programs.

The ultimate goal of the report is to make available data that will satisfy the basic purposes of the MVM '73 TV Science Experiment - a quantitative and highly accurate pictorial representation of both planets.

The report is divided into three sections:

- (1) Component Level.
- (2) Subsystem Bench Testing.
- (3) Thermal Vacuum.

2. COMPONENT-LEVEL CALIBRATIONS

The MVM '73 Television Subsystem (TVS) consists of five basic parts:

- (1) The Narrow-Angle Optics Telescope (NAO).
- (2) The Filter Wheel Assembly with eight filter positions.
(Wide-Angle Optics (WAO) System in Position #1.)
- (3) The Camera Head housing the Vidicon.
- (4) Four separate assemblies of Bus Electronics.
- (5) The Auxiliary Electronics Subassembly (AES).

The MVM '73 spacecraft is equipped with two identical cameras, "A" and "B", each of which is composed of parts (1), (2), and (3) (Figure 1). These are mounted in an approximately parallel position on the spacecraft scan platform. Parts (4) and (5) are shown in Figure 2. A centimeter scale in Figures 1 and 2 indicates the relative size of the components.

Beyond the required engineering acceptance tests, no special calibrations were performed on parts (4) and (5). However, it was necessary to calibrate a number of components in (1), (2), and (3) prior to their assembly and integration into the television subsystem. Specifically, they included the optics, filters, shutters, and vidicon. Component-level calibrations were necessary for three reasons:

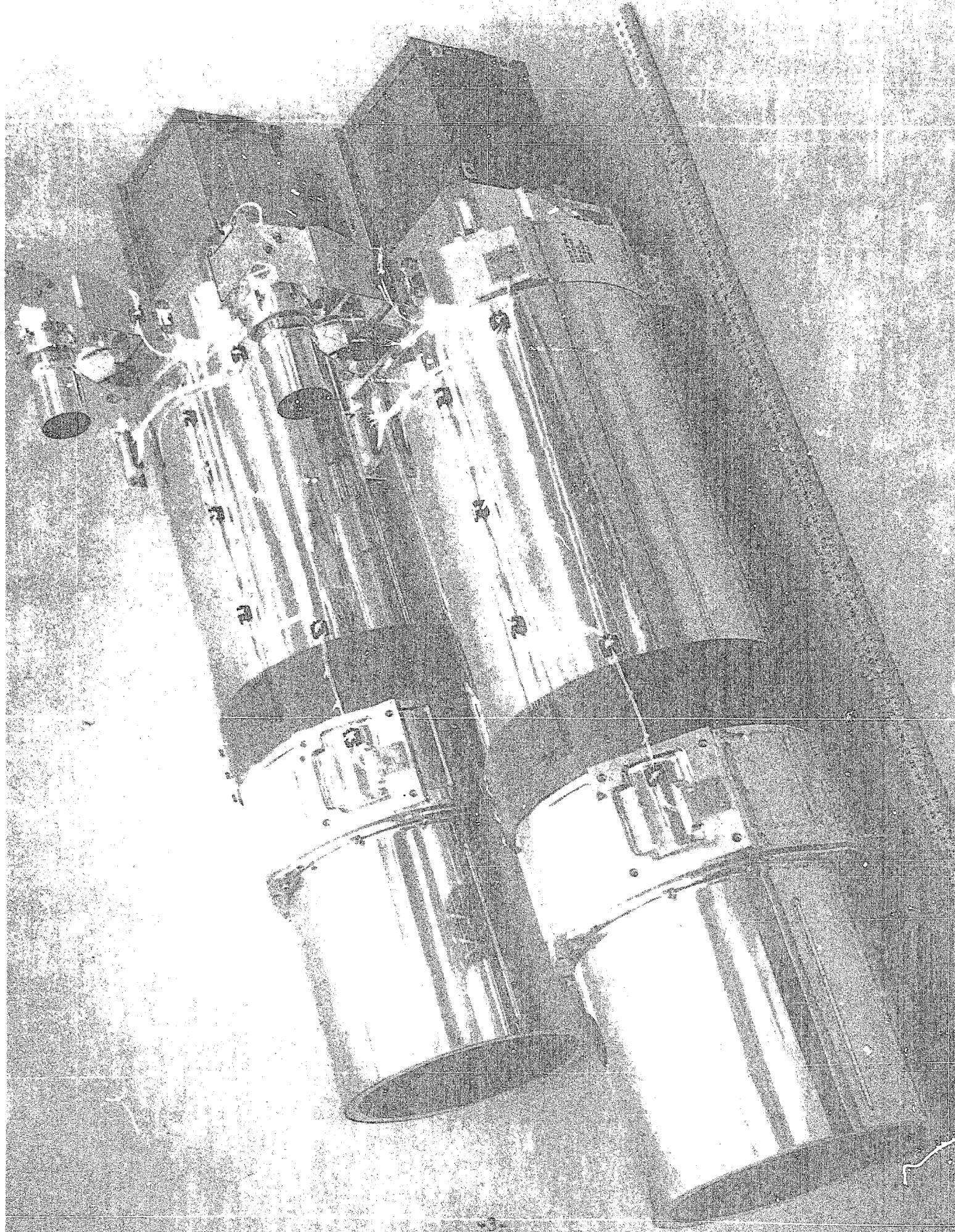
- (1) To verify that the manufactured component was acceptable for incorporation into the final assembly.
- (2) Various important photometric calculations required the knowledge of such parameters as spectral characteristics of the optics, filters, and vidicons.
- (3) The results of reseau mapping were mandatory in the subsystem-level geometric calibrations and could be done only at the component level when there was unrestricted accessibility of the vidicon tube.

2.1 OPTICS

2.1.1. Spectral Transmittance

Spectral transmittance of both the NAO and the WAO was measured on the JPL spectroradiometer. The same method as described in Reference 2 was used, but the spectroradiometer had been completely rebuilt and recalibrated, and the control rack was equipped with a paper tape punch.

Figure 3 shows schematically the spectral transmittance test setup. Figure 4 is a photograph of an actual test in process.



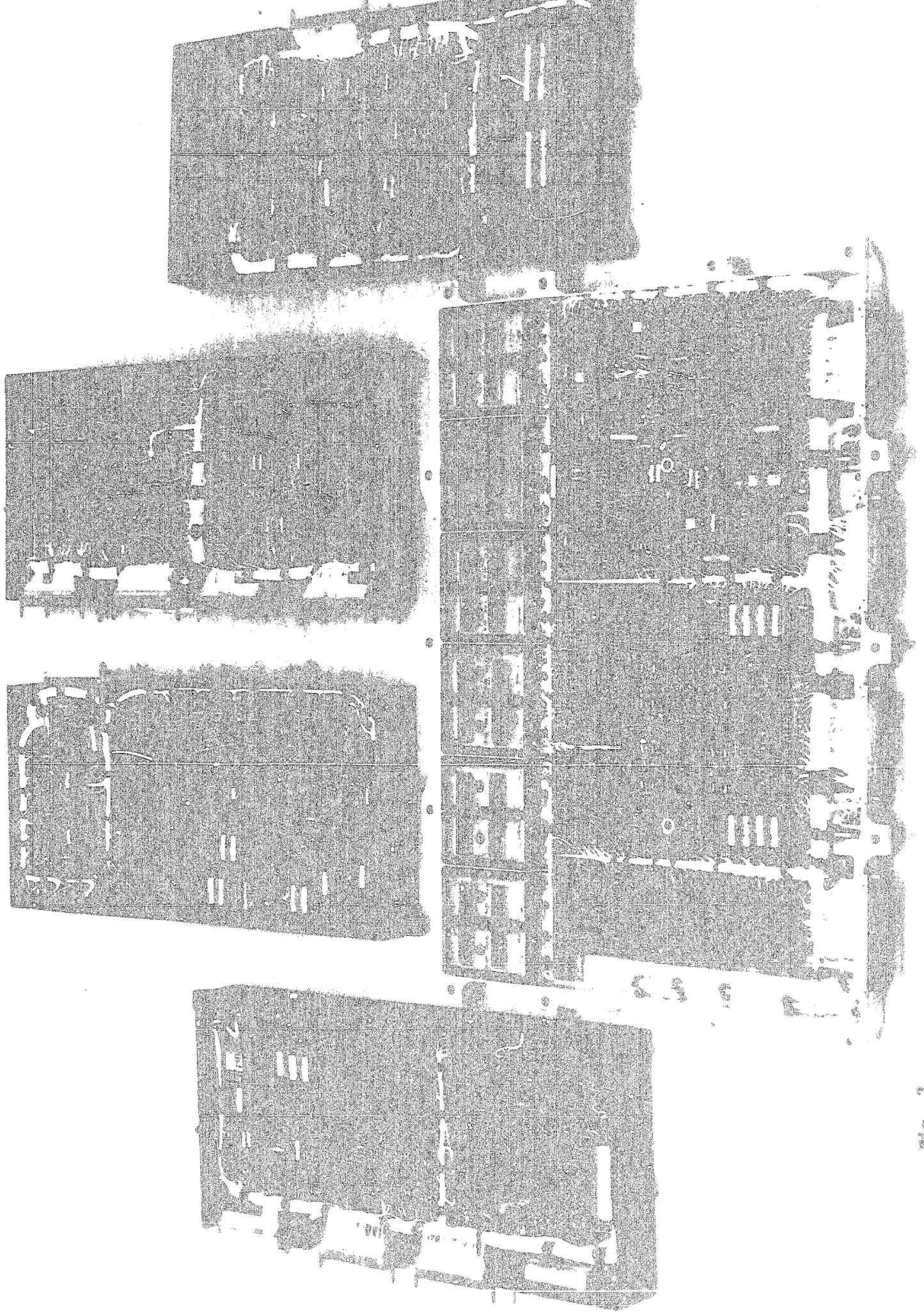


FIG. 2

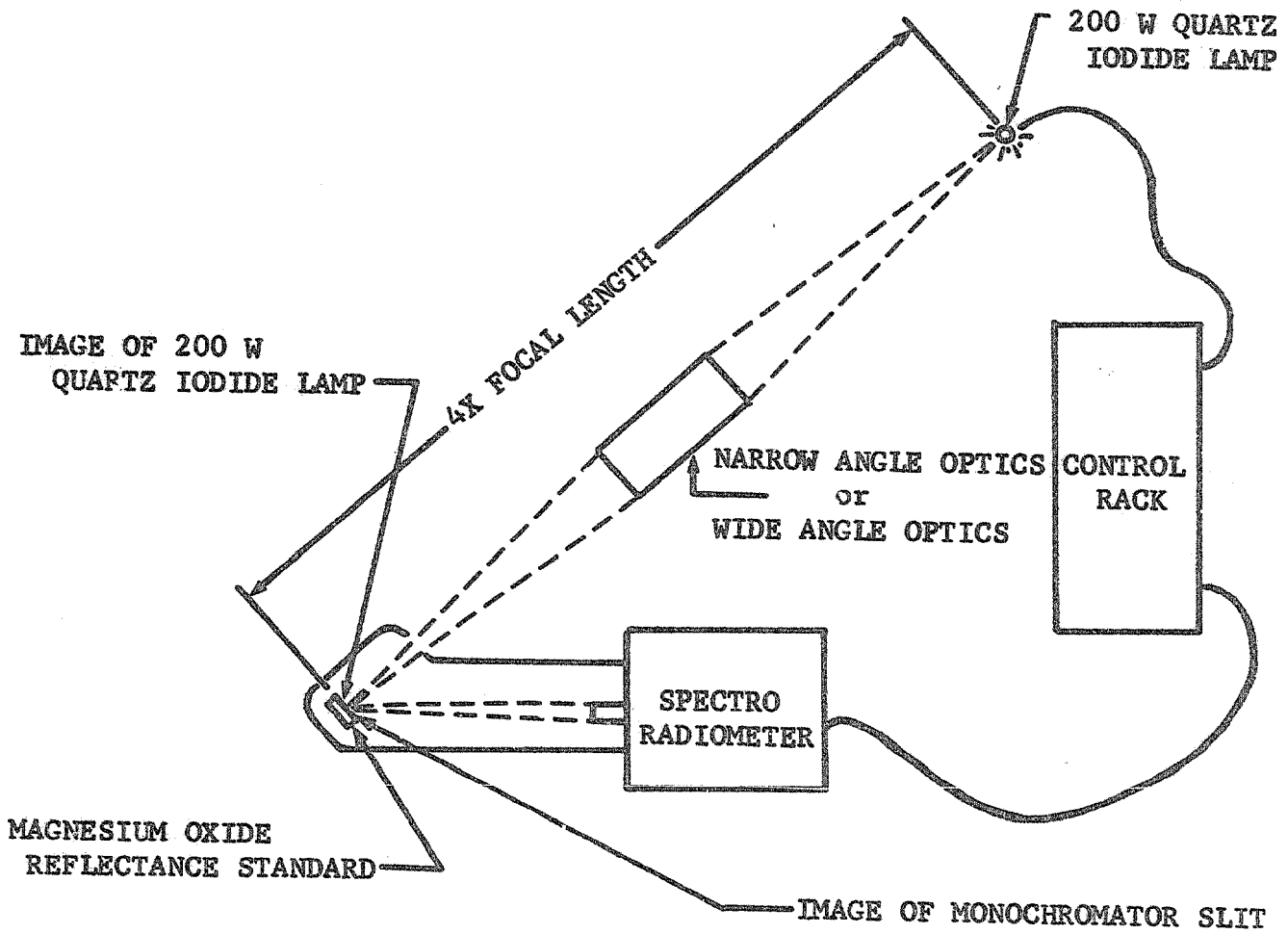


Fig. 3 SPECTRAL TRANSMITTANCE TEST CONFIGURATION

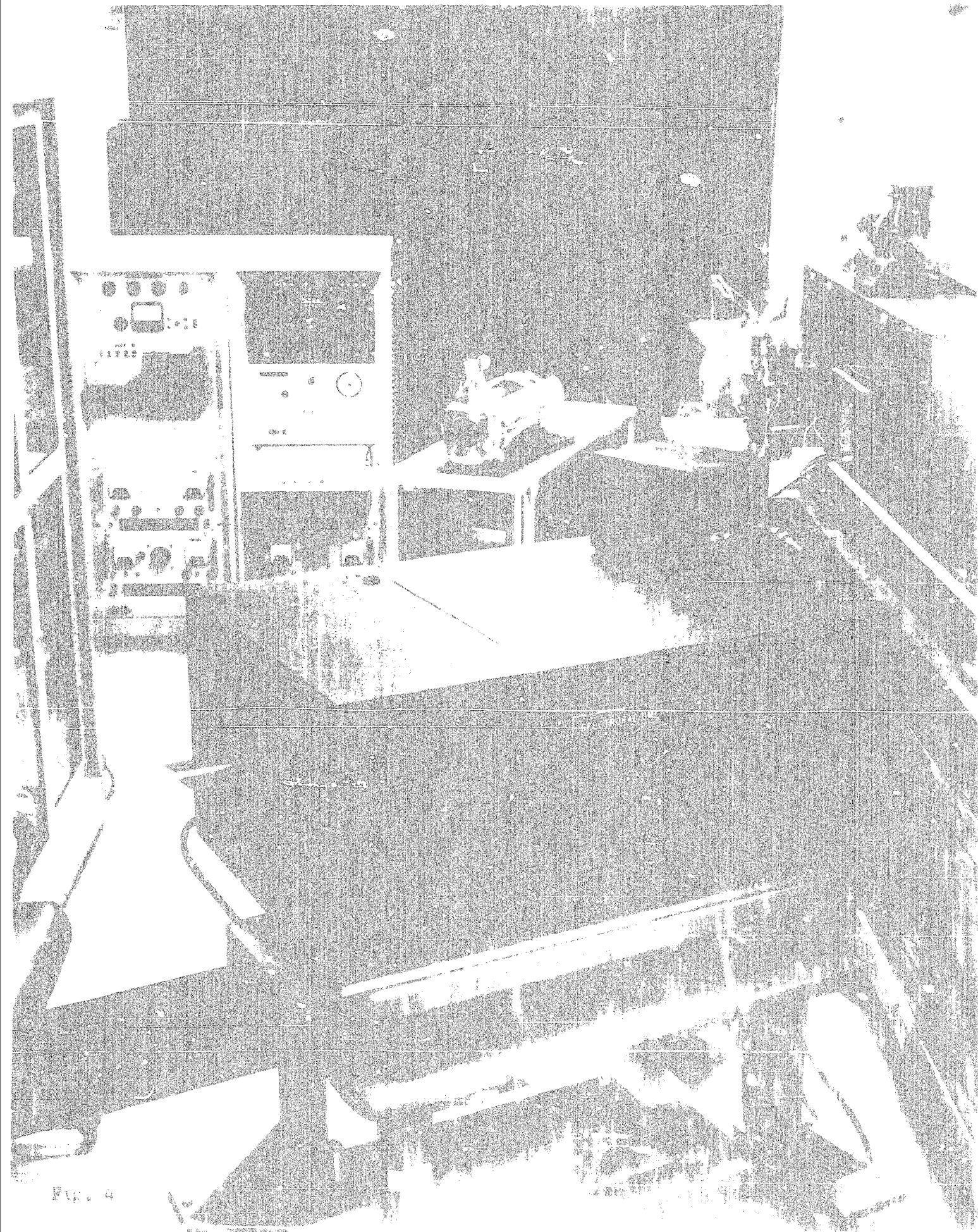


Fig. 4

The test was performed in two steps:

- (1) A 200-W quartz iodine lamp was mounted at a distance of approximately four times the focal length of the tested optics from the plaque (magnesium oxide reflectance standard). The amount of reflected radiation was then measured as a function of wavelength by the spectroradiometer and the collected data punched on a paper tape.
- (2) The tested optics system was then placed between the lamp and the plaque, the light beam was focused on a slit image and the procedure repeated. It is obvious that relative spectral transmittance is equal to the difference between the signal output of Step (1) and Step (2).

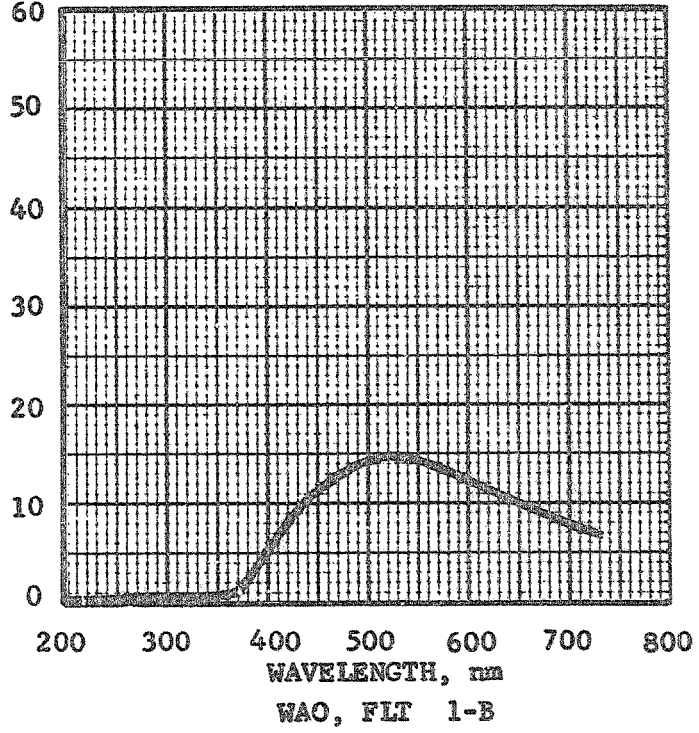
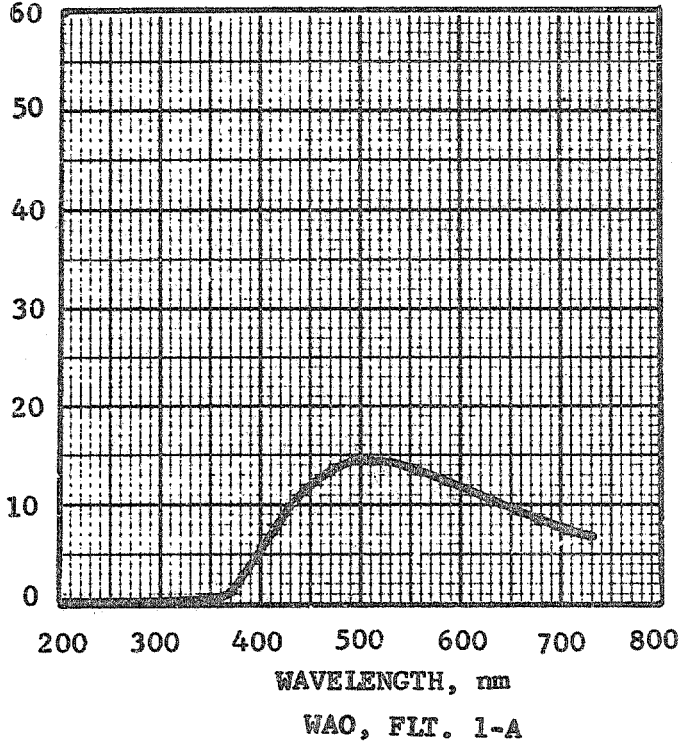
All four NAO flight telescopes were tested in this way. However, the WAO spectral characteristics are available only for Flight-1 lenses. The WAO were tested for Flight-1 only due to schedule problems. This test setup was performed for Flight-2 A and B only on the 50 mm lens, since the relay lens and filter wheel were not available when the Flight-1 WAO was tested. The curves (Figure 5) were scaled to show absolute transmittance at 555 nm, which was deduced from T-Stop No. results (see Section 2.1.2). The measurements were made between 245 and 725 nm at 5 nm intervals and their accuracy was $\pm 3\%$ or better.

It would be difficult to determine the exact accuracy of each individual test.

2.1.2. T-Stop Number

A reliable and effective method for T-Stop No. (T/#) measurement had been developed and tested for MM '71 calibration purposes. This was the method of choice for the MVM '73 calibration.

P
E
R
C
E
N
T
T
R
A
N
S
M
I
T
T
A
N
C
E



P
E
R
C
E
N
T
T
R
A
N
S
M
I
T
T
A
N
C
E

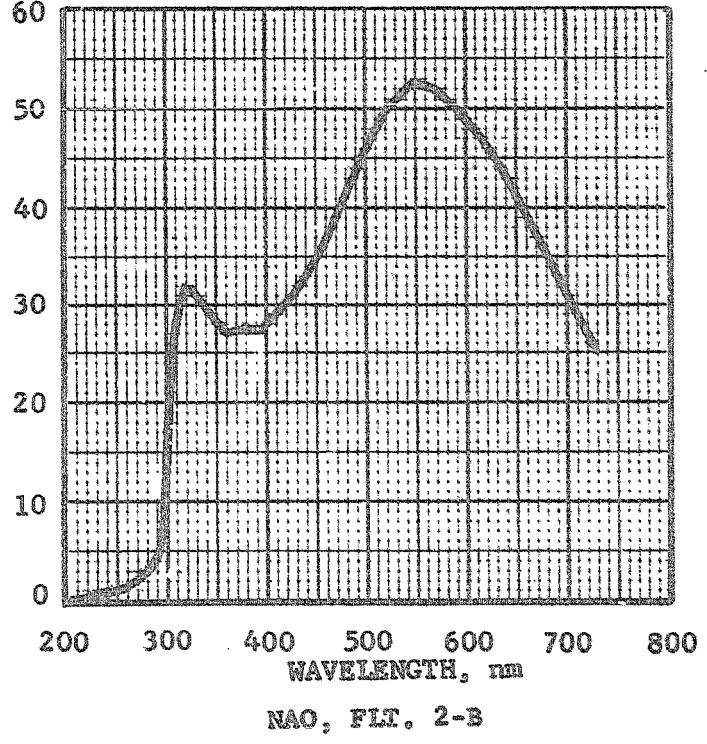
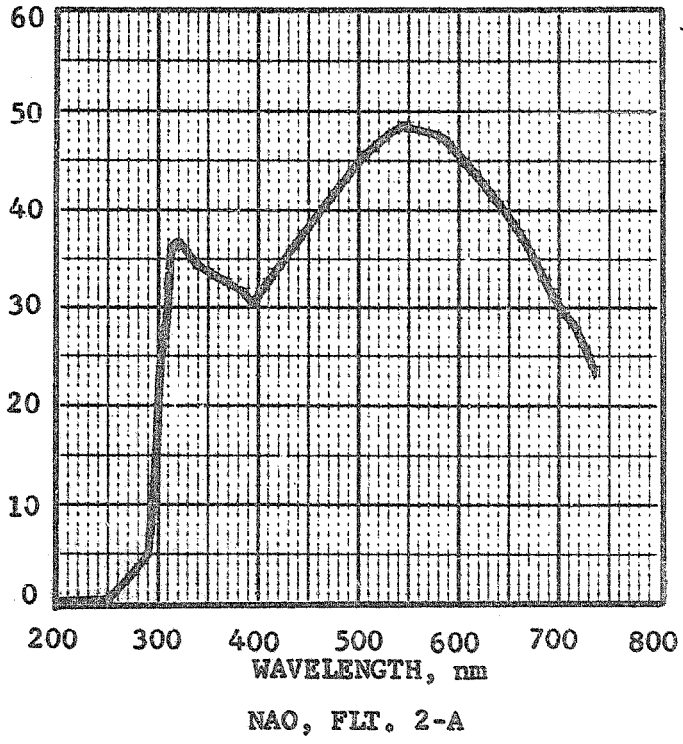


Fig. 5 SPECTRAL TRANSMITTANCE

The T/# of a lens is a function of its f-Stop No. (f/#) and its absolute transmittance, t , which includes the center obscuration of the telescope.

$$T/\# = \frac{f/\#}{\sqrt{t}}$$

This relationship is the basis for T/# determination. The calibration is performed in two steps:

- (1) A lens with 100% transmittance, $T/\# = f/\#$, is considered ideal. Thus, as shown in Figure 6B, an artificial optical system with perfect transmittance and known T/# can be constructed by placing an aperture of known diameter, D , at the light cannon face and erecting an imaginary image plane at distance L . The following relation for the T/# was deduced in Reference 2.

$$T/\# = \sqrt{\frac{1}{4} + (L/D)^2}$$

The relative light energy can now be measured at the axial point in the image plane for various aperture sizes. A plot of the square root of the relative energy versus the inverse value of the T/#, forms the calibration curve of the light cannon for the given test setup.

- (2) In the second step, the tested lens is placed between the light cannon and the imaginary image plane. Its entrance pupil is completely filled with flat-field illumination and the corresponding relative energy is measured at the same axial point. This value is then plotted on the calibration curve and the T/# of the optical system is found on the opposite scale as demonstrated in Figure 6A.

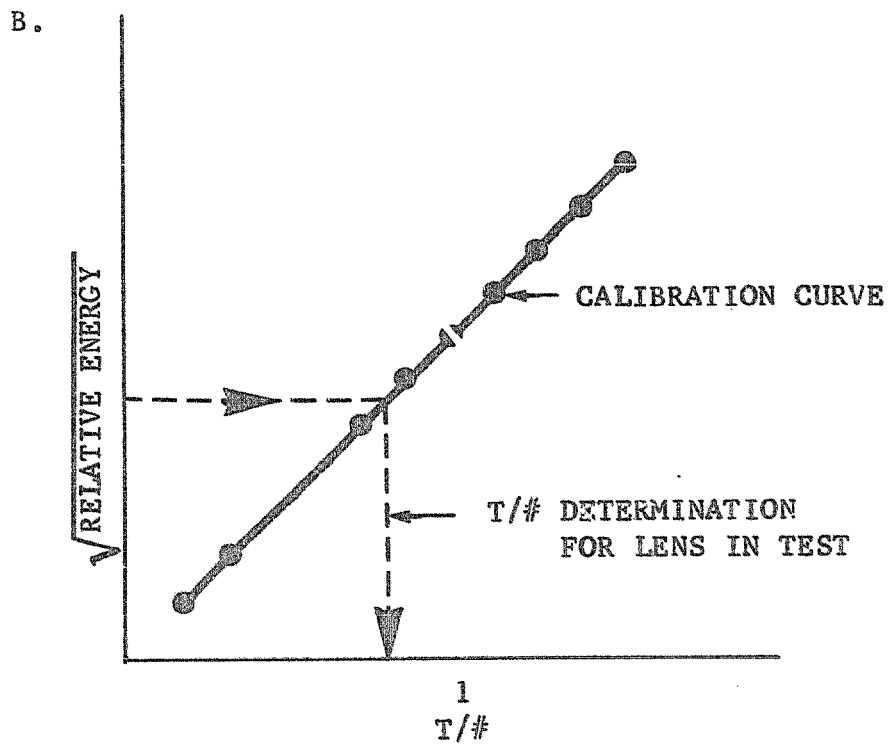
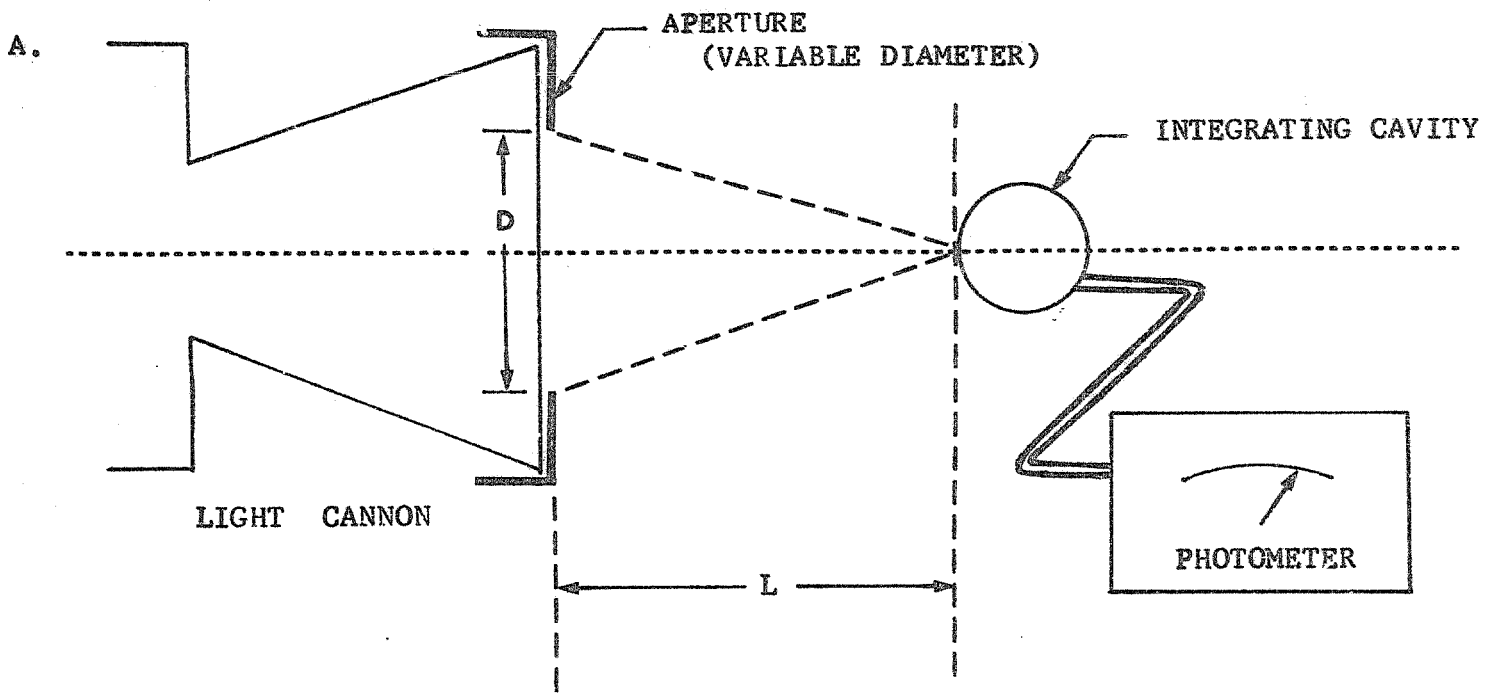


Fig. 6 T-Stop Number Determination : A. Light Cannon Calibration
B. Calibration Curve

A typical T/# measurement setup (Figure 7) shows the critical establishment of the imaginary image plane. (A special fixture had to be attached to the telescope to enable exact focusing at the opening of the integrating cavity.) The results of T/# measurements are summarized in Table 1, and they are all below the required $\pm 2\%$ accuracy limit (Reference 1). Once the T/# is known, the absolute transmittance of the telescope, as well as its accuracy, can be computed from the formula:

$$\tau = \left(\frac{f/\#}{T/\#} \right)^2$$

2.1.3. Polarization

The purpose of the component-level polarization test was twofold:

- (1) To determine the influence of the NAO upon the orientation of the polarization axis.
- (2) To determine the amount of polarization induced by the NAO.

Both these tests were applied to the NAO only, as the filter wheel was not mounted on the telescope.

Test (1) required reflected polarized light. A glass panel was set up at Brewster angle to the optical bench axis (Figure 8) and a 12-inch light cannon was used for its illumination. A polarizing filter was mounted on the bench to intercept the reflected polarized light. Using a photometer, the polarization axis was established with a $\pm 0.1^\circ$ accuracy. The NAO was then placed between the glass panel and the polarizing filter and the procedure repeated. Three independent sets of measurements were obtained for each telescope.

Both Flight-1 and Flight-2 NAO's were tested in this way, and the orientation differences were between 0.1° and 0.8° , which is well below the calibration requirement of $\pm 2.0^\circ$ (Ref. 1).

CAMERA	T-STOP NO.	NOMINAL f-STOP NO.	ABSOLUTE TRANSMITTANCE %	FILTER
FLT. 1-A, NAO	12.42 ± .10	8.5	46.8 ± .8	NONE
FLT. 1-A, WAO	Not Available	20.0	Not Available	WAF
FLT. 1-B, NAO	12.03 ± .10	8.5	49.9 ± .8	NONE
FLT. 1-B, WAO	54.27 ± .84	20.0	13.6 ± .2	WAF
FLT. 2-A, NAO	11.78 ± .04	8.5	52.1 ± .4	NONE
FLT. 2-A, WAO	Not Available	20.0	Not Available	WAF
FLT. 2-B, NAO	12.20 ± .10	8.5	48.5 ± .8	NONE
FLT. 2-B, WAO	Not Available	20.0	Not Available	WAF

TABLE 1. T-STOP NUMBER AND ABSOLUTE TRANSMITTANCE

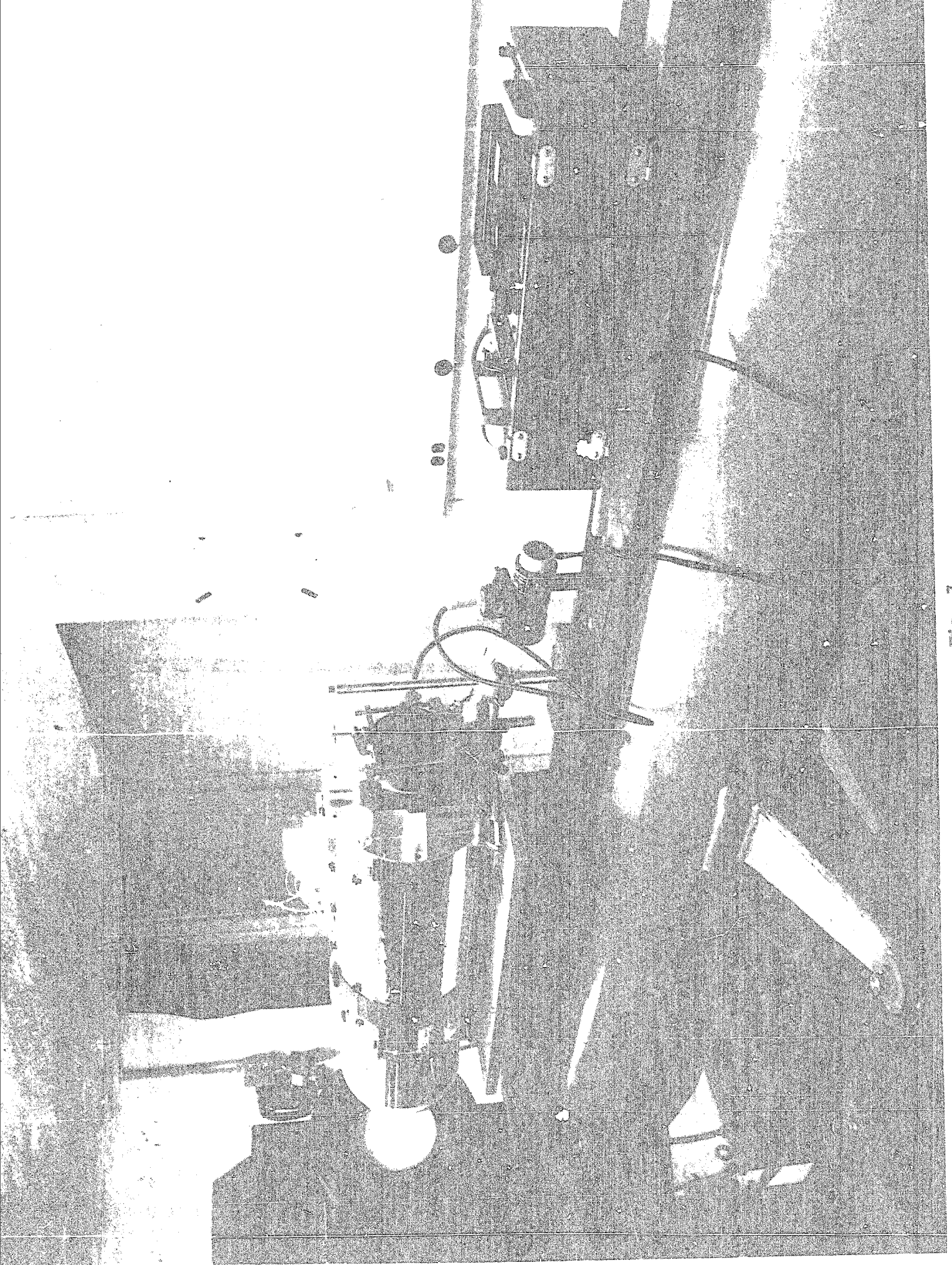
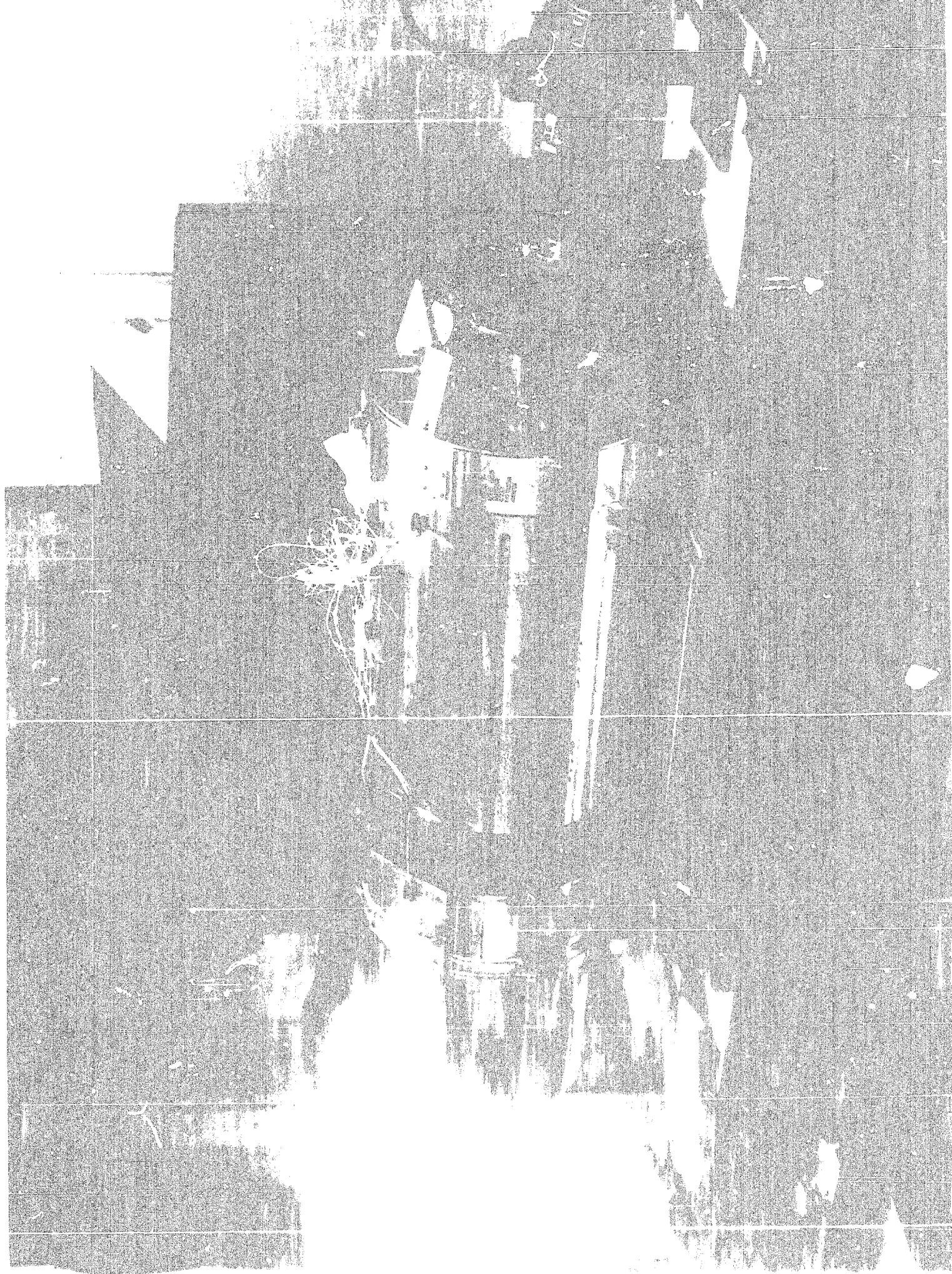


Fig. 7



30
31
32
33

The setup for test (2) was similar, except that unpolarized light reflected from a matte white surface was used. The polarizing filter was rotated 360° in steps of 5° , and the corresponding light energy was noted on the photometer. This procedure was repeated with the unpolarized light path passing through the NAO. Three independent sets of measurements were made for each telescope.

The differences for Flight 1-A, Flight 1-B, and Flight 2-B telescopes were found to be from $\pm 0.5\%$ to $\pm 4.0\%$; i.e., below the calibration requirement of $\pm 5.0\%$ (Reference 1). However, Flight 2-A results exceeded 12%, indicating that this NAO induces a substantial amount of polarization, the source of which has not been determined. It was suggested that the field corrector might contribute to the polarization leak, but results shown in Figure 9 prove this not to be the case. The test was also run with a red and blue filter to determine the spectral dependency of this induced polarization; it was very small (Figure 9).

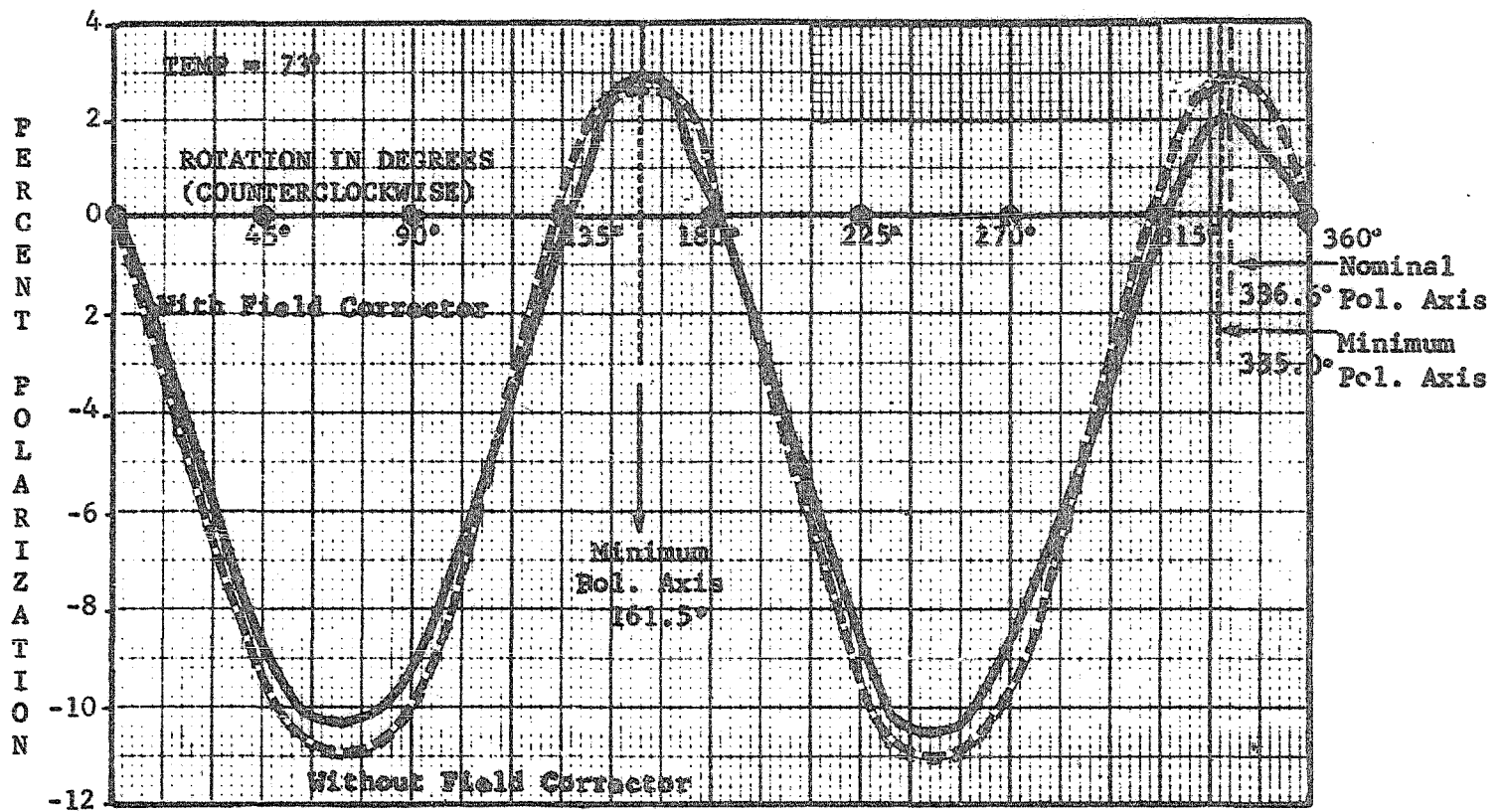
FILTERS

Each flight camera was equipped with a filter wheel containing eight filter positions:

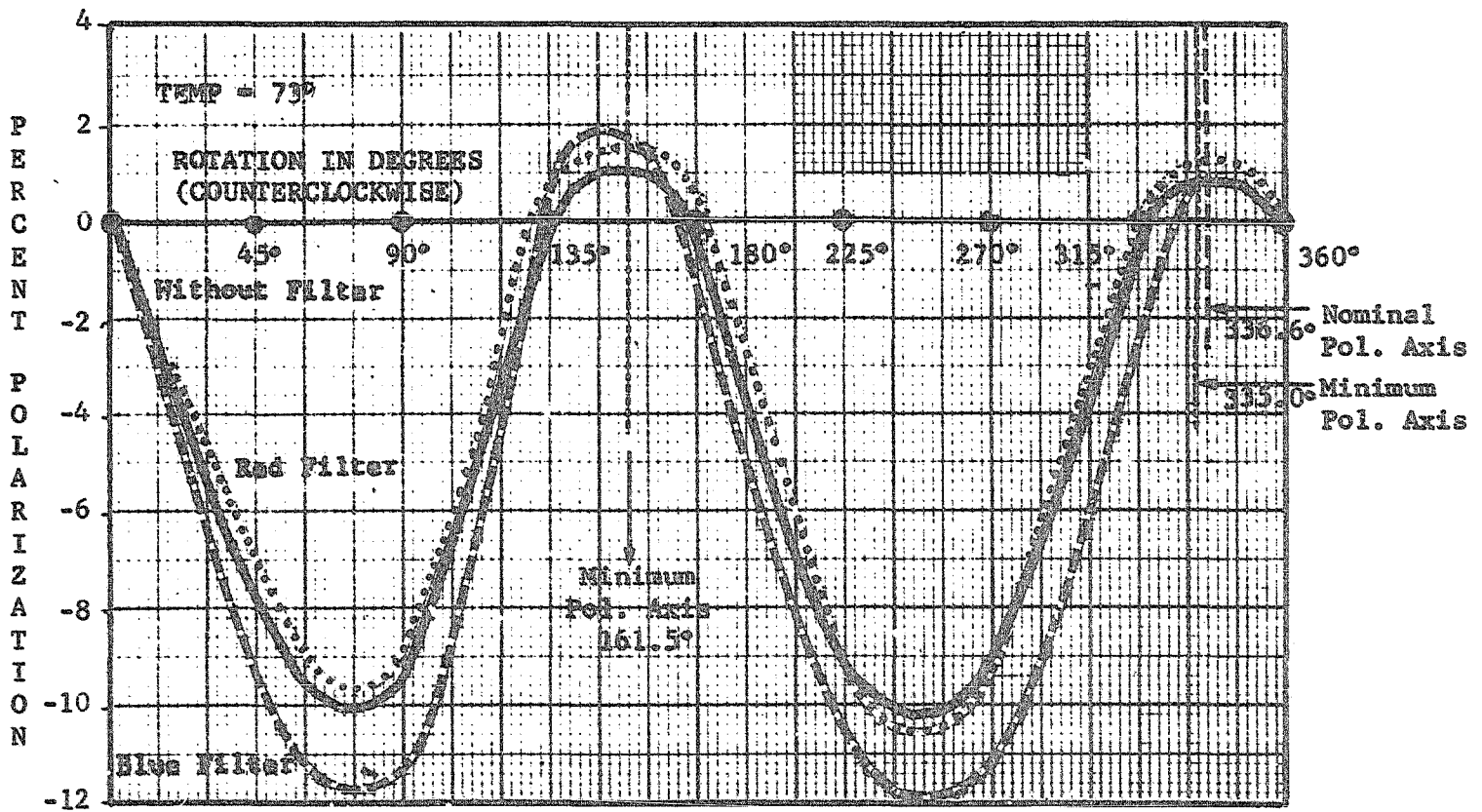
- 0 - Orange
- *1 - WAF (Wide-Angle Filter)
- 2 - Blue
- 3 - Ultraviolet Polarizer
- 4 - Minus Ultraviolet
- 5 - Clear
- 6 - Ultraviolet
- **7 - Fabry Lens

*WAF is a system of mirrors, fiber optics, and a relay lens which focuses the WAO on the vidicon. Spectral transmittance was ascertained in the optics tests.

**A special lens that focuses an image of the front corrector on the vidicon. It does not change the NAO spectral characteristics.



POLARIZATION



SPECTRAL DEPENDENCY OF POLARIZATION WITHOUT FIELD CORRECTOR

Fig. 9 POLARIZATION INDUCED BY NAO, FLT. 2-A

2.2.1. Spectral Transmittance

Spectral transmittance of filters 0, 2, 4, 5, and 6 was measured on a Bausch and Lomb Spectronic 505 Spectrophotometer. Periodic monitoring of a gas discharge lamp of known spectral characteristics insured calibration of the instrument. A wavelength precision, of the spectrophotometer, of 1 nm and transmittance accuracy of $\pm 3\%$ had previously been determined.

The spectral transmittance of Filter 3 was measured on the JPL spectroradiometer. The inherent difficulties of measuring the spectral properties of polarized light were overcome by placing the filter between two integrating cavities. Representative curves are shown in Figures 10-11 for each filter tested.

2.2.2. Polarization Axis

It was necessary to determine the axis of polarization of the ultraviolet polarizer filter, prior to its being mounted in the filter wheel. This was accomplished using a goniophotometer, an instrument which generates a light beam with a known polarization axis. The tested filter was placed in the light path and rotated until the point of minimum transmission (extinction) was determined. A notch was ground in the filter edge 90° from the minimum axis, marking the position of the polarization pass axis.

The notched lens was placed in the filter wheel so that the polarization pass axis would be parallel to the line direction of the vidicon faceplate (Figure 12). Subsequent testing of the filter in the filter wheel assembly yielded an accuracy level below the $\pm 2^\circ$ of rotation required by Reference 1. However, the actual orientation of the axis is also determined by opto-mechanical alignment and by eventual vidicon raster rotation. As so many factors enter into the exact positioning, the final orientation of the polarization axis was stated as $90^\circ \pm 3^\circ$.

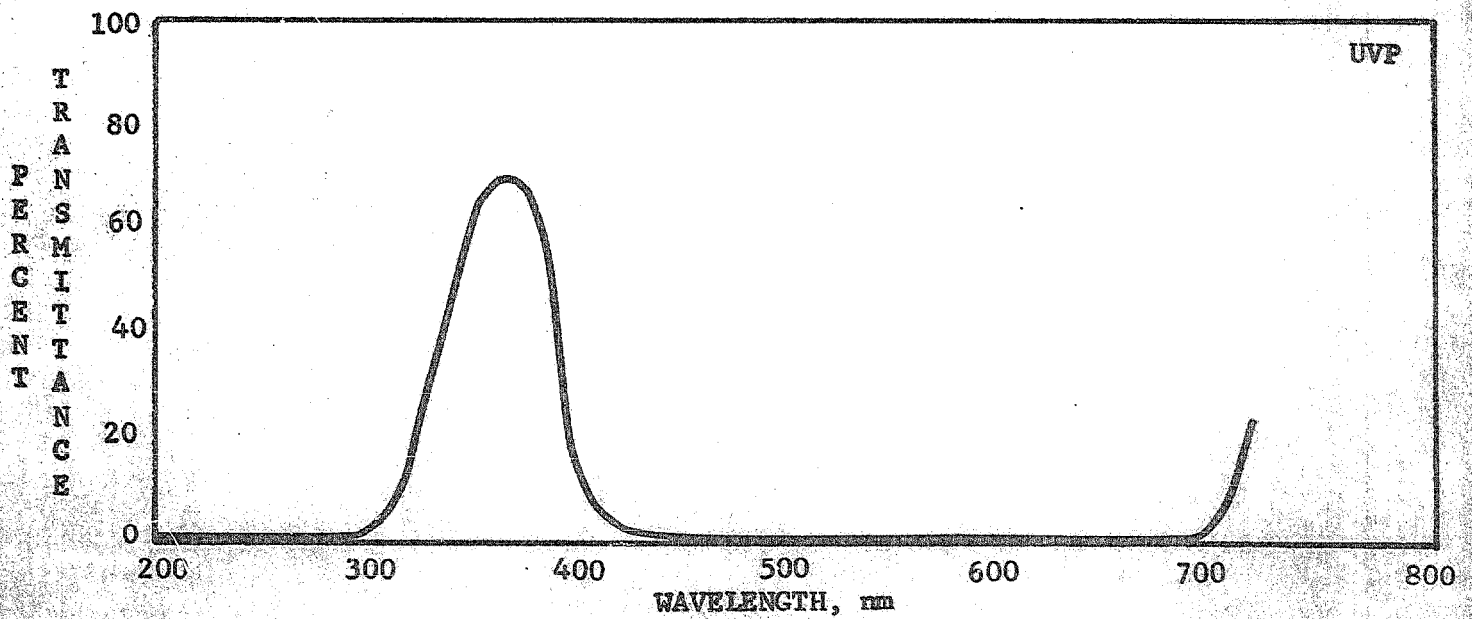
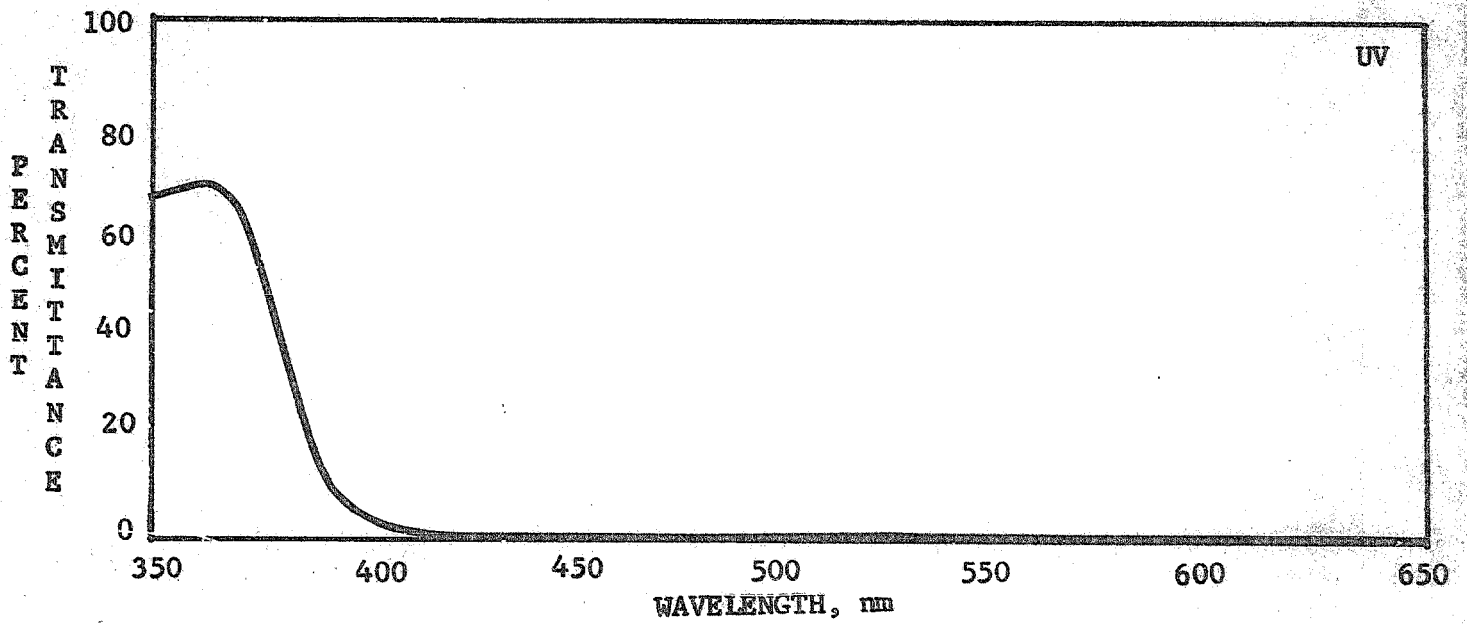
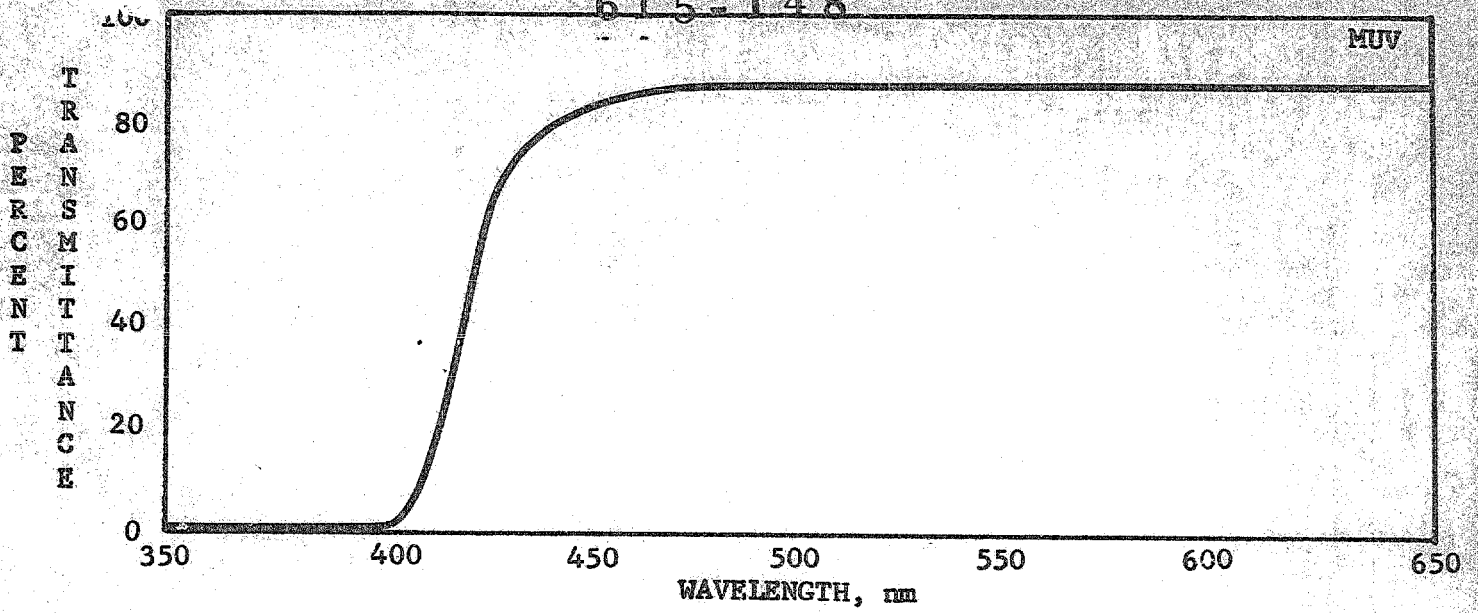


Fig. 11 SPECTRAL TRANSMITTANCE, FLT. 2

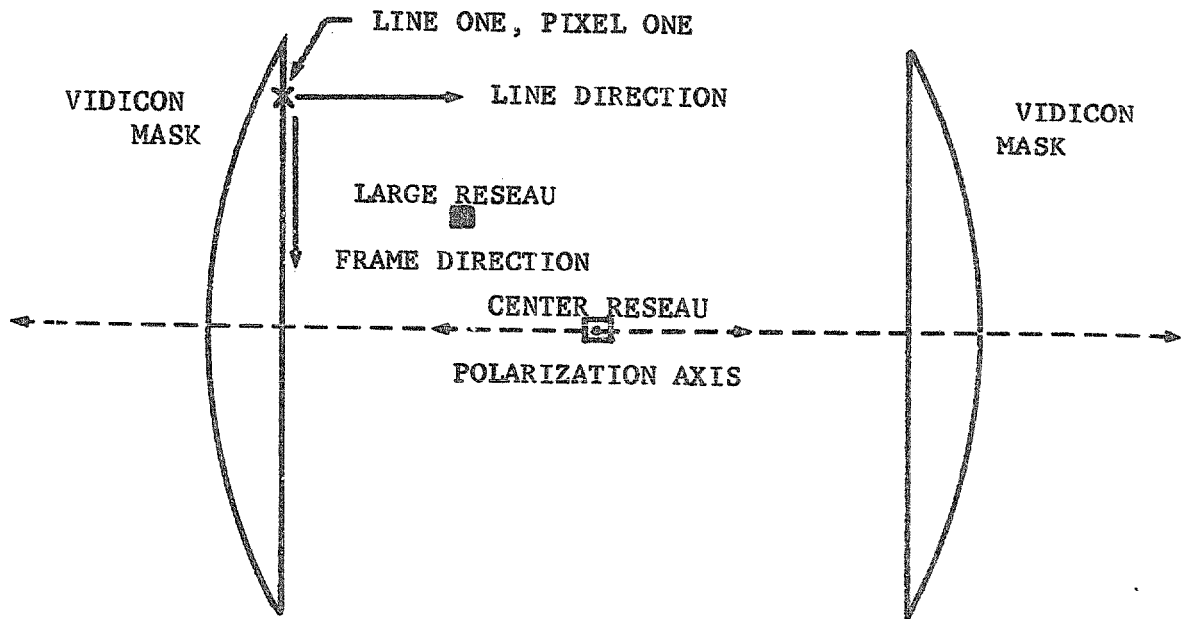


Fig. 12 DIRECTION OF THE POLARIZATION AXIS ON THE VIDICON FACE PLATE

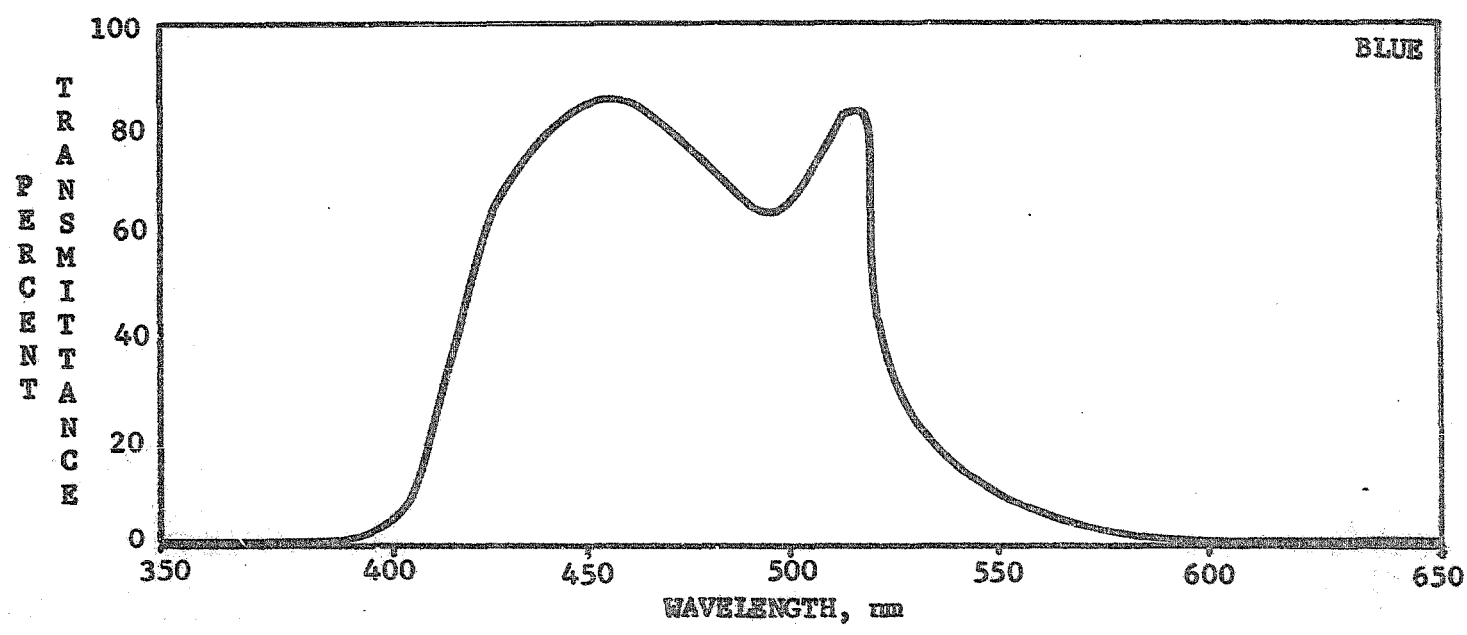
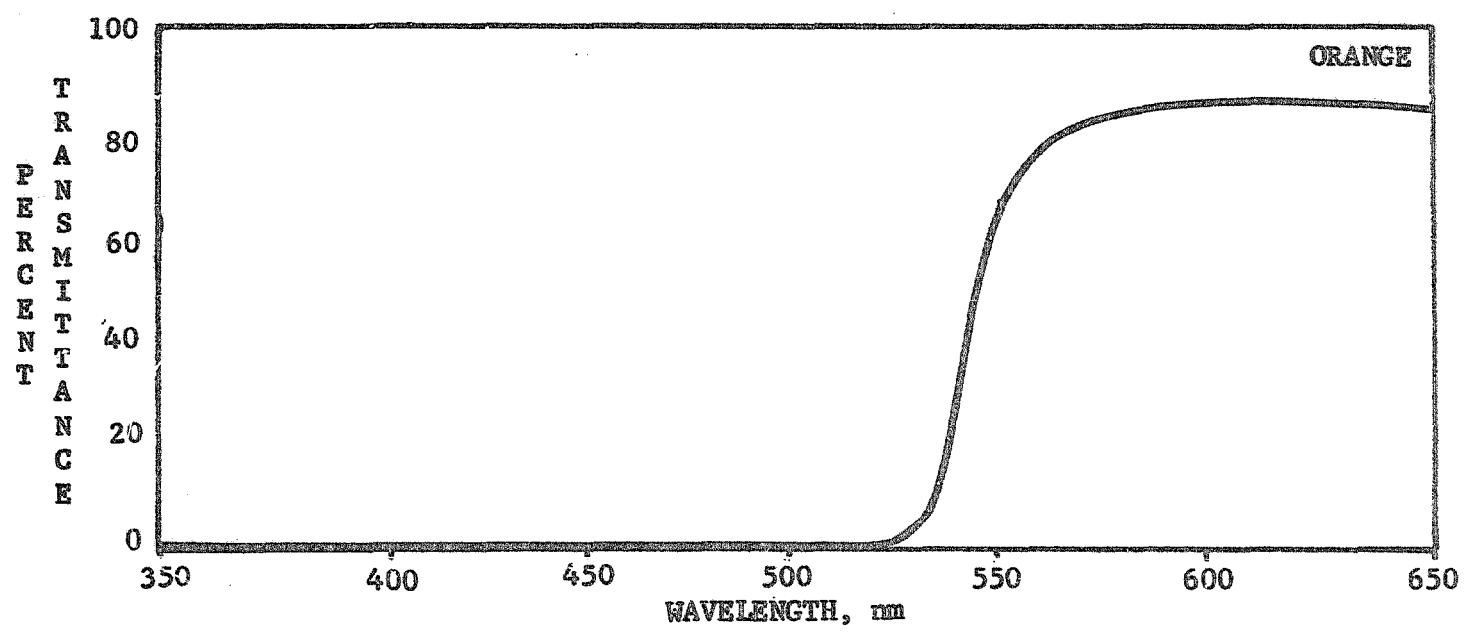
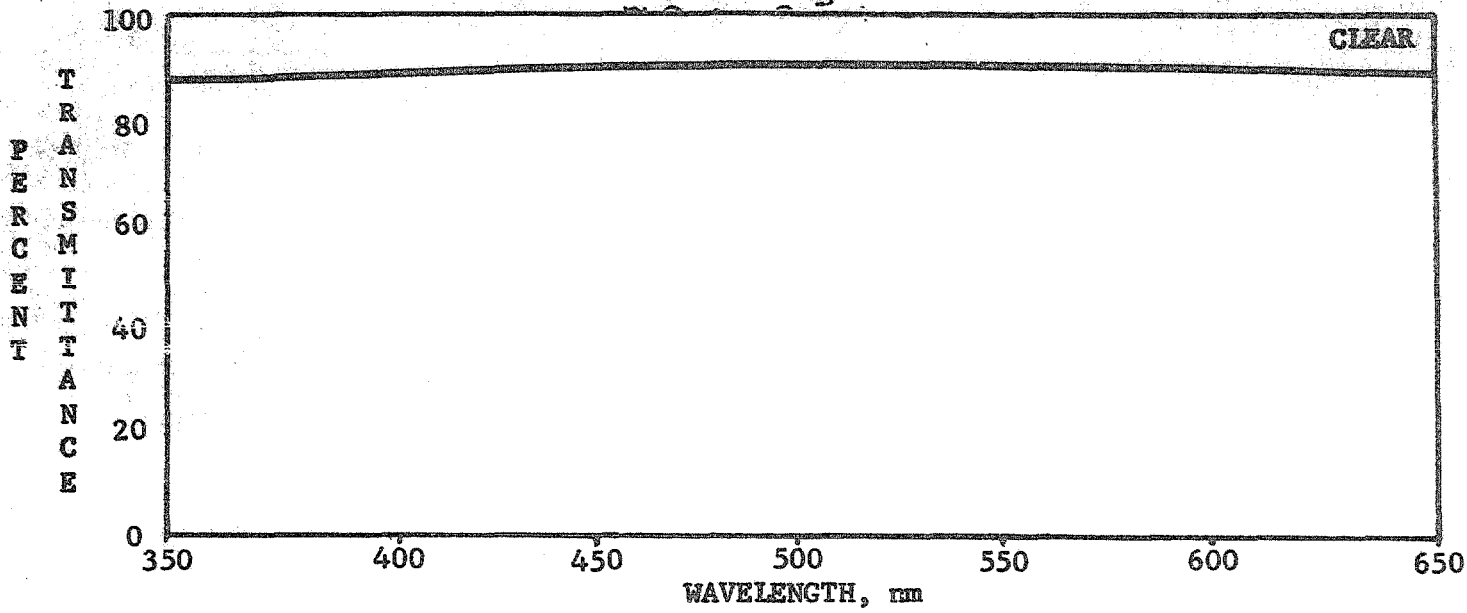


Fig. 10 SPECTRAL TRANSMITTANCE, FLT. 2

2.3 SHUTTERS

2.3.1. Shutter Characteristics

The shutters are of the focal-plane type with two blades: one blade opens the aperture, the other covers the aperture after the desired exposure interval. The exposure time is controlled by the Flight Data Subsystem (FDS) which provides a separate pulse to start each of the two shutter blades. The time between pulses is defined by the formula:

$$t = .81633 (4 + i) 2^{(j-1)} \text{ msec}$$

$$i = 0, 1, 2, 3$$

$$j = 1, 2, 3, \dots, 12$$

Each shutter assembly has a different response to commands due primarily to differing frictional forces. Therefore, the actual exposure time should be derived as follows:

$$t = .81633 (r + i) 2^{(j-i)} - \bar{\delta}$$

The appropriate value for $\bar{\delta}$ is obtained by determining the mean difference between commanded exposure time and the actual average exposure time measured at five places across the aperture. Since the shutter delay $\bar{\delta}$ is a mechanical effect imposed by a specific mechanism, the value is essentially independent of commanded exposure time.

2.3.2. Exposure Table and Shading

Exposure and shading data were obtained by testing in a thermal environment at a temperature range from -15° C to $+35^{\circ}$ C. The shutter test fixture permitted measuring shutter characteristics by successively illuminating five photo-transistors with collimated light passing through the test shutter. The five photo-transistors were equally spaced over a 0.5-inch interval in the direction of shutter blade travel. Average exposure

time is the average of the exposure times of each of the five photo-transistors and is given in Table 2 for all cameras. The standard deviation was also calculated, and served as a measure of exposure repeatability at various temperatures. In addition, shading of the deviation from the average exposure across the frame has been determined (Figure 13). The precision of the performed observations was better than 20 microseconds of time resolution.

2.4. VIDICONS

2.4.1. Spectral Response

The relative spectral response was measured for each vidicon. In the initial phases of the program this information was used for selection of the tubes and for gain-setting calculations. This measurement is an important part of component-level calibrations, as it complements other spectral transmittance data of the system.

Measurements were made in the wavelength band from 300 to 620 nm, utilizing a monochromatic stimuli within this region. The constant output current method was used; i.e., the power of the monochromator lamp was adjusted for each selected wavelength so that the vidicon output current was kept constant. The varying power input, required to achieve this constant level, constitutes the spectral response curve of the vidicon when normalized and plotted against the wavelength. The obtained results are given in Figure 14. Each curve was normalized to show 100% response at its peak and the accuracy, based on a comparison test, was well below the required 10% relative radiometry (Reference 1).

2.4.2. Reseau Map

To correct the geometric distortion of vidicon images induced by the electrostatic and magnetic focusing systems, a pattern of metallic marks was deposited upon the inside surface of the vidicon window prior to application of the photo-conduction layers. Careful calibration of the

SHUTTER SERIAL NUMBER	-15° C		+5° C		+25° C		+35° C	
	COMM.	EXPOSED	COMM.	EXPOSED	COMM.	EXPOSED	COMM.	EXPOSED
007 (FLT. 1-A)	25.710	24.167	25.695	24.253	25.695	24.325	25.680	24.214
006 (FLT. 1-B)	25.705	23.417	25.690	23.371	25.680	23.316	25.680	23.425
011 (FLT. 2-A)	25.710	24.885	25.685	24.849	25.705	24.989	25.695	24.944
008 (FLT. 2-B)	25.695	23.073	25.685	23.170	25.670	23.110	25.700	23.352

EXPOSURE TIMES

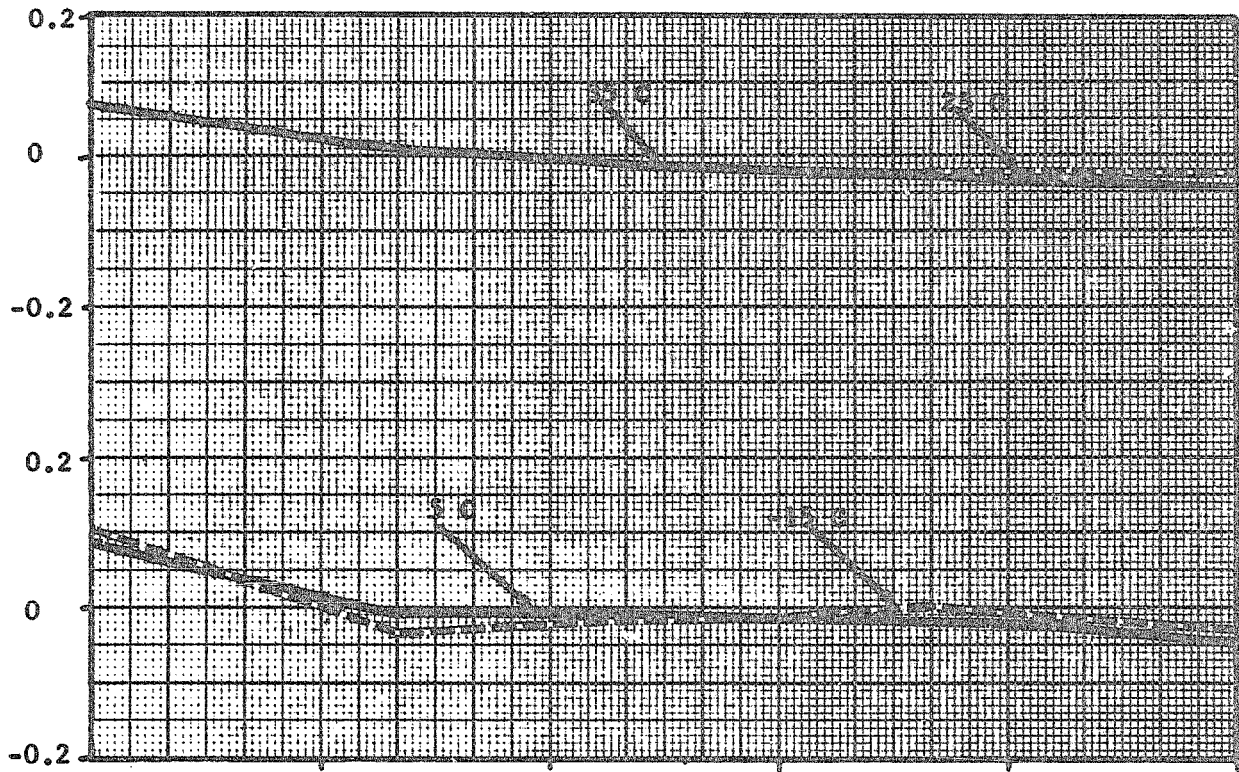
SHUTTER SERIAL NUMBER	EXPOSURE TIME STANDARD DEVIATION, MS			
	-15° C	+5° C	+25° C	+35° C
007 (FLT. 1-A)	±.059	±.052	±.034	±.056
006 (FLT. 1-B)	±.072	±.042	±.057	±.086
011 (FLT. 2-A)	±.049	±.104	±.060	±.034
008 (FLT. 2-B)	±.030	±.059	±.018	±.023

COMMANDED EXPOSURE TIME = 25.7 MS

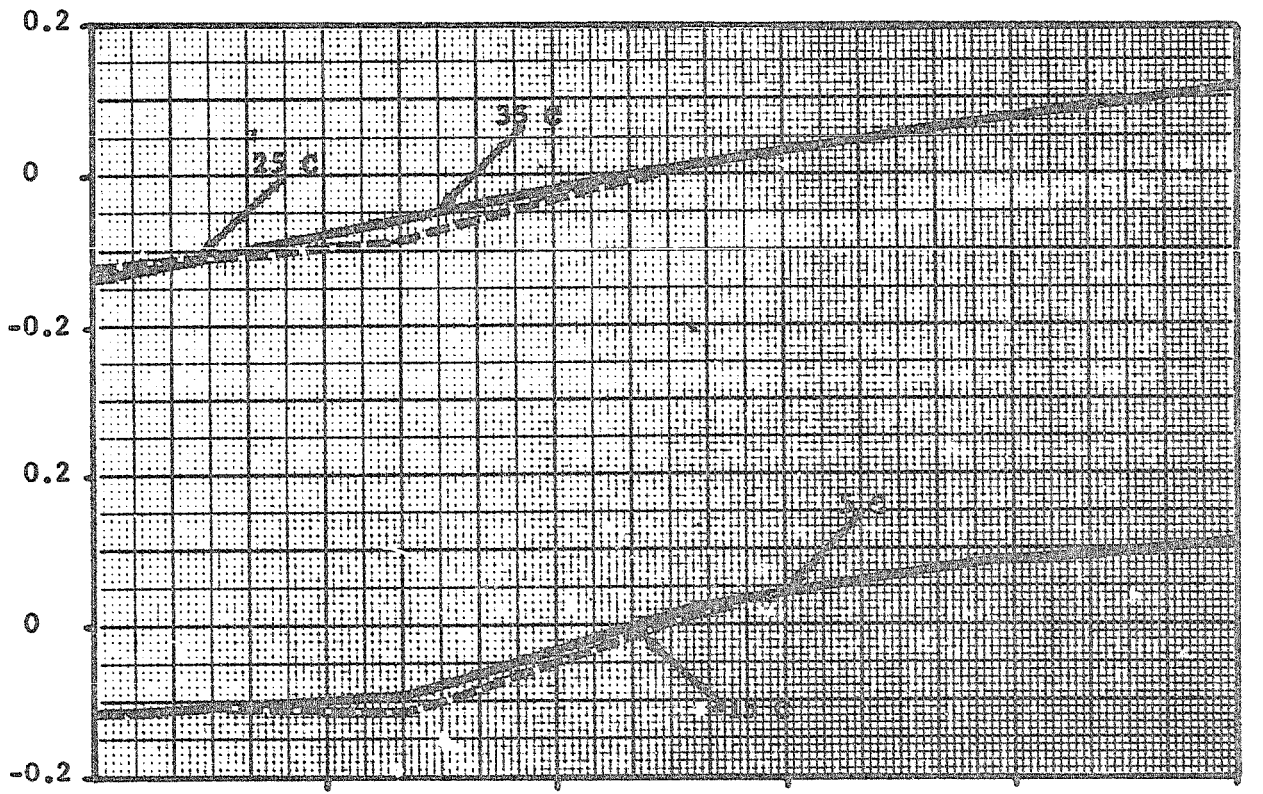
REPEATABILITY

TABLE 2. SHUTTER EXPOSURE TIMES AND REPEATABILITY

DEVIATION FROM AVERAGE EXPOSURE IN MSEC



SHUTTER S/N 011, FLT. 2-A



DISTANCE ACROSS APERTURE, INCH
 SHUTTER S/N 008, FLT. 2-B

Fig. 13 EXPOSURE SHADING (50V, 1320 μ f, 25.7 msec COMMAND)

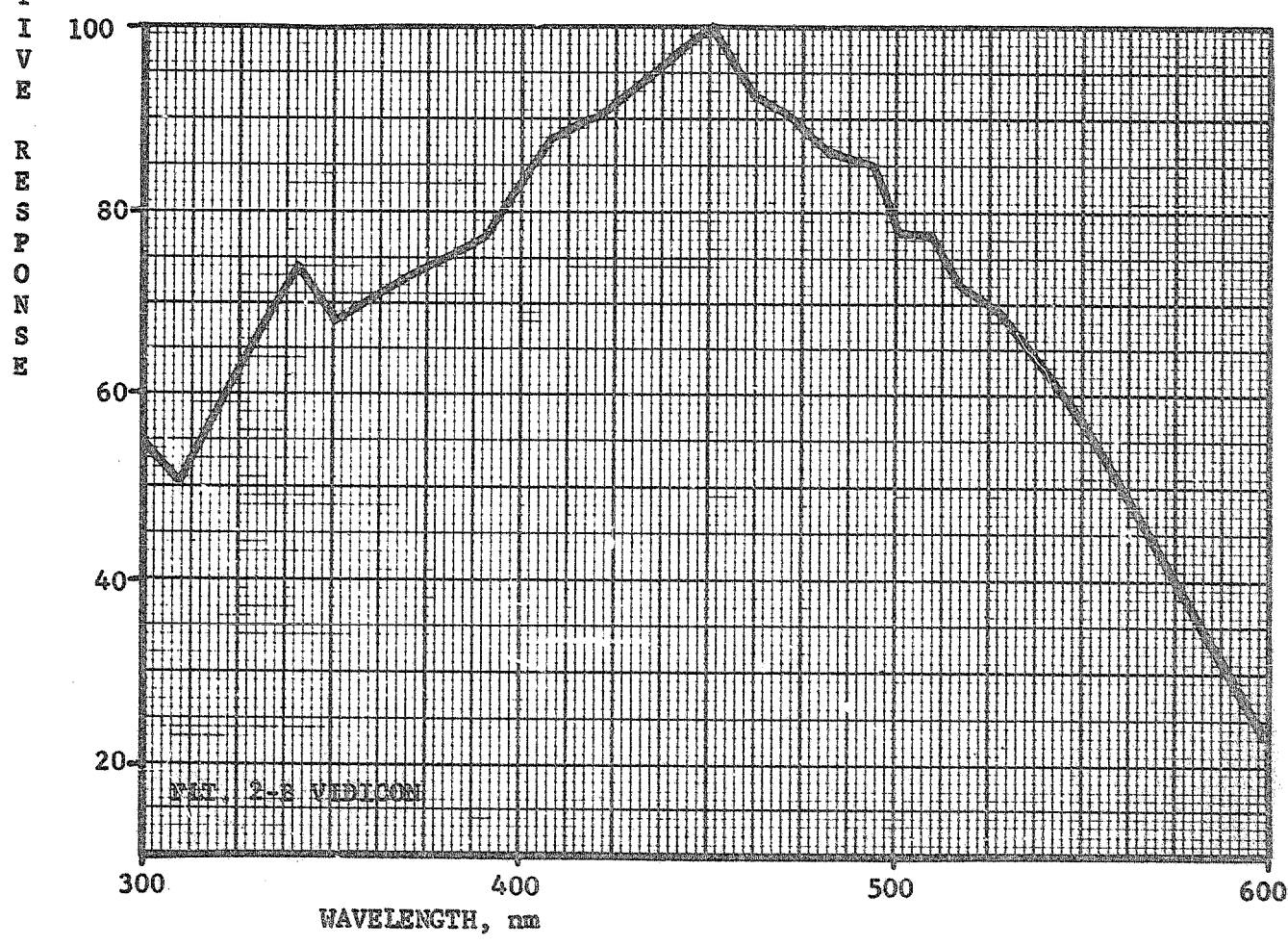
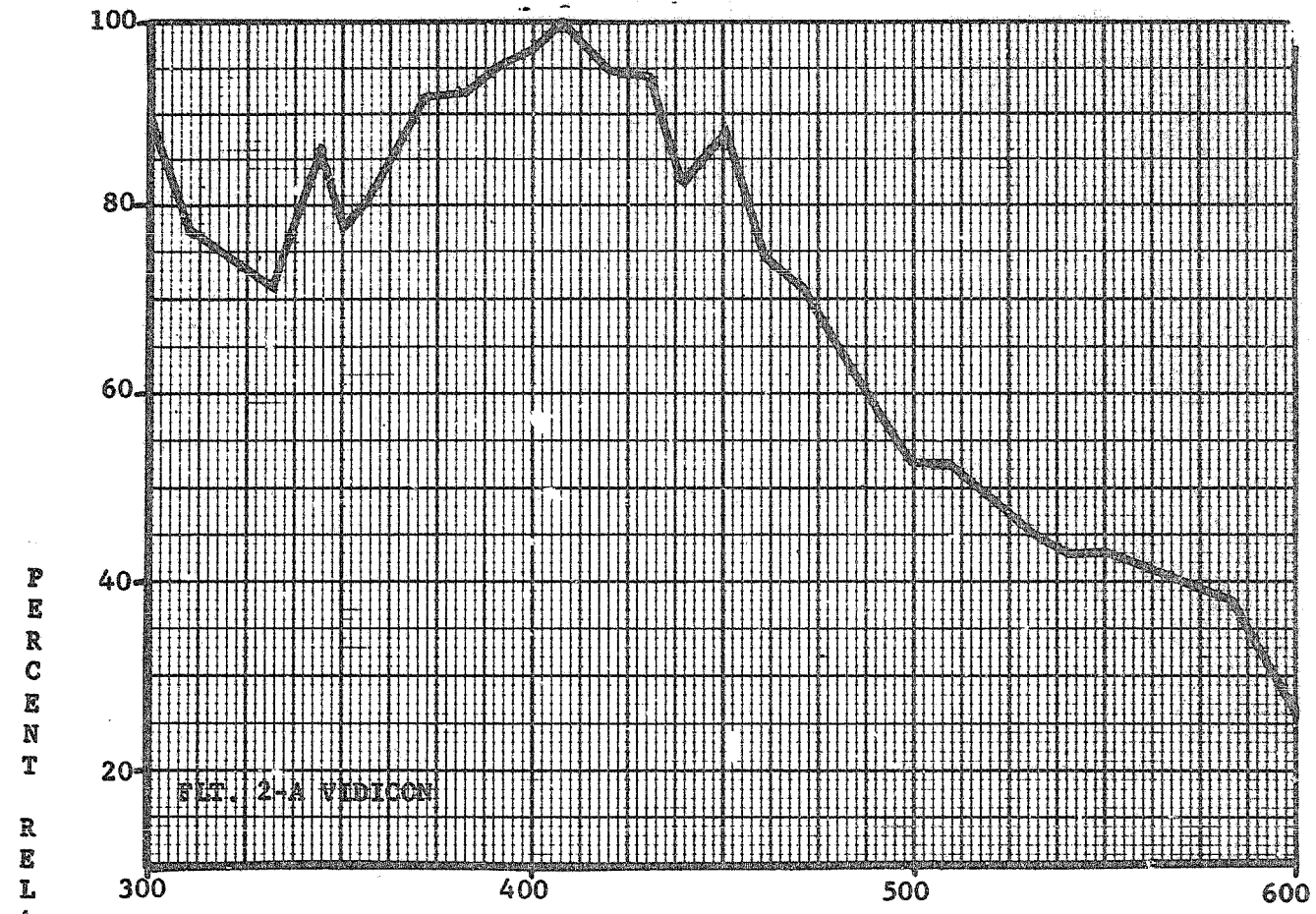


Fig. 14 RELATIVE SPECTRAL RESPONSE

distortions, comparing image location of the reseaus to known locations on the vidicon tube, would allow computer reduction of geometric distortions.

Exact measurement of the x-y coordinate positions of the center of each reseau (reseaus touching the vidicon mask were measured at the center of the area where the mask edge crossed the reseau) was performed on the Moore Universal Measuring Machine using a 150 x microscope. The obtained observational accuracy was determined to be $\pm .001$ mm as compared with the required accuracy of $\pm .002$ (Reference 1). The reseau grid was aligned with the x-y table of the optical comparator and all grid deviations measured.

Reseau marks deposited on the vidicon varied greatly in size and shape from the specified square, having side dimensions of .025 mm to .043 mm.

Results of calibration are organized by reseau pattern type. The schematics of the 63 reseau pattern, Flight 1-A, and the 111 reseau pattern, Flight 1-B, 2-A, 2-B vidicons, can be found in Figures 15 and 16 respectively. X-Y coordinates of the reseaus on the Flight 2-A and 2-B vidicons are listed in Tables 3 and 4.

3. SUBSYSTEM LEVEL CALIBRATIONS

3.1. LIGHT SOURCES

Primary light source used for radiometric calibration was the 12" light cannon(Figure 17); consisting of two 1600 -watt Xenon high-pressure arc discharge lamps in an integrating cavity, a variable iris diaphragm, a conical integrating cavity, and a 12" diameter diffuser. Xenon lamps provide a spectrum similar to the solar spectrum.

Smaller 2" light cannons (a single Xenon lamp in an integrating cavity) were coupled to a Celestron reverse collimating telescope(Fig. 18) to provide an 8" diameter collimated beam. Two units of this type were utilized where it was impractical to employ the 12" light cannon.

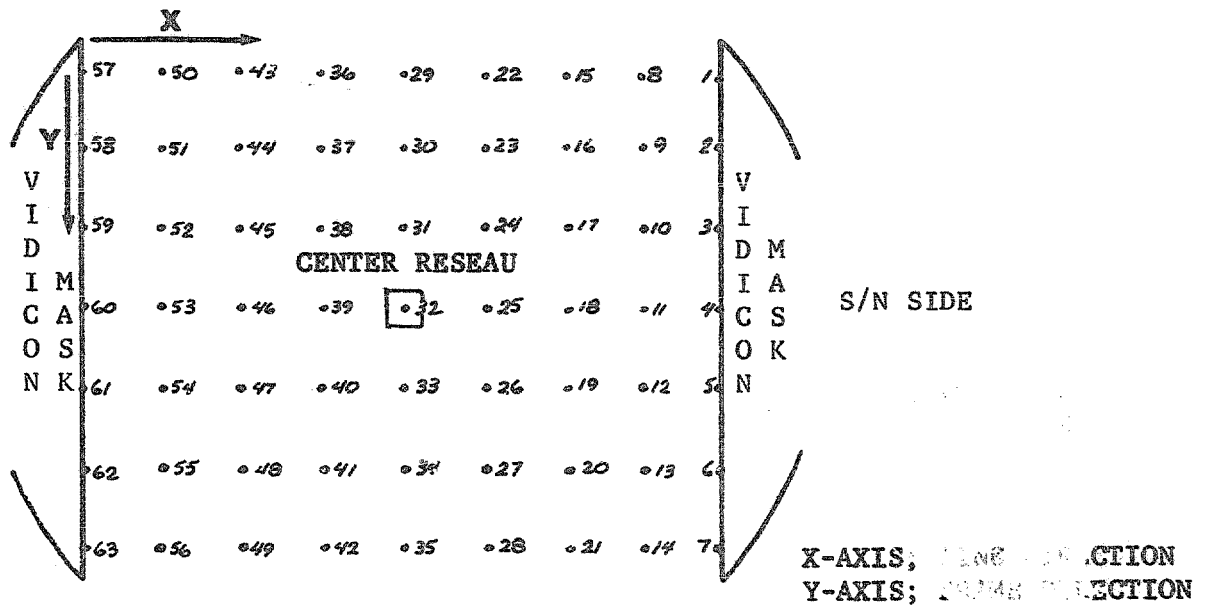


Fig. 15 VIDICON RESEAU GRID FLIGHT 1-A, 63 RESEAU PATTERN

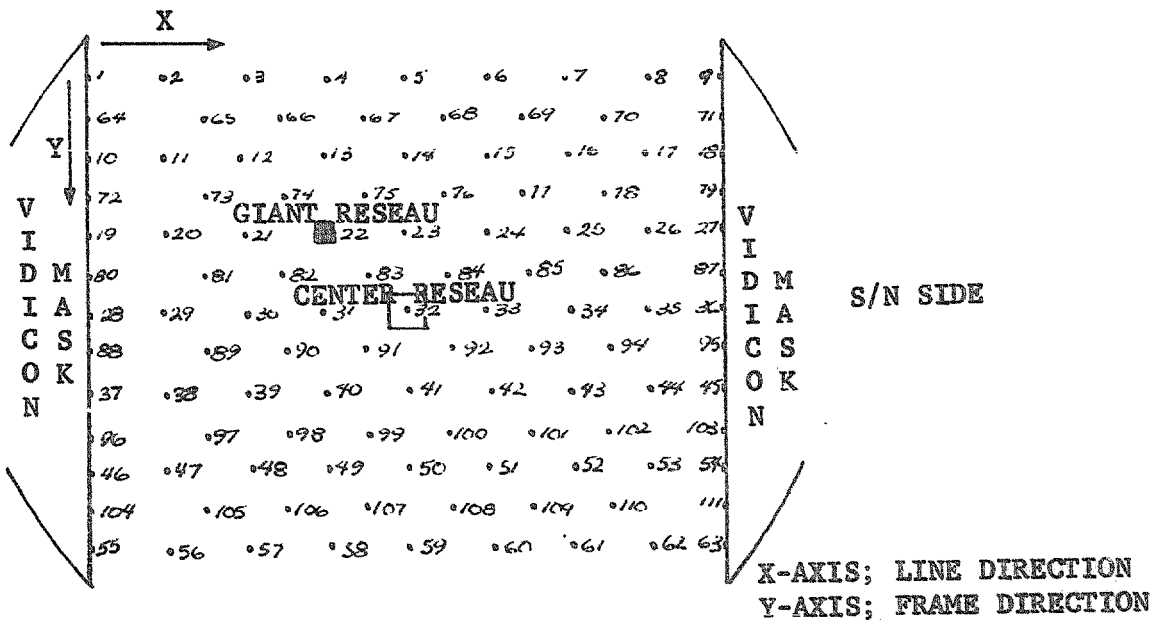


Fig. 16 VIDICON RESEAU GRID FLIGHT 1-B, 2-A, 2-B, 111 RESEAU PATTERN

RESEAU	X	Y	RESEAU	X	Y	RESEAU	X	Y
1	-.18836	-.24304	38	.10630	-.10644	75	-.03560	.10636
2	-.16556	↓	39	.16532	-.10644	76	.03550	↓
3	-.14112	↓	40	-.18836	-.07100	77	.10630	↓
4	-.10654	↓	41	-.14112	↓	78	.16532	↓
5	-.07024	↓	42	-.07024	↓	79	-.18836	.14188
6	-.03560	↓	43	.00000	↓	80	-.14112	↓
7	.00000	↓	44	.07000	↓	81	-.07024	↓
8	.03550	↓	45	.14090	↓	82	.00000	↓
9	.07000	↓	46	.18810	↓	83	.07000	↓
10	.10630	↓	47	-.16556	-.03546	84	.14090	↓
11	.14090	↓	48	-.10654	↓	85	.18810	↓
12	.16532	↓	49	-.03560	↓	86	-.16556	.17732
13	.18810	↓	50	.03550	↓	87	-.10654	↓
14	-.18836	-.21284	51	.10630	↓	88	-.03560	↓
15	-.14112	↓	52	.16532	↓	89	.03550	↓
16	-.07024	↓	53	-.18836	.00000	90	.10630	↓
17	.00000	↓	54	-.14112	↓	91	.16532	↓
18	.07000	↓	55	-.07024	↓	92	-.18836	.21284
19	.14090	↓	56	.00000	↓	93	-.14112	↓
20	.18810	↓	57	.07000	↓	94	-.07024	↓
21	-.16556	-.17730	58	.14090	↓	95	.00000	↓
22	-.10654	↓	59	.18810	↓	96	.07000	↓
23	-.03560	↓	60	-.16556	.03558	97	.14090	↓
24	.03550	↓	61	-.10654	↓	98	.18810	↓
25	.10630	↓	62	-.03560	↓	99	-.18836	.24302
26	.16532	↓	63	.03550	↓	100	-.16556	↓
27	-.18836	-.14186	64	.10630	↓	101	-.14112	↓
28	-.14112	↓	65	.16532	↓	102	-.10654	↓
29	-.07024	↓	66	-.18836	.07100	103	-.07024	↓
30	.00000	↓	67	-.14112	↓	104	-.03560	↓
31	.07000	↓	68	-.07024	↓	105	.00000	↓
32	.14090	↓	69	.00000	↓	106	.03550	↓
33	.18810	↓	70	.07000	↓	107	.07000	↓
34	-.16556	-.10644	71	.14090	↓	108	.10630	↓
35	-.10654	↓	72	.18810	↓	109	.14090	↓
36	-.03560	↓	73	-.16556	.10636	110	.16532	↓
37	.03550	↓	74	-.10654	.10636	111	.18810	↓

TABLE 3. FLT. 2-A VIDICON RESEAU LOCATIONS, INCHES

RESEAU	X	Y	RESEAU	X	Y	RESEAU	X	Y
1	-.18823	-.24310	38	.10635	-.10652	75	-.03552	.10644
2	-.16549	↓	39	.16537	-.10652	76	.03546	↓
3	-.14104	↓	40	-.18823	-.07096	77	.10635	↓
4	-.10646	↓	41	-.14104	↓	78	.16537	↓
5	-.07004	↓	42	-.07004	↓	79	-.18823	.14188
6	-.03552	↓	43	.00000	↓	80	-.14104	↓
7	.00000	↓	44	.07008	↓	81	-.07004	↓
8	.03546	↓	45	.14100	↓	82	.00000	↓
9	.07008	↓	46	.18822	↓	83	.07008	↓
10	.10635	↓	47	-.16549	-.03548	84	.14100	↓
11	.14100	↓	48	-.10646	↓	85	.18822	↓
12	.16537	↓	49	-.03552	↓	86	-.16549	.17733
13	.18822	↓	50	.03546	↓	87	-.10646	↓
14	-.18823	-.21292	51	.10635	↓	88	-.03552	↓
15	-.14104	↓	52	.16537	↓	89	.03546	↓
16	-.07004	↓	53	-.18823	.00000	90	.10635	↓
17	.00000	↓	54	-.14104	↓	91	.16537	↓
18	.07008	↓	55	-.07004	↓	92	-.18823	.21272
19	.14100	↓	56	.00000	↓	93	-.14104	↓
20	.18822	↓	57	.07008	↓	94	-.07004	↓
21	-.16549	-.17750	58	.14100	↓	95	.00000	↓
22	-.10646	↓	59	.18822	↓	96	.07008	↓
23	-.03552	↓	60	-.16549	.03544	97	.14100	↓
24	.03546	↓	61	-.10646	↓	98	.18822	↓
25	.10635	↓	62	-.03552	↓	99	-.18823	.24286
26	.16537	↓	63	.03546	↓	100	-.16549	↓
27	-.18823	-.14194	64	.10635	↓	101	-.14104	↓
28	-.14104	↓	65	.16537	↓	102	-.10646	↓
29	-.07004	↓	66	-.18823	.07092	103	-.07004	↓
30	.00000	↓	67	-.14104	↓	104	-.03552	↓
31	.07008	↓	68	-.07004	↓	105	.00000	↓
32	.14100	↓	69	.00000	↓	106	.03546	↓
33	.18822	↓	70	.07008	↓	107	.07008	↓
34	-.16549	-.10652	71	.14100	↓	108	.10635	↓
35	-.10646	↓	72	.18822	↓	109	.14100	↓
36	-.03552	↓	73	-.16549	.10644	110	.16537	↓
37	.03546	↓	74	-.10646	.10644	111	.18822	↓

TABLE 4. FLT. 2-B VIDICON RESEAU LOCATIONS, INCHES

3.1.1. Spectral Characteristics

Prior to MVM'73 calibration, the 12" light cannon was updated to transmit UV. Following disassembly and refurbishment during which the lamps were replaced and a plexiglass diffuser which transmits UV was added, the light cannon was recalibrated to establish a new "Snyder" curve and new flat-field light curves. The radiance distribution was measured across the exit diffuser at .5" intervals at 100 and 1000 Foot Lambert levels using a Gamma Model 700 Photometer (Figure 19). Calibration of the 12" light cannon was checked and updated prior to and following each series of calibrations.

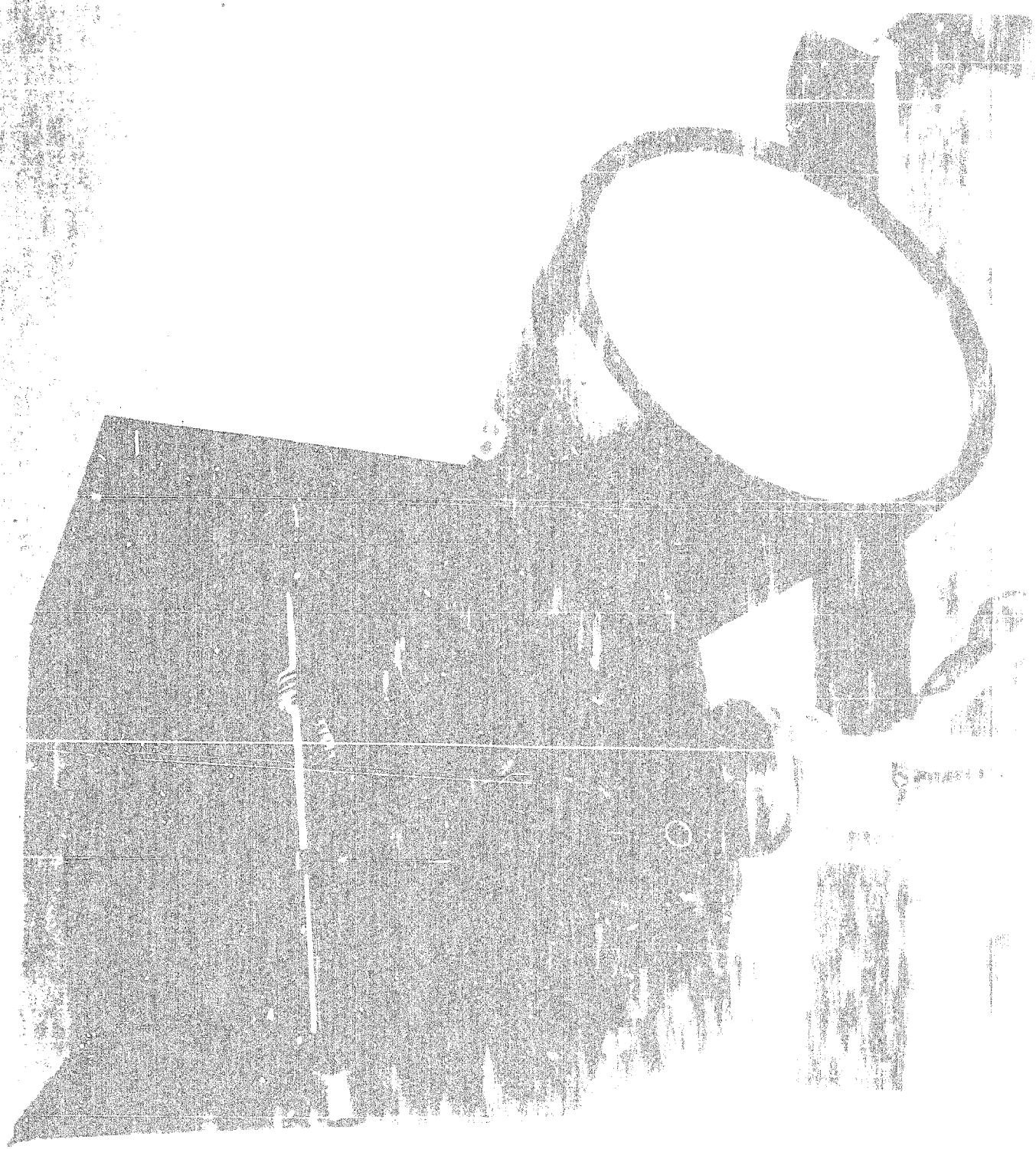
The secondary mirror in the MVM'73 catadioptric cassegrain telescope obscures the central 3.5" area of the 12" light cannon. Limiting aperture stops of 7" cut out the sharp fall-off near the edges. Thus the variation of significant radiance across the exit of the light cannon is only about $\pm 2\%$.

The bench calibrations were run with the diffuser of the light cannon approximately 20 mm from the front of each flight camera subsystem. As the hyperfocal distance of the telescope in these subsystems is 16 km, each point on the diffuser is out of focus on the vidicon. It was concluded that a uniform field of illumination was provided to each vidicon to an accuracy of less than 1%.

The spectral radiance characteristics of the 12-inch light cannon were determined using the JPL Spectroradiometer to compare light cannon output with that of a 200-watt quartz-iodine standard of spectral radiance. The relative spectral radiance of the 12-inch light cannon is shown in Figure 20. The color temperature is approximately 5000° K.

3.1.2. Determination of Source Radiance

A potential source of error, encountered in these calibrations, was that no adequate method was available to make absolute, in situ, measurements of the radiance of the light cannon diffuser plate during each radiometric test. For this reason, the method used during Mariner 9 TV Subsystem



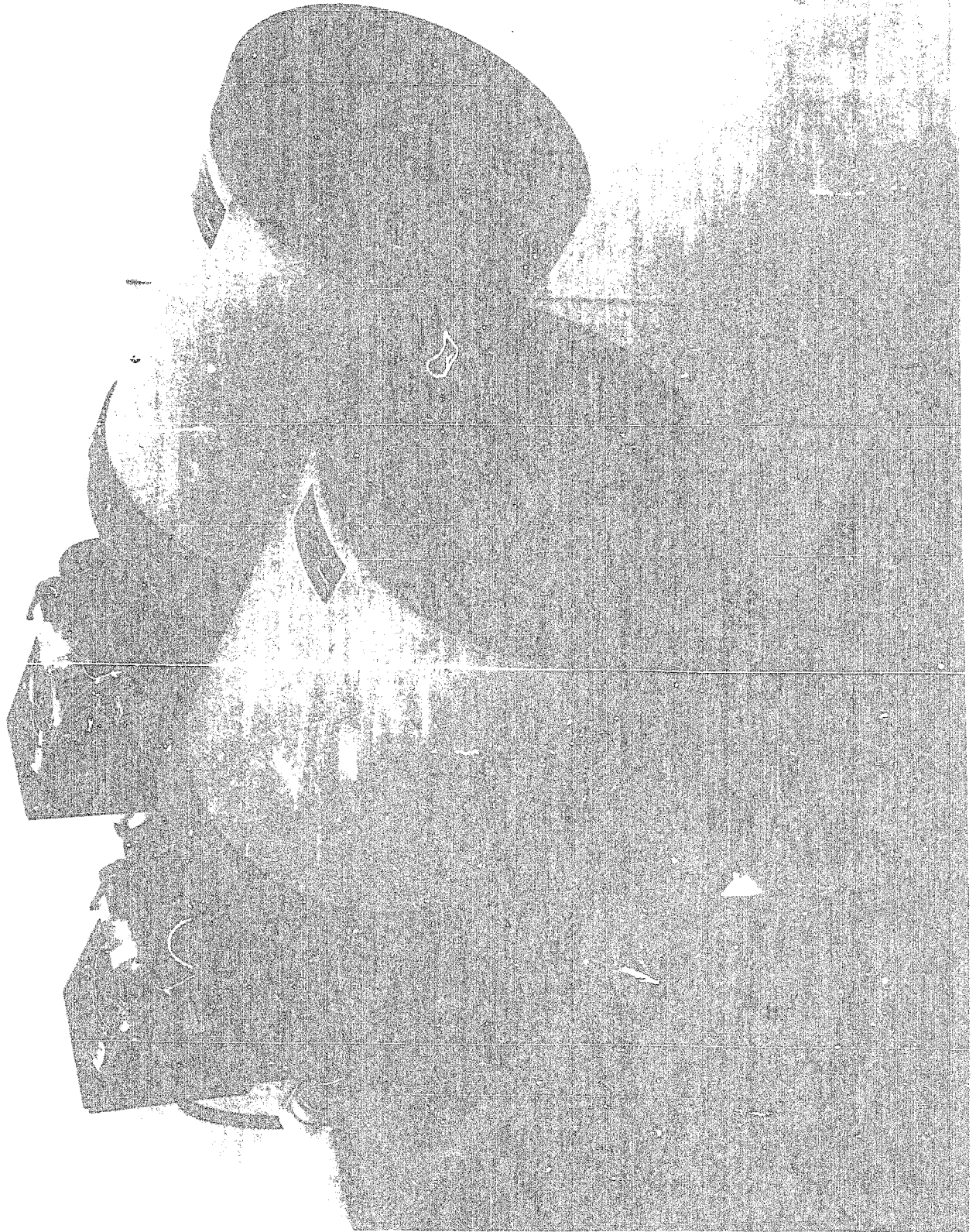


FIG. 18

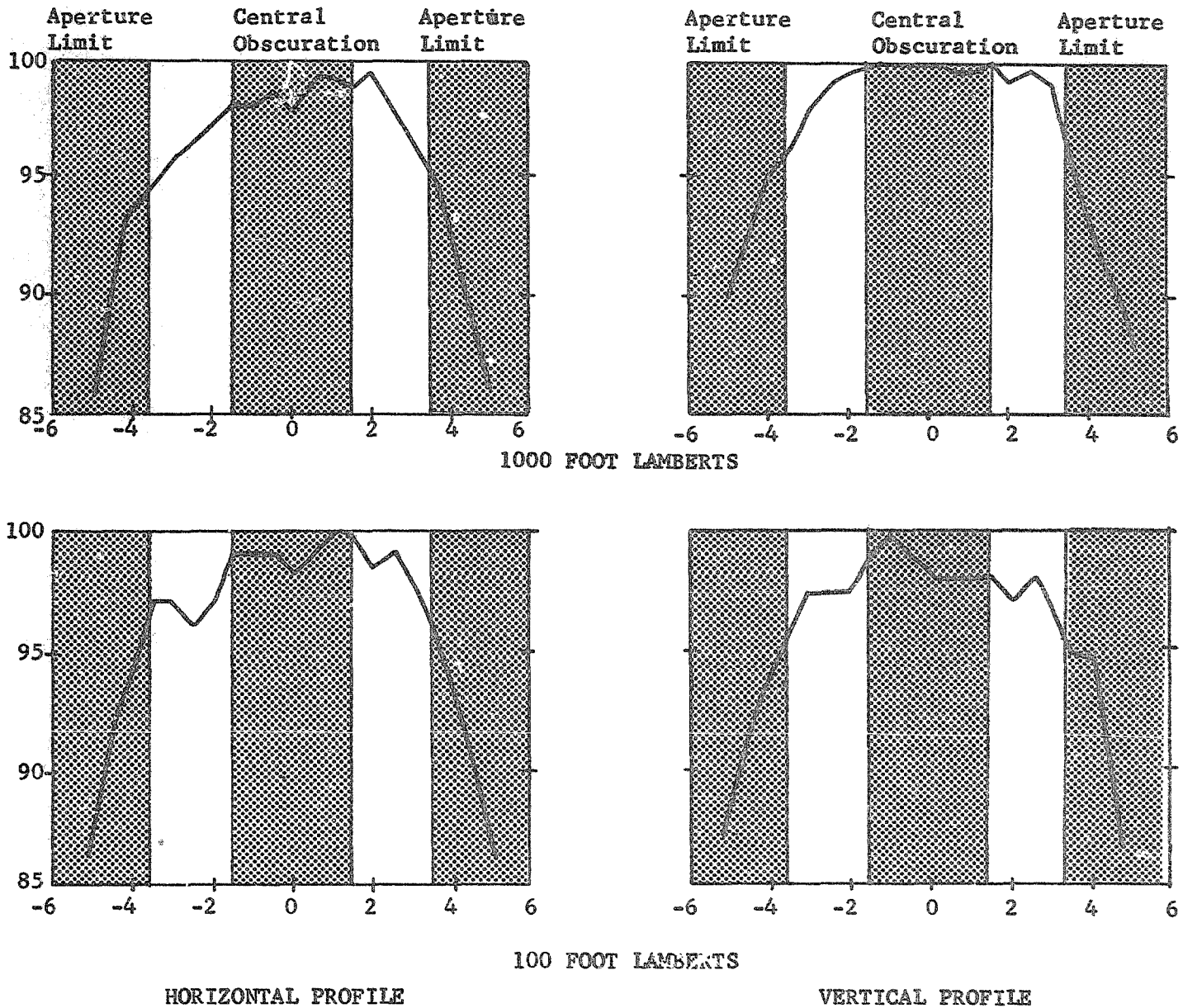


Fig. 19 FIELD FLATNESS OF THE 12 INCH LIGHT CANNON

43

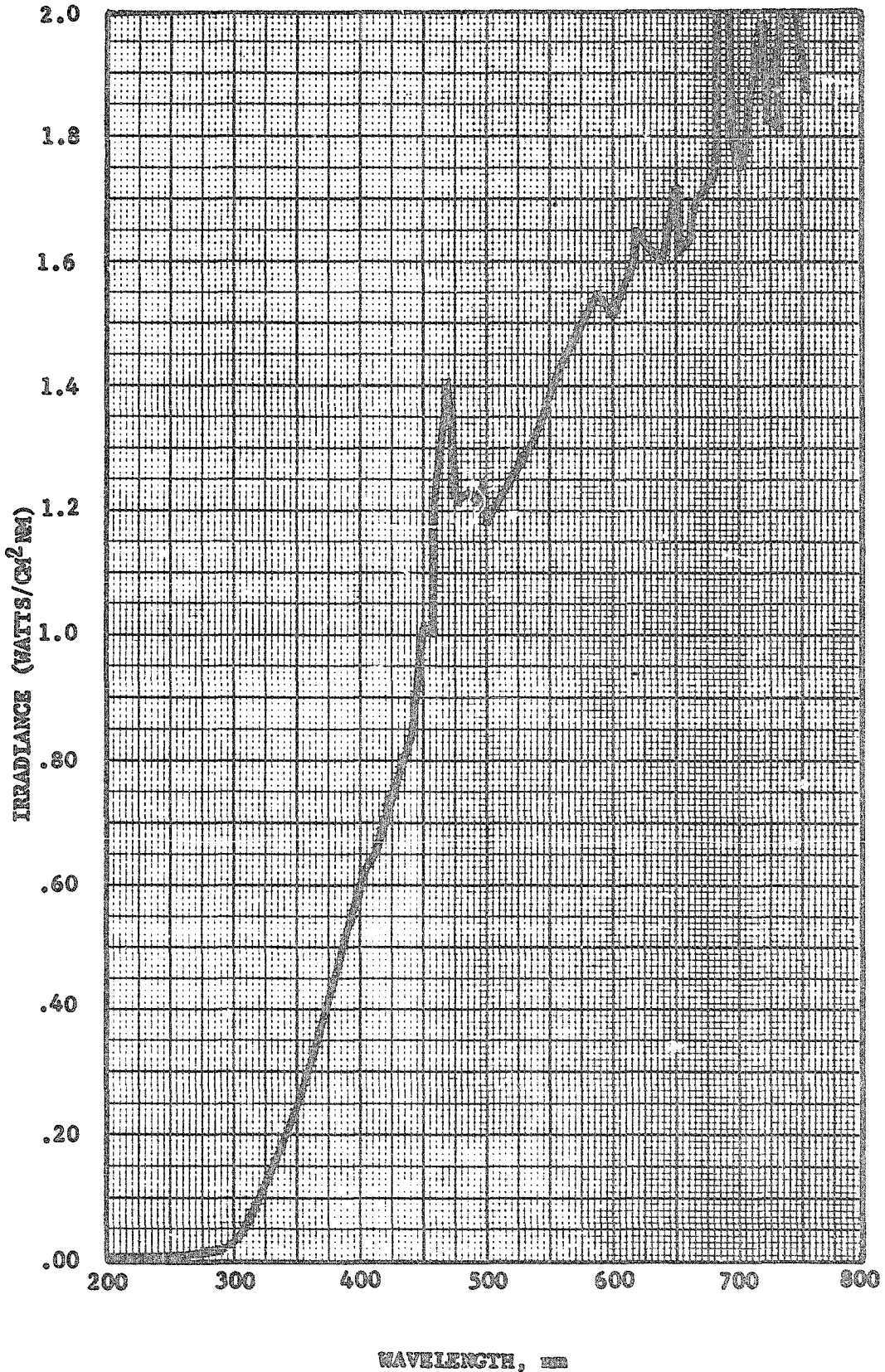


Fig. 20 RELATIVE SPECTRAL RESPONSE

12 INCH LIGHT CANNON

calibration (Reference 2, p. 41) was utilized for calibrating the Mariner 10 TV Subsystems. This technique provided relative measurements which could later be converted to absolute values. A Snyder curve of inverse transmittance for the 12-inch light cannon appears in Figure 21.

All source radiance readings were expressed in RFL's (Relative Foot Lamberts). A conversion factor was subsequently determined to yield absolute radiometric units.

3.1.3. Error Estimation

A brief assessment was made of possible sources of error in the radiance determinations of the calibration light sources. The following factors were taken into account:

- (1) The light cannon output tended to drift slightly over the duration of a radiometric test sequence.
- (2) Subsequent measurements determined that the luminance of JPL standard lamps varied between 98.5 and 102.5 foot Lamberts.
- (3) Backlash in the gear train between the light cannon iris and the Veeder root counter was estimated to introduce a possible error of ± 0.5 on the Veeder root scale.

Values for possible Δ RFL's were determined (Figure 22). At 100 relative foot Lamberts, a maximum absolute error in source radiance of $\pm 5.2\%$ was possible. At 4500 relative foot Lamberts, the maximum error in source radiance was $\pm 3.9\%$. Though not a rigorous error estimation, the values provided some quantitative assessment of the magnitude of source radiance errors introduced into the radiometric calibration.

3.2 RADIOMETRY

The MVM television cameras were put through exhaustive tests at the subsystem and spacecraft levels. The most important test involved

LIGHT
CANNON
FOR
CALIBRATION

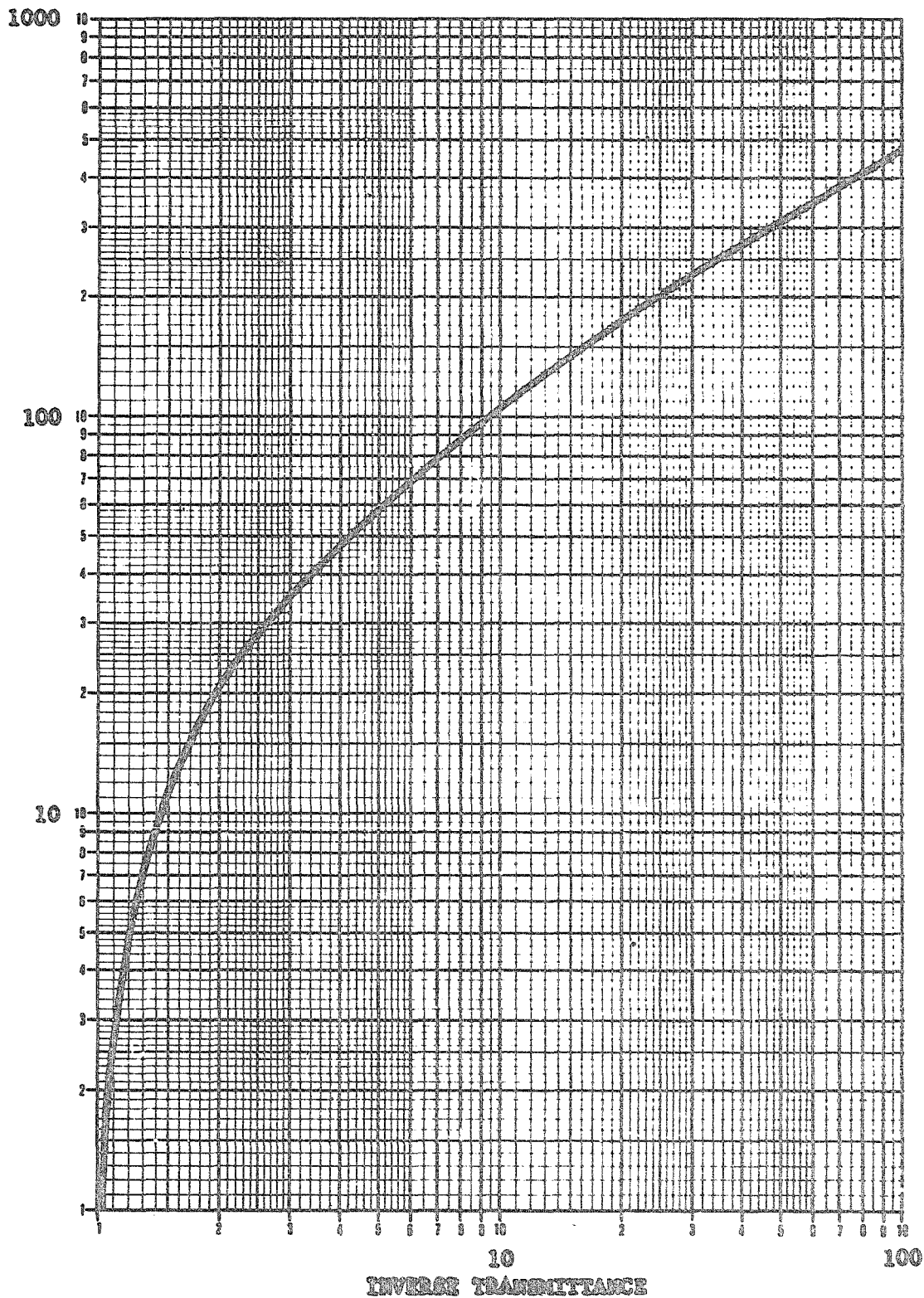


Fig. 21 TYPICAL IRIS CALIBRATION CURVE 12 INCH LIGHT CANNON

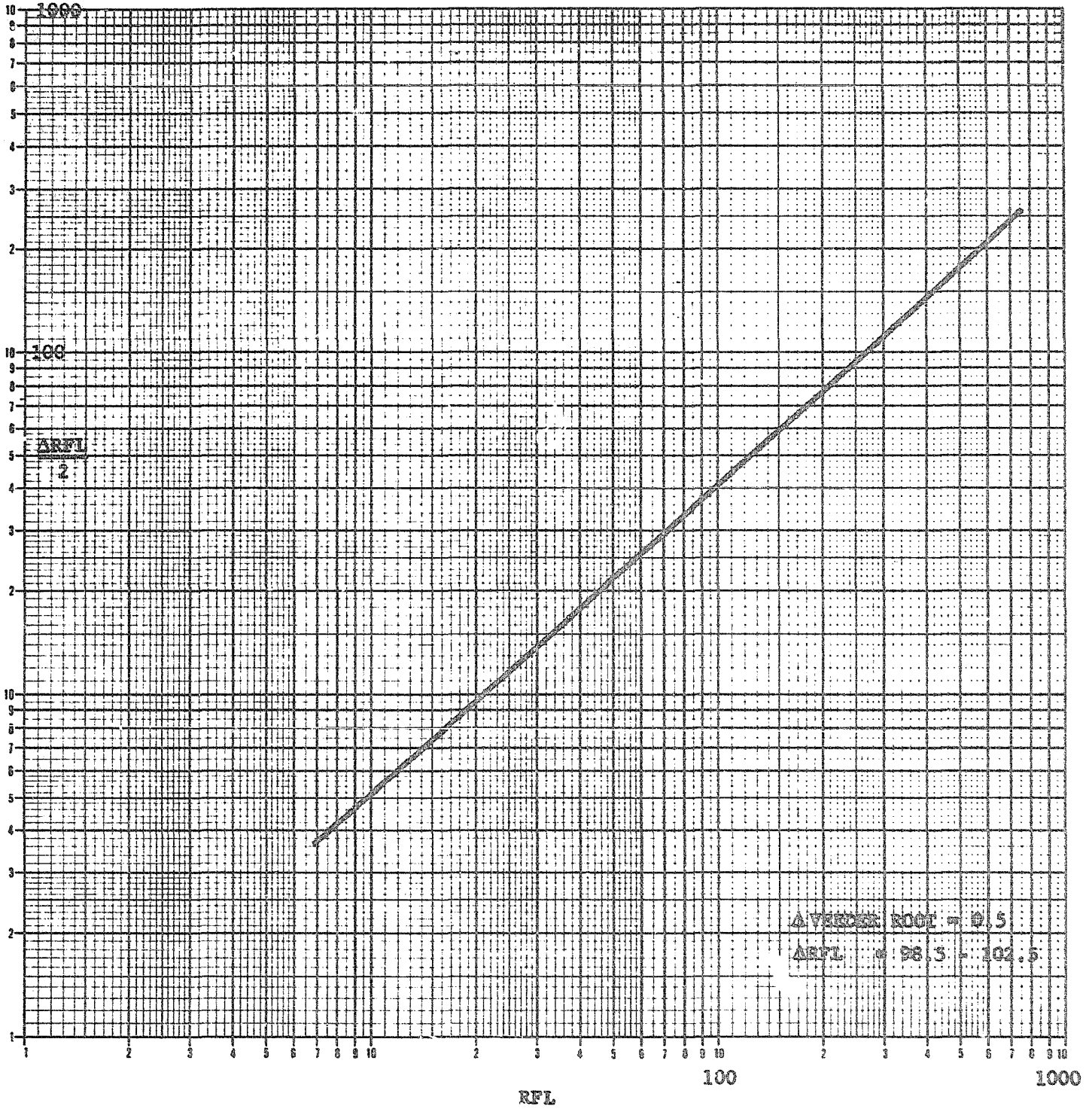


Fig.22 12 INCH LIGHT CANNON RADIANCE ERROR CURVE

taking a series of flat-field exposures using the calibrated 12-inch light cannon. These results were recorded digitally on magnetic tape during the test and used in the IPL to completely characterize each picture element on each flight vidicon.

3.2.1 Shutter Performance

3.2.1.1. Reciprocity

Reciprocity of a system requires that the response through the vidicons is a function only of energy incident on the vidicon and independent of exposure time. In order to prove or disprove the reciprocity factor, several series of light transfer tests were run, some with high illumination and short exposure times, others with low illumination and long exposure times (Figure 23). Since the initial results seemed to indicate that the systems were not reciprocal, another testing procedure was developed. Here the flat-field illumination and the exposure time were reciprocally adjusted, attempting to achieve the same average output DN over a range of exposure times. The results of these tests were plotted in terms of sensitivity $(\overline{DN} - \text{Dark Current})/\text{Exposure}$, which if the systems were reciprocal, would be independent of exposure time (Figures 24 - 25). Such was not the case for Flight 1-A, where major discrepancies seemed to occur at short exposure times. Some simple calculations showed that if exposure times were varied by about a millisecond, more reciprocal results could be obtained.

A further analysis of tests and results seemed to indicate that some other anomaly, such as shutter offset or incorrect estimate of exposure, was causing the discrepancy in the reciprocity curves.

3.2.1.2. Offset

A major factor in the calibration of radiometric response is the knowledge of the exact exposure time. As described in Section 2.3 due to the shutter assembly design, factors such as frictional forces caused a

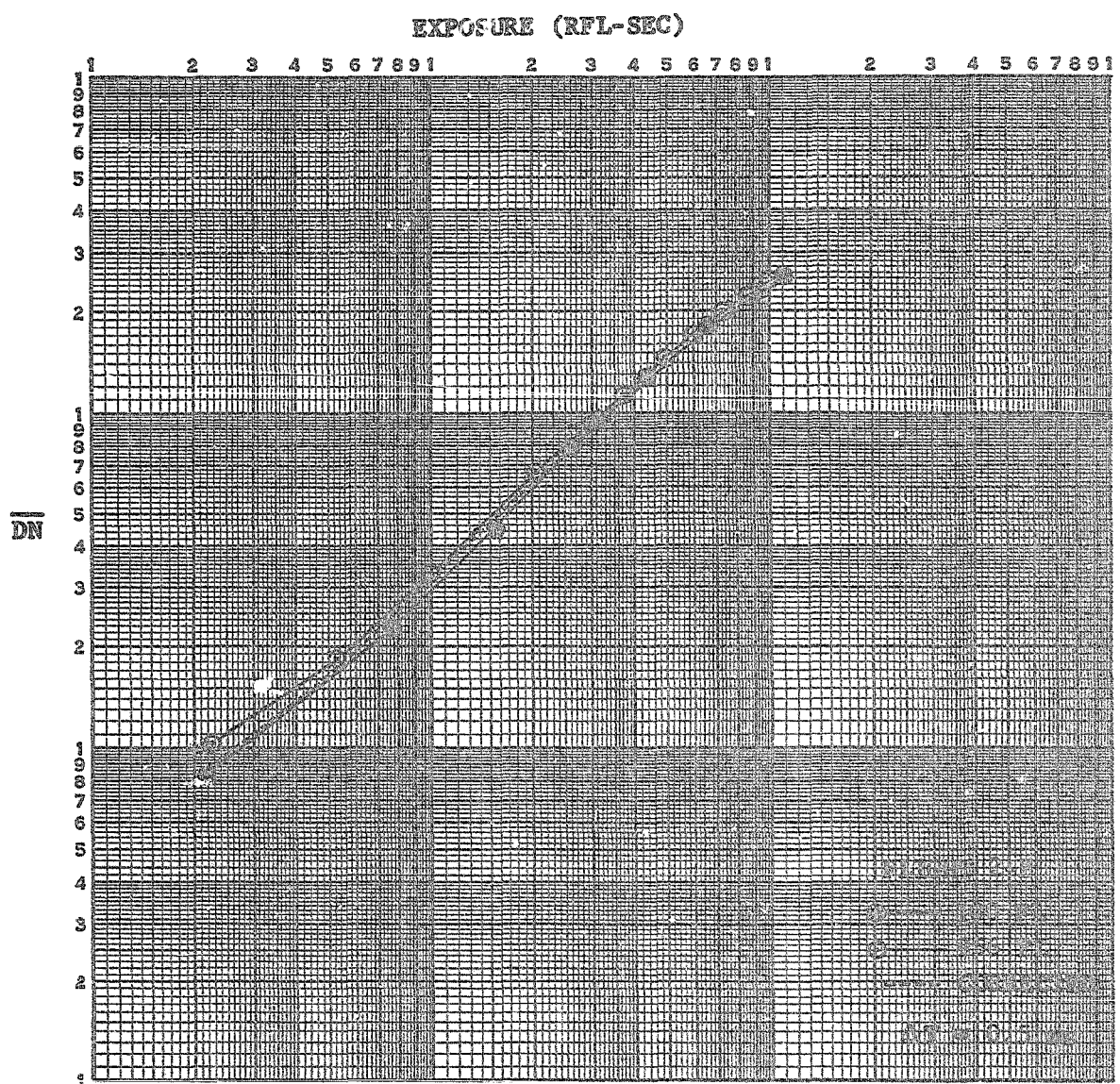
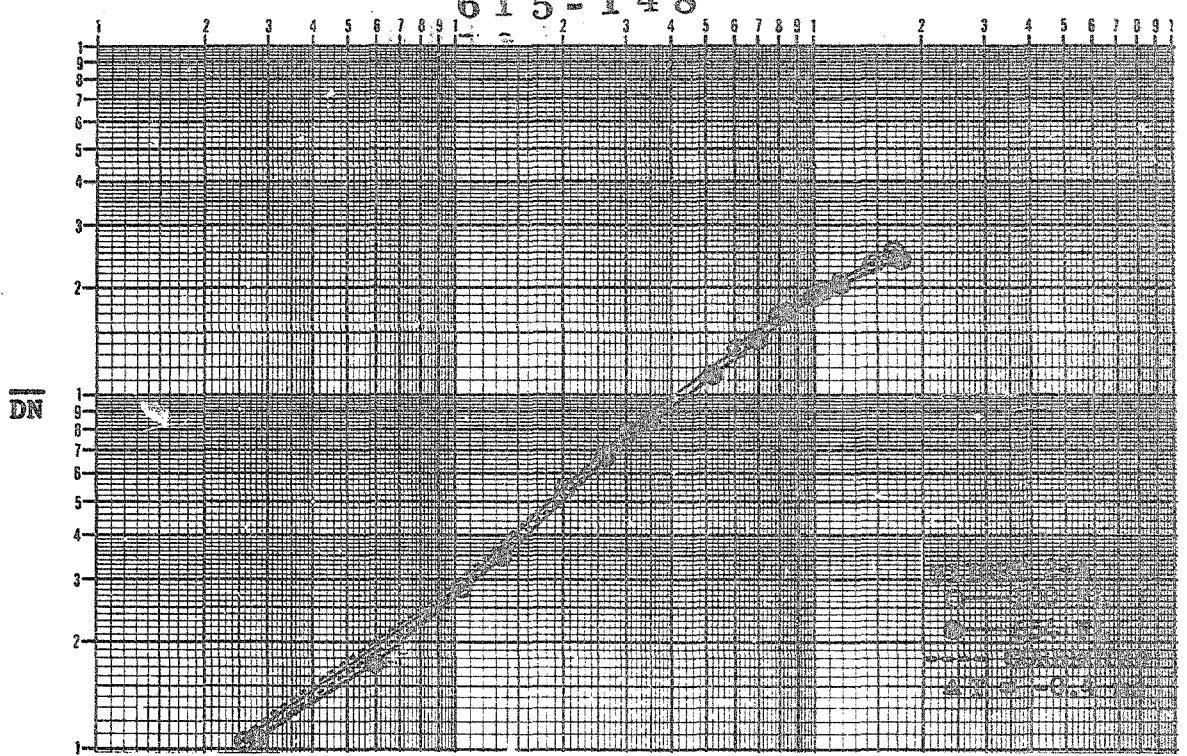


Fig. 23 LIGHT TRANSFER CURVES, LOW AND HIGH LEVEL LIGHT

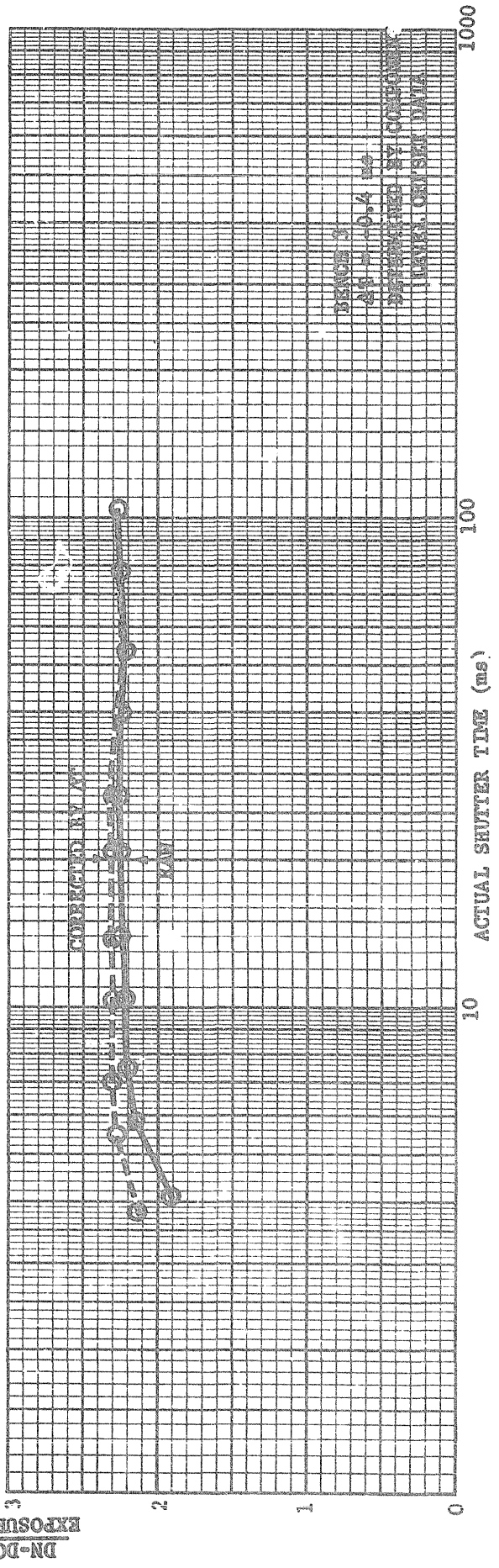
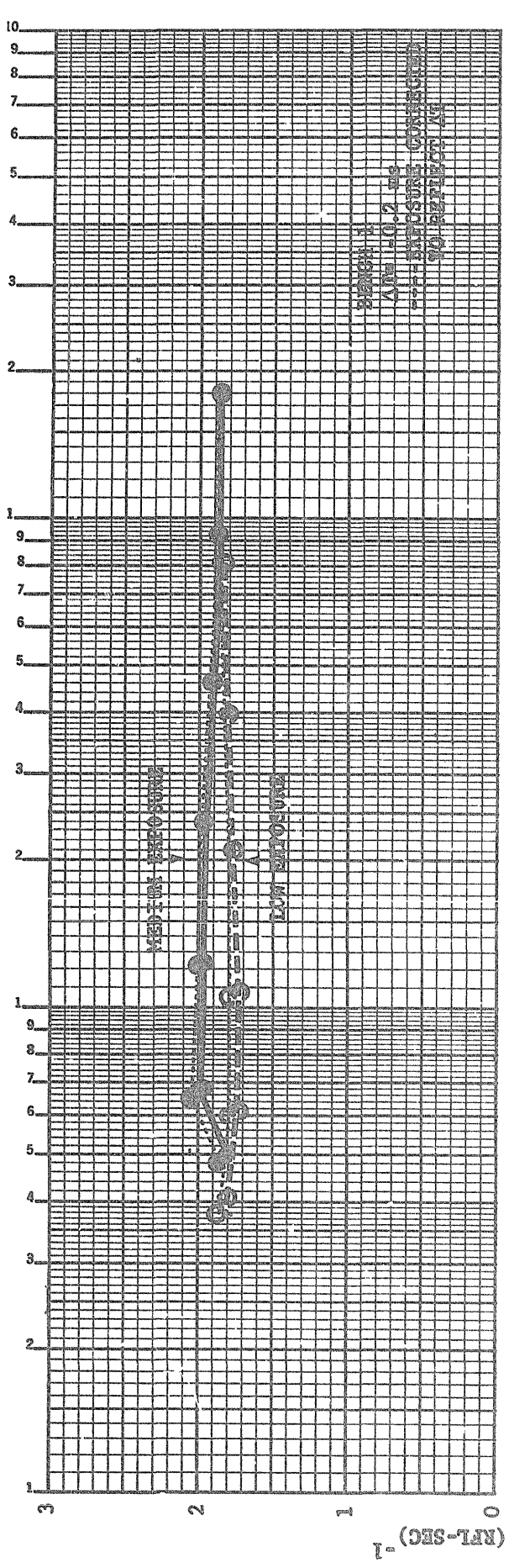


Fig. 24 RECIPROCITY, FLIGHT 2-A

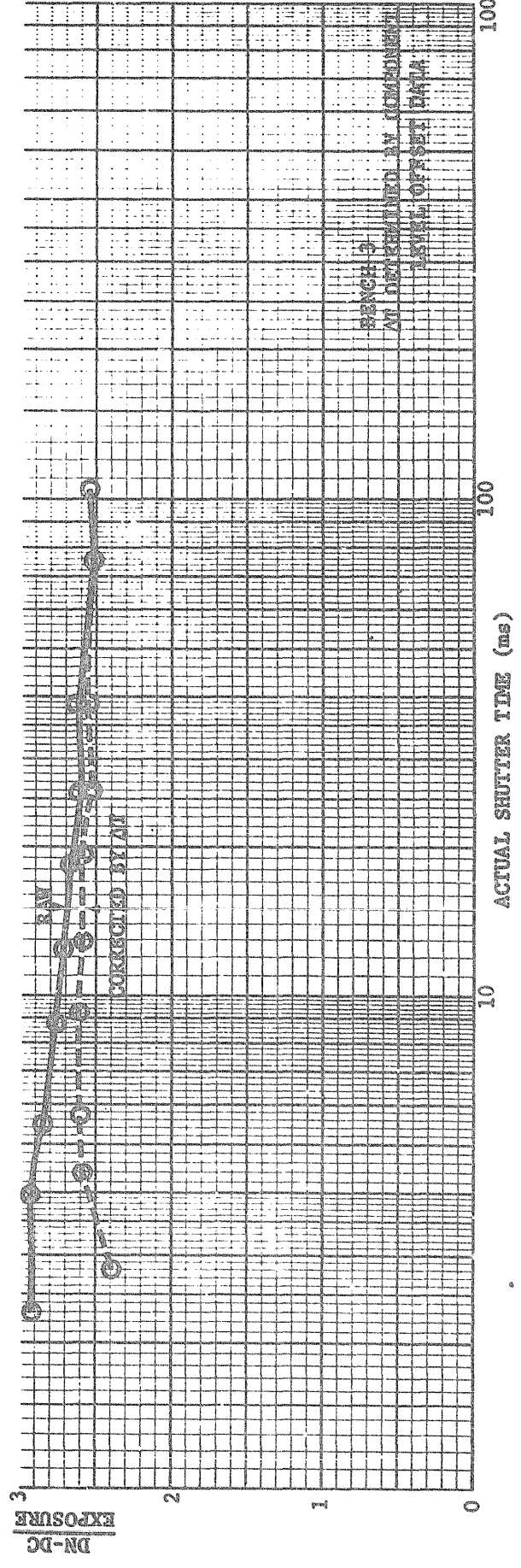
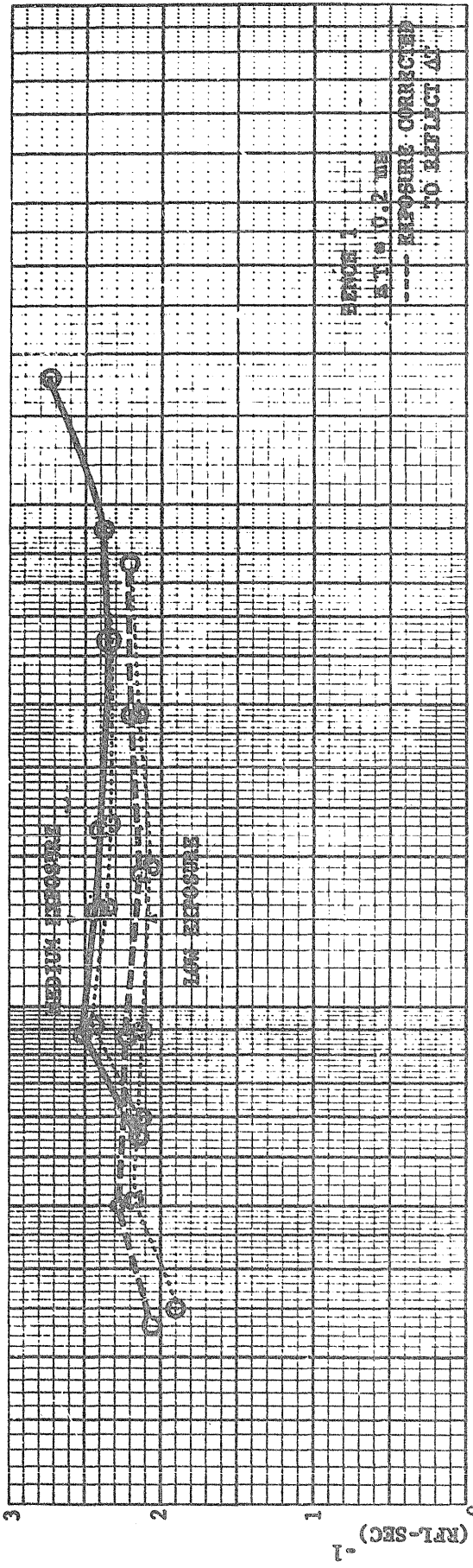


FIG. 25 RECIPROCALITY, FLIGHT 2-B

difference between the commanded and the actual exposure times. These "shutter offsets" for both flight systems were measured during component calibration (Table 5).

At the subsystem level of calibration, discrepancies in the light transfer curves indicated that these values of shutter offset might be incorrect. In order to assess whether incorrect exposure times caused these discrepancies, light transfer data were recalculated and replotted assuming a slightly different shutter offset for each system (dashed lines Figures 24 - 25). The results indicated that the assumed shutter offset values yielded more consistent results and that shutter offset errors might indeed be the source of the discrepancies.

Since the discrepancies in reciprocity and light transfer data were never satisfactorily resolved it is strongly suggested that actual exposures be carefully measured at the subsystem level in the future to eliminate exposure time as a possible source of error.

3.2.2. Light Leak

Light leak is defined as light reaching the vidicon when the shutter is inhibited. Tests for both on-axis and off-axis light leaks were performed using the procedures described schematically in Figure 26. The procedure can be divided into four basic steps:

- (1) All lights are out, camera is completely covered, shutter is inhibited, automatic light flooding is on and so is the beam. These conditions result in gradual erasure of the video signal until dark current is recorded in Frame 11.
- (2) During Frame 12, both the beam and light flooding are inhibited causing the dark current to build up. During Frame 22 the beam and light flooding are activated and the dark current buildup is recorded in Frame 23.

TVS	SHUTTER S/N	ORIGINAL OFFSET	CORRELATION	CORRECTED OFFSET
1A	007	1.370 msec	- 1.2 msec	0.170 msec
1B	006	2.364 msec	+ 0.5 msec	2.864 msec
2A	011	0.716 msec	- 0.4 msec	0.316 msec
2B	008	2.560 msec	+ 0.5 msec	3.060 msec

TABLE 5. SHUTTER OFFSET CORRECTION BASED ON

BENCH 3 TESTS

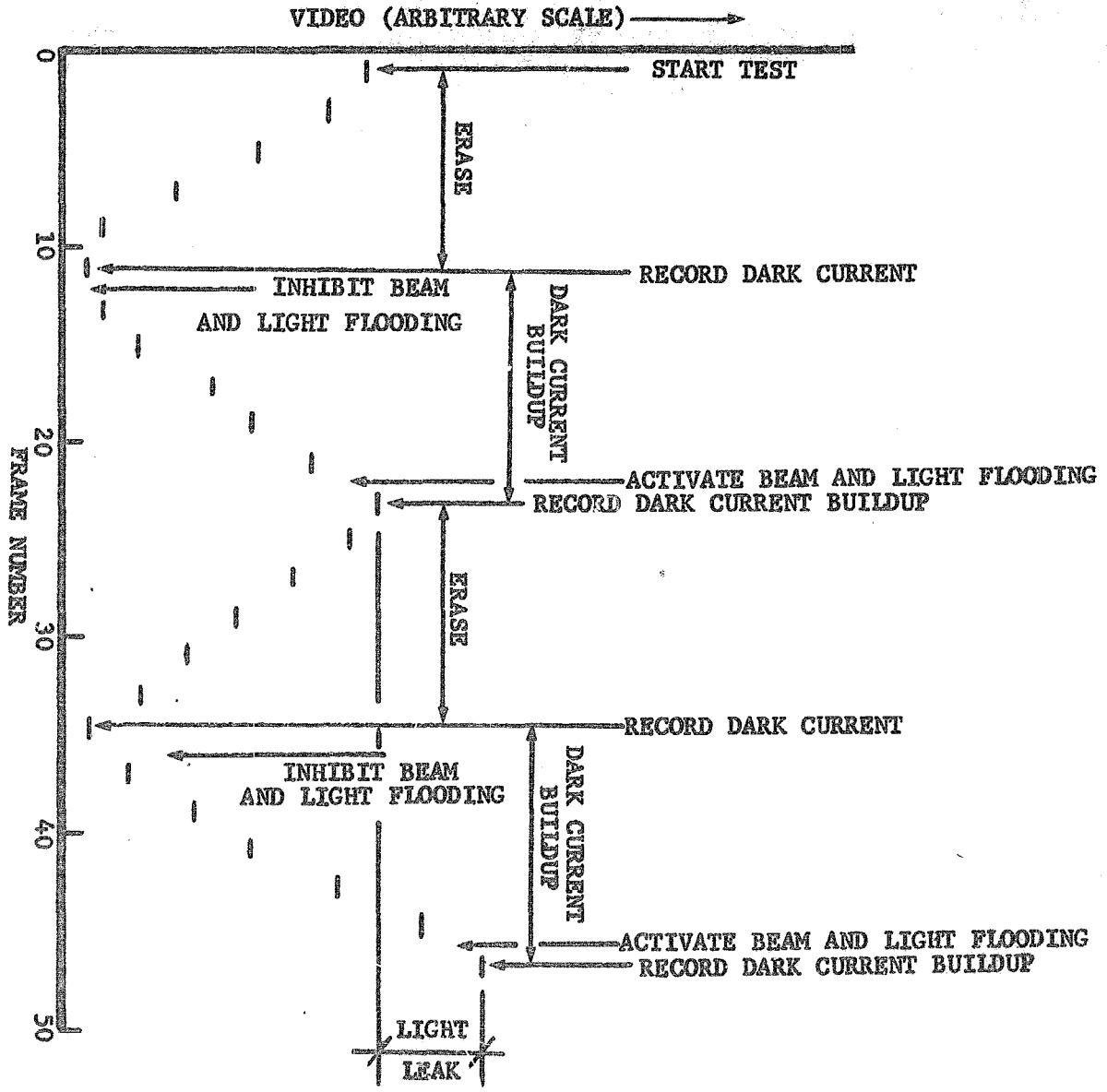


FIG. 26 LIGHT LEAK CALIBRATION PROCEDURE

FRAMES 1 THROUGH 35, LIGHT OFF, CAMERA COVERED
FRAMES 37 THROUGH 47, LIGHT ON, CAMERA UNCOVERED

- (3) Step No. 1 is repeated and the resulting dark current is recorded in Frame 35.
- (4) Step No. 2 is repeated at the same time the light source is turned on to maximum intensity during Frame 36. The final dark current buildup is recorded in Frame 47 and the test is terminated. Any difference between video outputs of Frames 23 and 47 is caused by light leaks in the system.

The on-axis light leak was calibrated with a 12-inch light cannon placed in front of the NAO camera while the off-axis determination was based upon multiple 150 W floodlights mounted on both sides of the camera head at right angles to the optical axis. In either case, the filter wheel was in Position 5 (clear).

Each of the four cameras was tested at least twice on both axial modes, and the light leak never exceeded 0.5 DN/frame cycle (Table 6).

3.2.3. Residual Image and Hysteresis

Residual image is the phenomena which occurs as the result of failure of the erase cycle to completely neutralize the charge on the photo-cathode. Residue from the preceding image is then visible in the succeeding image.

In the case of light transfer sequences, residual image is evidenced by hysteresis between the response to light transfer sequences at increasing exposure levels and those made at decreasing exposure levels. As this was a problem on the MM '71 system, procedures were devised to detect the influence of residual image (Figure 27).

The test consisted of 25 cycles that were arranged in a 5 x 5 matrix according to flat-field and reference target exposure times. Each cycle was performed in seven steps:

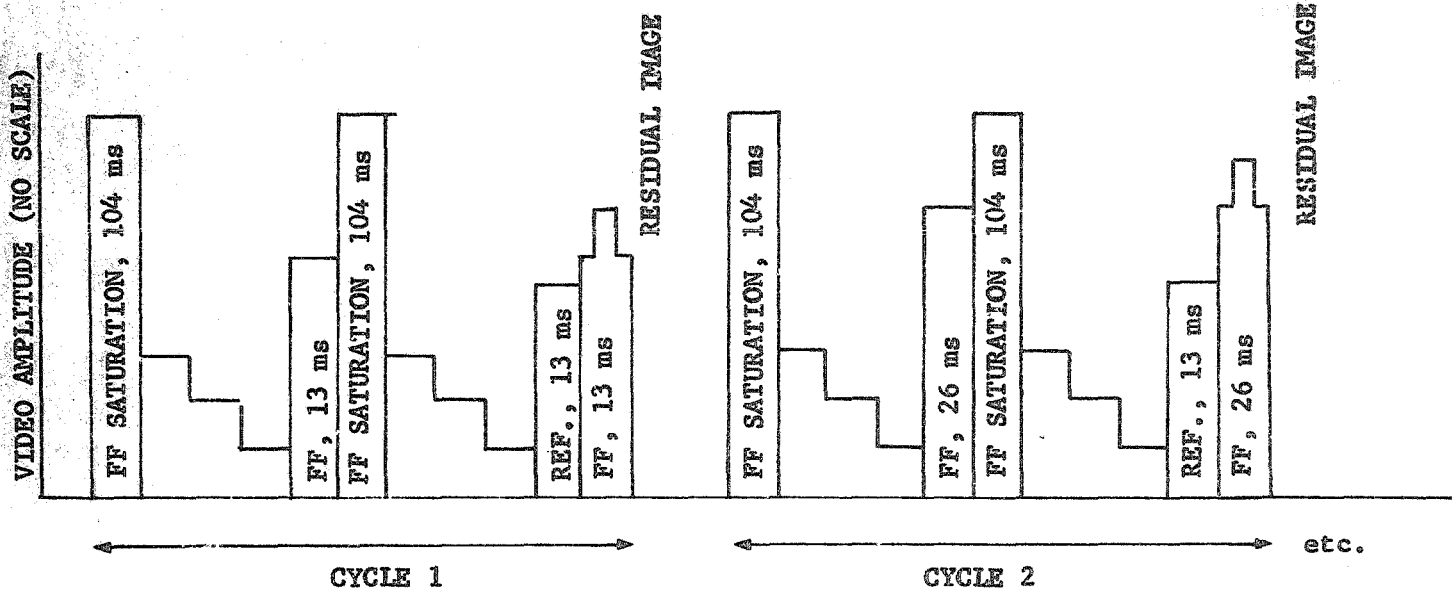
FRAME NO.	SHUTTER	EXPOSURE	BEAM	LIGHT FLOOD	RECORD	MEAN DN	SIGMA
<u>OFF AXIS A CAMERA</u>							
1001-9	Inhibit	Camera Covered - No Illumination	On	On	No		
1011	Inhibit	↓	On	On	Yes	6.42	2.80
1013-21	Inhibit		Off	Off	No		
1023	Inhibit		On	On	Yes	56.18	10.66
1025-33	Inhibit		On	On	No		
1035	Inhibit	↓	On	On	Yes	6.48	2.83
1037-45	Inhibit	Camera Uncovered 150 W Light	Off	Off	No		
1047	Inhibit	Camera Covered - No Illumination	On	On	Yes	58.02	10.97
<u>OFF AXIS B CAMERA</u>							
2001-9	Inhibit	Camera Covered - No Illumination	On	On	No		
2011	Inhibit	↓	On	On	Yes	5.65	3.48
2013-21	Inhibit		Off	Off	No		
2023	Inhibit		On	On	Yes	74.26	15.69
2025-33	Inhibit		On	On	No		
2035	Inhibit	↓	On	On	Yes	5.75	3.52
2037-45	Inhibit	Camera Uncovered 150 W Light	Off	Off	No		
2047	Inhibit	Camera Covered - No Illumination	On	On	Yes	77.48	16.21

TABLE 6. SUMMARY OF LIGHT LEAK TESTS, FLIGHT 2 BENCH 2

FRAME NO.	SHUTTER	EXPOSURE	BEAM	LIGHT FLOOD	RECORD	MEAN DN	SIGMA
ON AXIS							
B CAMERA - BENCH 2 - TEST 33 2/7/73							
3001-9	Inhibit	Camera Covered - No Illumination	On	On	No		
3011	Inhibit	↓	On	On	Yes	6.01	3.66
3013-21	Inhibit		Off	Off	No		
3023	Inhibit		On	On	Yes	74.48	15.73
3025-33	Inhibit		On	On	No		
3035	Inhibit		On	On	Yes	6.00	3.65
3037-45	Inhibit	Camera Uncovered - 150 W Light	Off	Off	No		
3047	Inhibit	Camera Covered - No Illumination	On	On	Yes	76.77	18.16

AXIS	CAMERA	$DN_{Exposed} - DN_{Covered}$	
Off	A	1.78 DN	(~ 0.3 DN/Frame Cycle)
Off	B	3.12 DN	(~ 0.5 DN/Frame Cycle)
On	A	1.90 DN	(~ 0.3 DN/Frame Cycle)
On	B	2.30 DN	(~ 0.4 DN/Frame Cycle)

TABLE 6. (CONT.) SUMMARY OF LIGHT LEAK TESTS



FLAT FIELD LIGHT EXPOSURE, ms

REFERENCE TARGET EXPOSURE, ms		13	26	52	78	104
	13	CYCLE 1	2	3	4	CYCLE 5
	26	6	7	8	9	10
	52	11	12	CYCLE 13	14	15
	78	16	17	18	19	20
	104	CYCLE 21	22	23	24	CYCLE 25

Fig. 27 RESIDUAL IMAGE TEST CYCLES

- (1) Almost saturated flat-field frame at 104 μ sec.
- (2) Erasure by using three inhibited shutter frames.
- (3) Flat-field frame at selected exposure time X.
- (4) Same as Step 1.
- (5) Same as Step 2.
- (6) Reference target frame at selected exposure time Y.
- (7) Same as Step 3.

Any difference in video output amplitude between Step 3 and 7 was due to the residual image influence of the reference target taken in Step 6. As can be seen, the 5 x 5 matrix was designed in such a way that the entire DN range of the television subsystem was covered. However, the MVM '73 cameras were equipped with an automatic light system to flood the vidicon after each exposure. Therefore, as no significant residual image build-up was expected, only cycles No. 1, 5, 13, 21, and 25 were performed.

The obtained results (Figures 28 - 29) (Tables 7 - 8) confirmed the favorable conclusion based on hysteresis calibration. Both Flight 1 and Flight 2 cameras were tested for residual image influence and in all of these cases, it was found to be below 1 DN. It can, thus, be said that automatic light flooding is indeed an effective tool for residual image elimination.

3.2.4. Vidicon Shading

Vidicon shading for filters other than clear was recorded in line plots taken along the vertical (SS = 450), horizontal (SL = 350), and both diagonals through the frames in the "2-point" L/T sequences. The mean DN, refers to that along the line plot.

For clear filter positions "3-D" plots were produced showing in greater detail the shading surface. Frames selected had reseaus removed and were

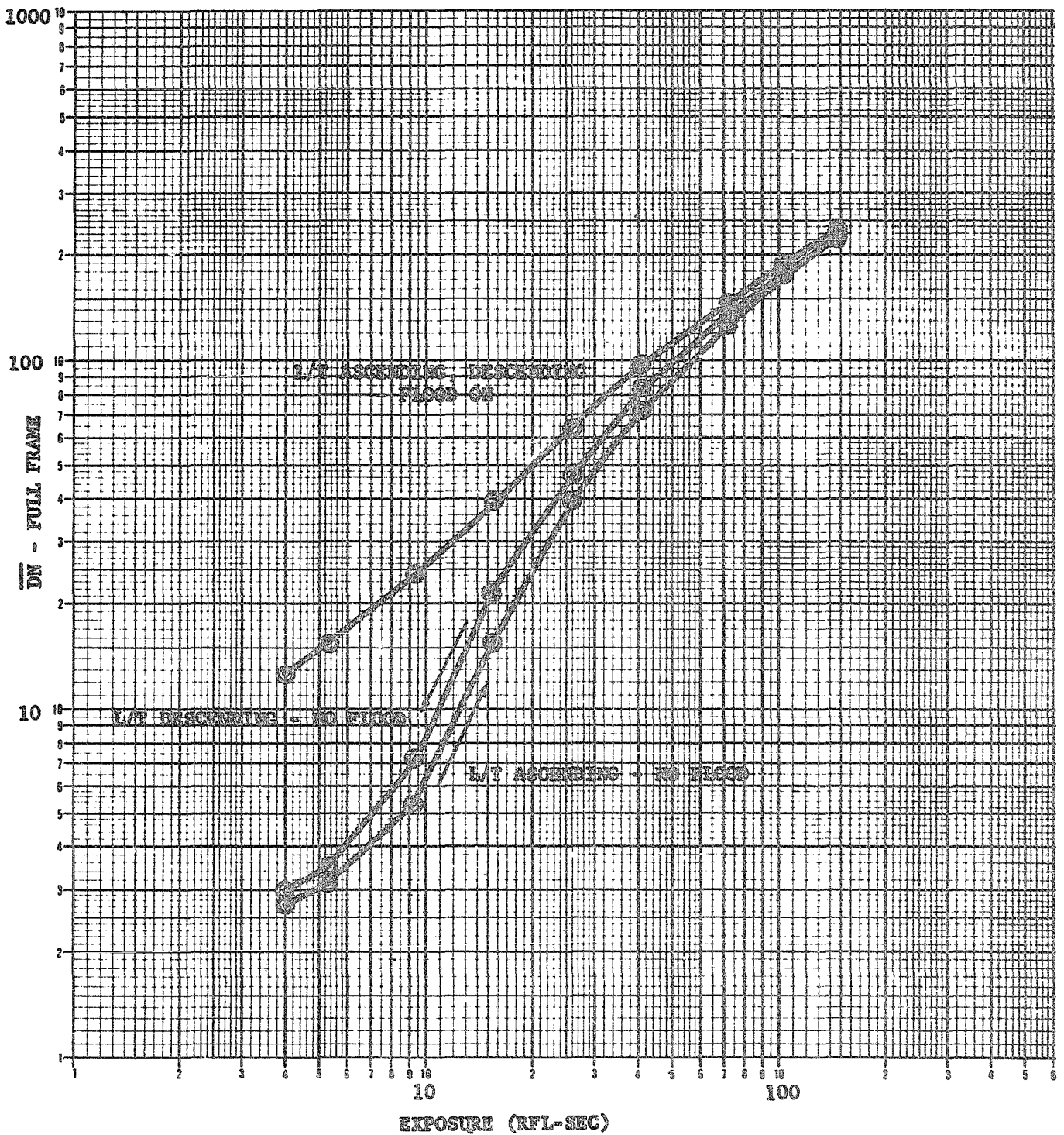


Fig. 28 HYSTERESIS ANALYSIS - FLIGHT 2-A BENCH 2

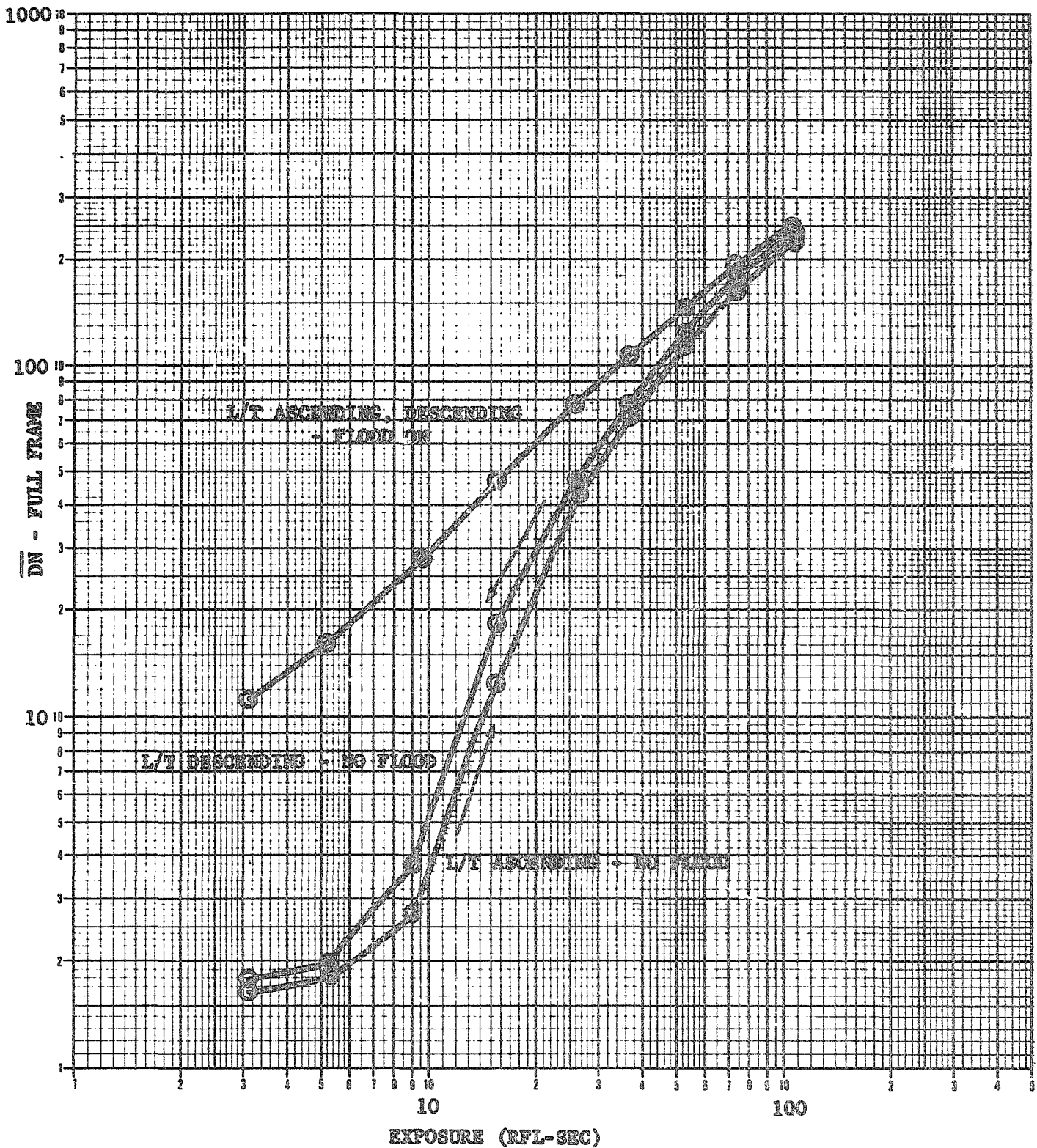


Fig. 29 HYSTERESIS ANALYSIS - FLIGHT 2-B BENCH

C
A
M
E
R
A
A

EXPOSURE	FLOOD Δ DN	NO FLOOD Δ DN
4.0099	0.1074	0.1807
5.3161	0.1084	0.4097
9.2344	0.1358	2.1422
15.7653	0.1254	5.1011
26.2143	0.2094	7.5067
41.8873	0.1163	8.2206
73.2343	0.0807	8.1892
104.5783	0.1084	6.4684
146.3783	0.1773	3.3245

C
A
M
E
R
A
B

3.1725	0.1330	0.0459
5.1317	0.0597	0.1600
9.0500	0.0952	1.1065
15.5809	0.1686	6.1506
26.0299	0.1857	7.9641
36.4779	0.1851	9.4069
52.1519	0.5485	11.0945
73.0499	0.1148	12.1072
104.3939	0.0346	7.1382

TABLE 7. HYSTERESIS ANALYSIS, FLIGHT 2

RESOLUTION TARGET

RELATIVE EXPOSURE

F
L
A
T
M
E
F
A
I
N
E
L
D
N

I
M
A
G
E

	X	4X	8X
41	Residual < 1 DN		Residual = 1 DN
144		Residual ≤ 1 DN	
240	Residual ≤ 1 DN		Residual ≤ 1 DN

FLIGHT 1-B, BENCH 1

	X	4X	8X
39	Residual < 1 DN		Residual = 1 DN
149		Residual ≤ 1 DN	
237	Residual ≤ 1 DN		Residual ≤ 1 DN

FLIGHT 1-B, BENCH 1

TABLE 8. RESIDUAL IMAGE

sampled at every 12th line and 12th sample. The data were projected onto a plane generated in the computer at DN = 0 and rotated so that line 1 - sample 1 was displayed at top center with the line direction diagonal to the right (Figures 30 - 31). Using the calibration results, an interpolated relationship between input brightness and output DN for each pixel can be generated and used to restore accuracy to flight data.

3.2.5. Filter Response

3.2.5.1. Bench Test Light Transfer

During Bench 1 and Bench 2, full (9 exposure level) flat-field light transfer sequences were obtained for all filter positions on the four flight subsystems. At Bench three, where test conditions most nearly represented the flight conditions, 9 exposure sequences were taken only in the Clear and Orange filter positions. Low and medium exposure levels (two point) were taken for minus UV, UV, Blue, and UV Polarizer filters. These sequences have been plotted together in Figure 32.

Sequences to test the Fabry lens for in-flight radiometric calibrations differed from the other filters in that the measurements of light transfer had to be made at two aperture openings (Figure 33). In determining light transfer curves for the WAO assembly, a sample region centered over the brightest portion of the field of view was selected. A Farrand 35^o collimator was used as physical constraints made the use of the 12" light cannon impossible. The resultant plot appears in Figure 34.

3.2.5.2. Relative Filter Factors

A set of relative filter factors was established for each flight vidicon system (Table 9). These were determined, at a particular DN output, by taking the ratio of the exposure through each filter to that of the clear filter.

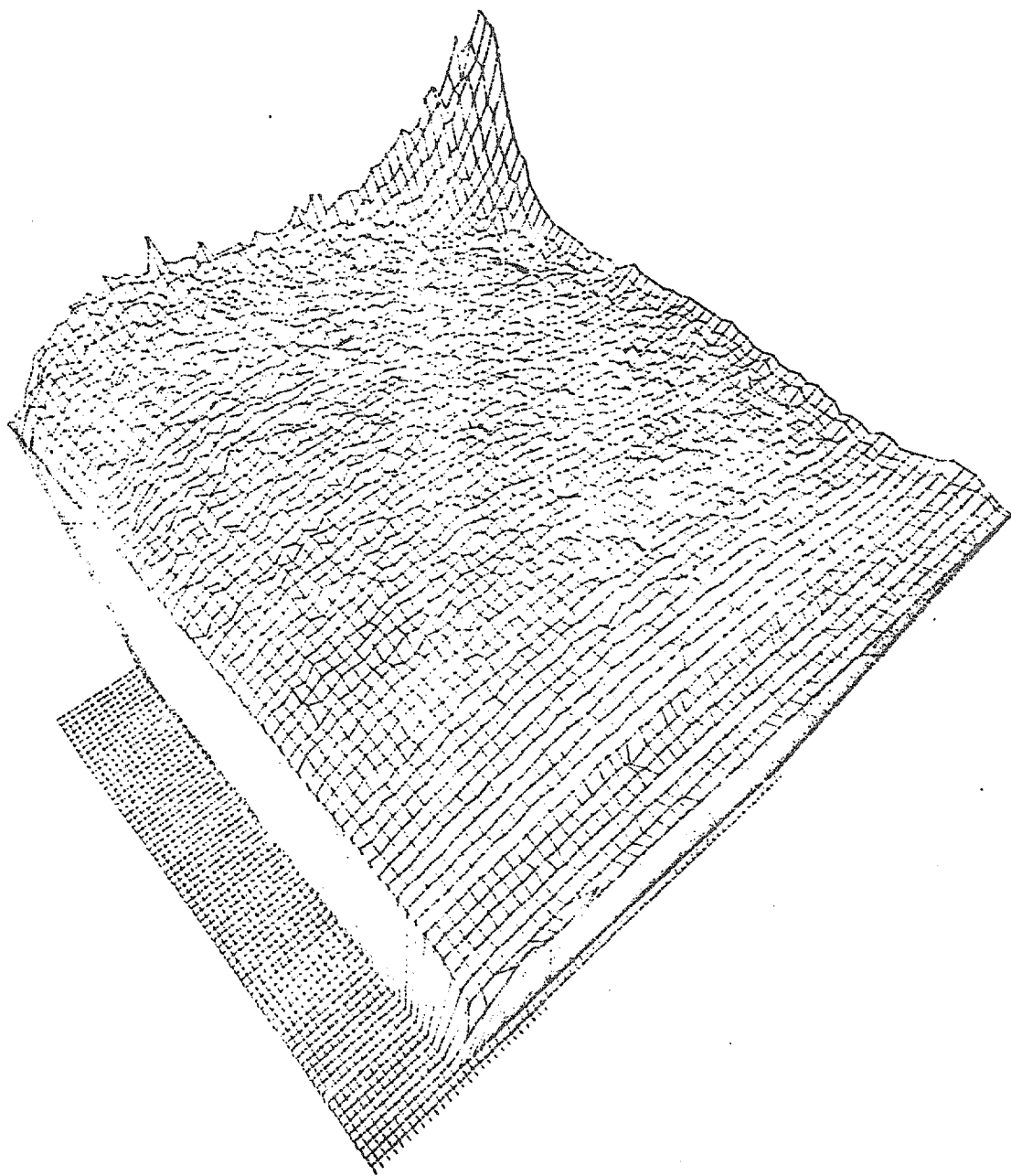


Fig. 30 VIDICON SHADING - FLIGHT 2-A

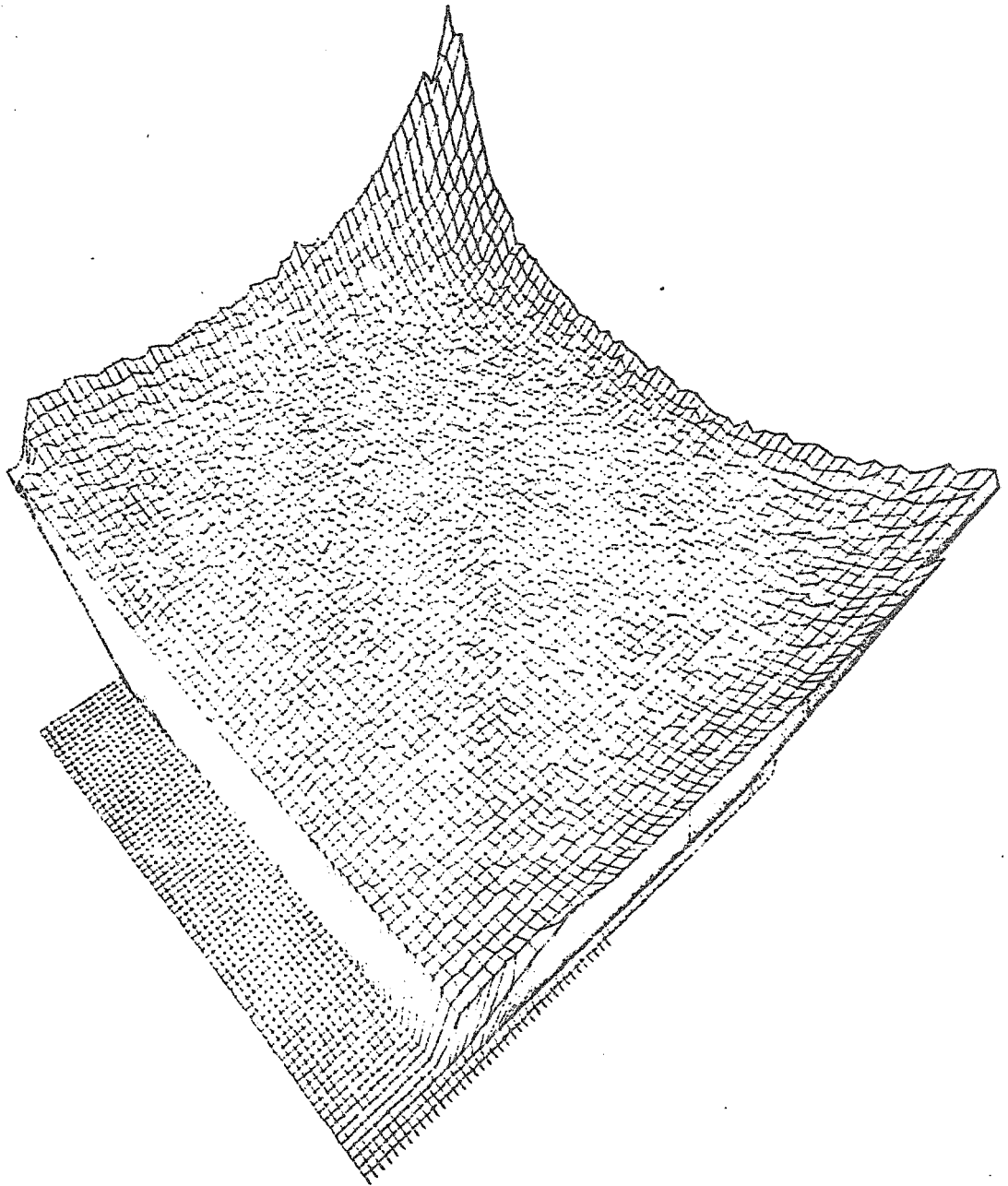


Fig. 31 VIDICON SHADING - FLIGHT 2-B

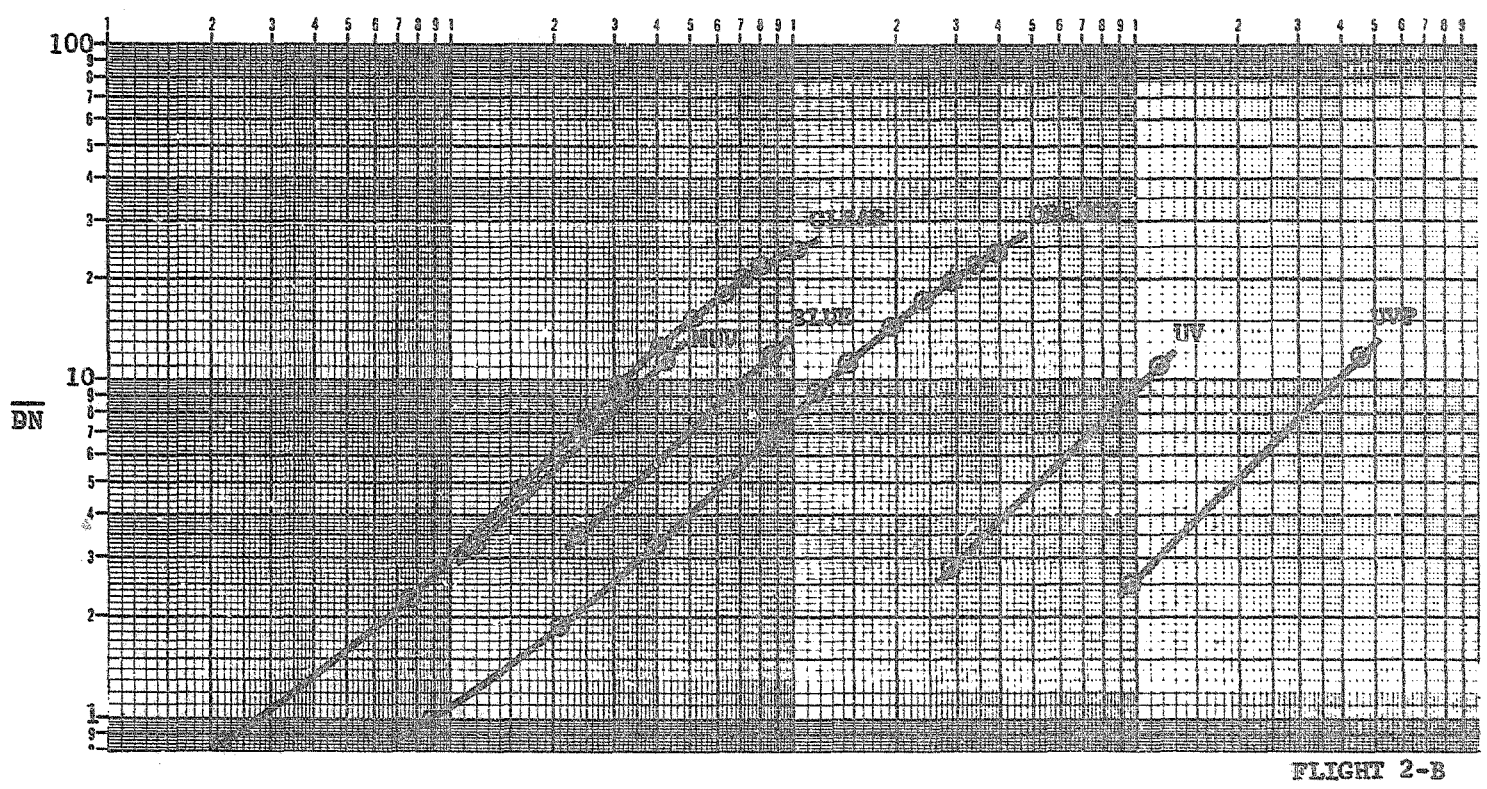
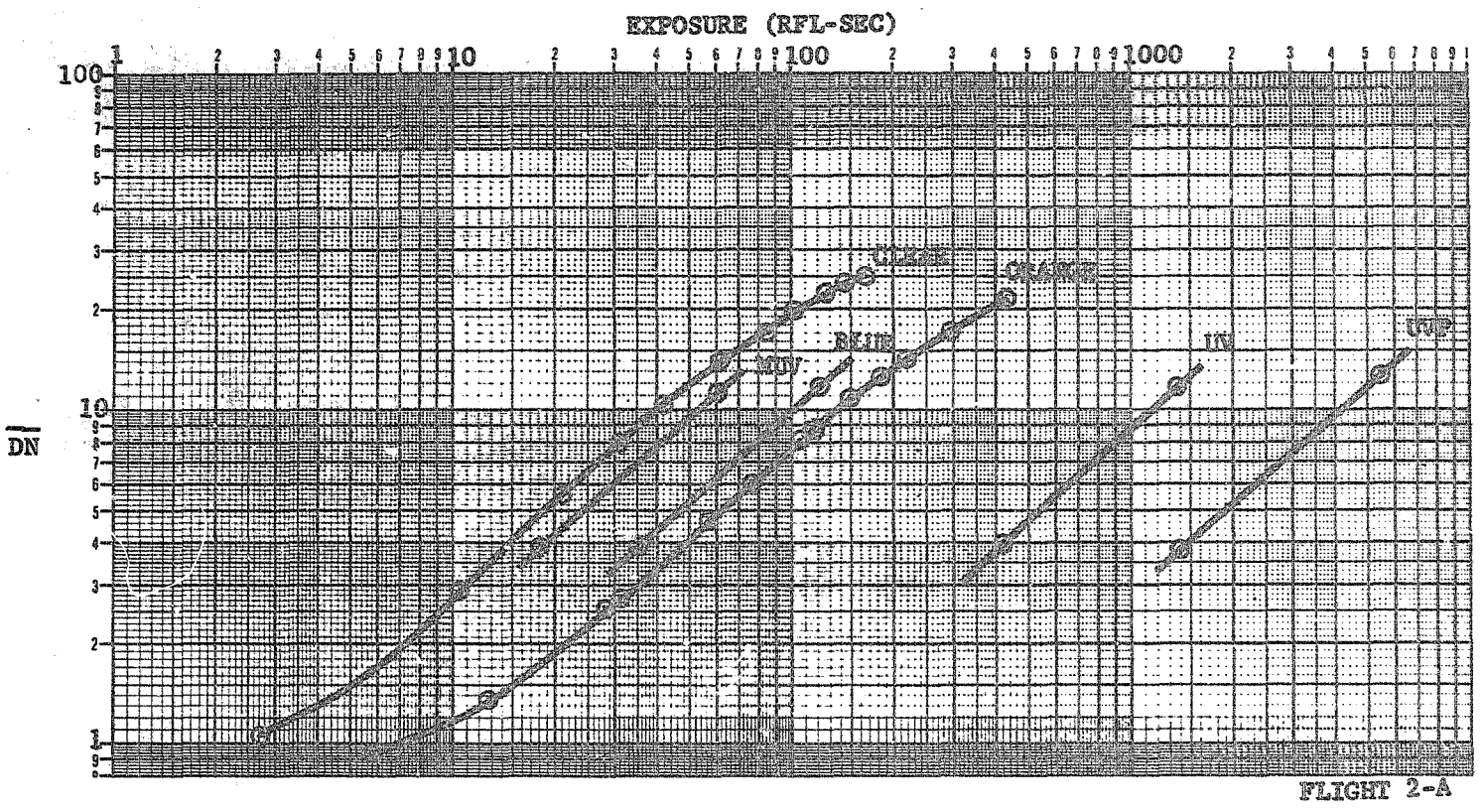


Fig. 32 FLAT FIELD RESPONSE (BENCH 3)

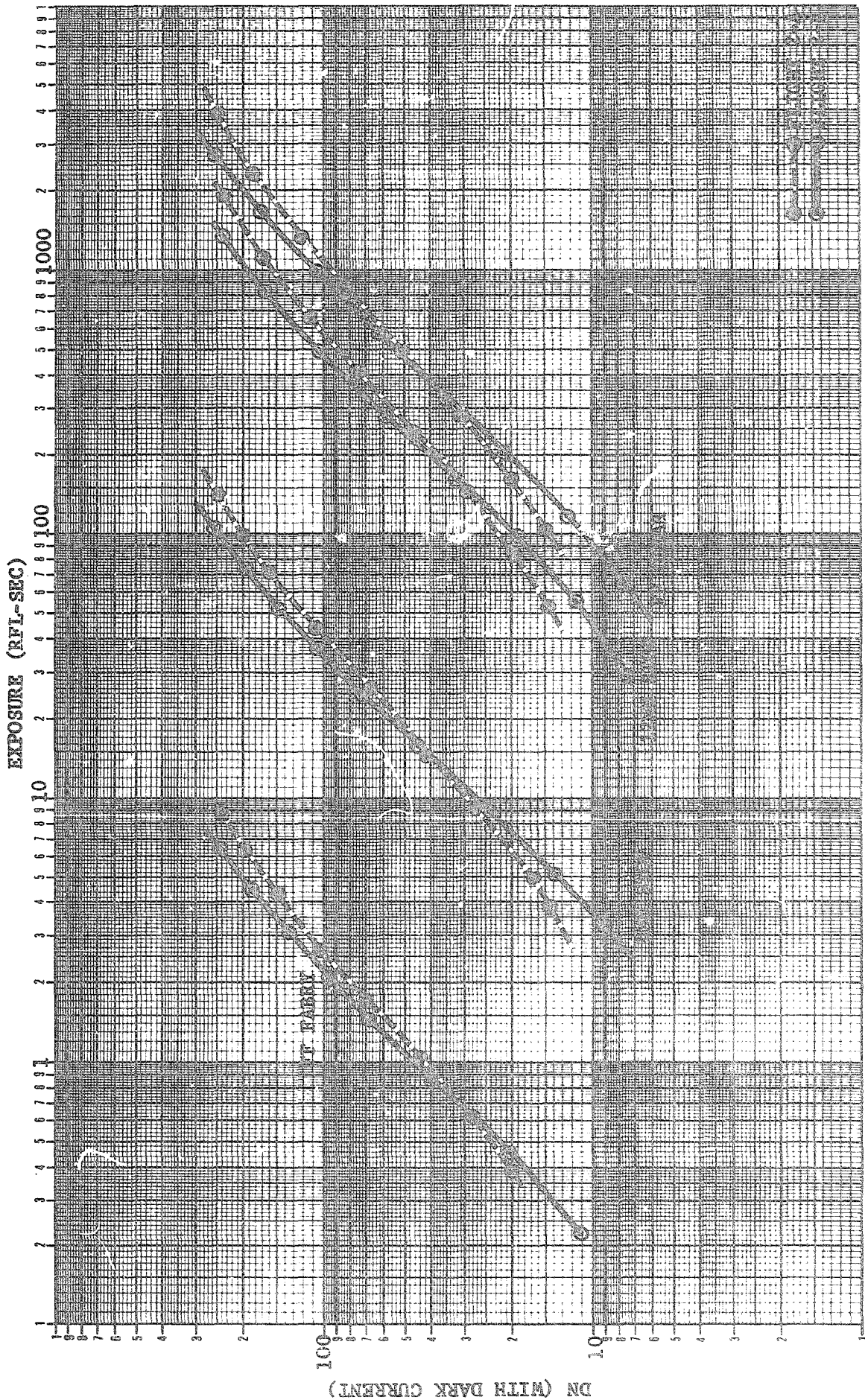


FIG. 33 FABRY ANALYSIS, FLIGHT 2

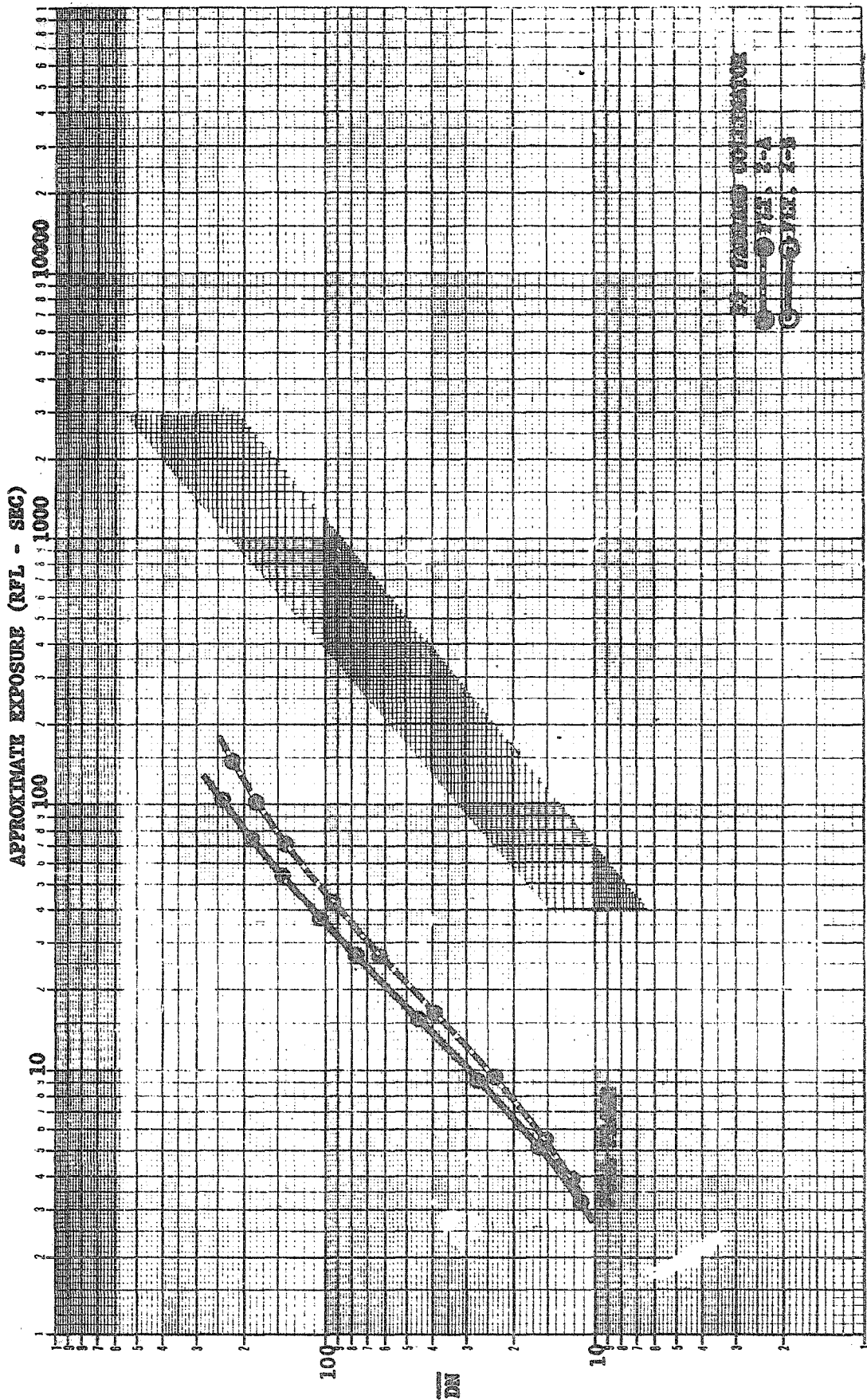


FIG. 34 I/T CURVE, WAF

FILTER	\overline{DN}	A CAMERA		B CAMERA	
		EXPOSURE	RFF	EXPOSURE	RFF
0 (OR)	38	44.5	3.13	46.2	3.61
0 (OR)	128	190.0	3.39	163.0	3.79
1 (WAF)	64	535.0	20.42	405.0	18.93
1 (WAF)	128	1790.0	20.00	860.0	19.11
2 (BLUE)	38	34.5	2.43	26.5	2.07
2 (BLUE)	128	138.0	2.46	94.0	2.19
3 (UVP)	38	1390.5	97.89	1095.0	88.55
3 (UVP)	128	5600.0	100.00	5200.0	120.93
4 (MUV)	38	17.5	1.23	13.8	1.08
4 (MUV)	128	71.0	1.27	50.0	1.16
5 (CLR)	38	14.2	1.0	12.8	1.0
5 (CLR)	128	56.0	1.0	43.0	1.0
6 (UV)	38	405.0	28.52	405.0	31.64
6 (UV)	128	1580.0	28.21	1380.0	32.09

TABLE 9. RELATIVE FILTER FACTORS (WAF,#1, BASED ON BENCH 2,
OTHERS BENCH 3)

The values compare fairly well with those determined from component data. Relative filter factors obtained in WAF calibration are also listed in Table 9.

3.2.6 Veiling Glare

Veiling glare is defined as unfocused light reaching the vidicon when the shutter is open. In planetary photography, it may occur when the camera is pointed at a small segment of a brightly illuminated surface. Inasmuch as veiling glare reduces the image contrast, all effort was made during the design and manufacture of the MVM '73 cameras to keep it at an absolute minimum. The calibration was performed in the JPL Optical Tunnel on the Askania Bench, as shown schematically in Figure 35.

The optics, baffles, and a black hole were aligned by placing a small light cannon behind the telescope focal plane, which provided a centralizing light beam. It was interesting to notice that in this configuration the scattered light was dominated by violet when viewed in front of the telescope from an off-axis position. The screen was a 6 x 8 foot styrofoam sheet capable of being raised to various heights above the optical axis. It was illuminated by three photo-floods and two sun-guns, mounted in one transverse line.

A photomultiplier tube was used to detect the transmitted light energy. It was first coupled with a fiber-optics probe fed by a 4" integrating sphere attached to the telescope at the focal plane. Later, the photomultiplier tube was coupled directly to the telescope in response to the violet hue observed during the setup.

A series of photomultiplier readings was taken with the illuminated screen in different positions; within the field of view, within the stray field of view, and completely outside both fields (Table 10). The output of the black hole represented the reference basis. Data reduction was implemented in two different ways: first by simple comparison of the

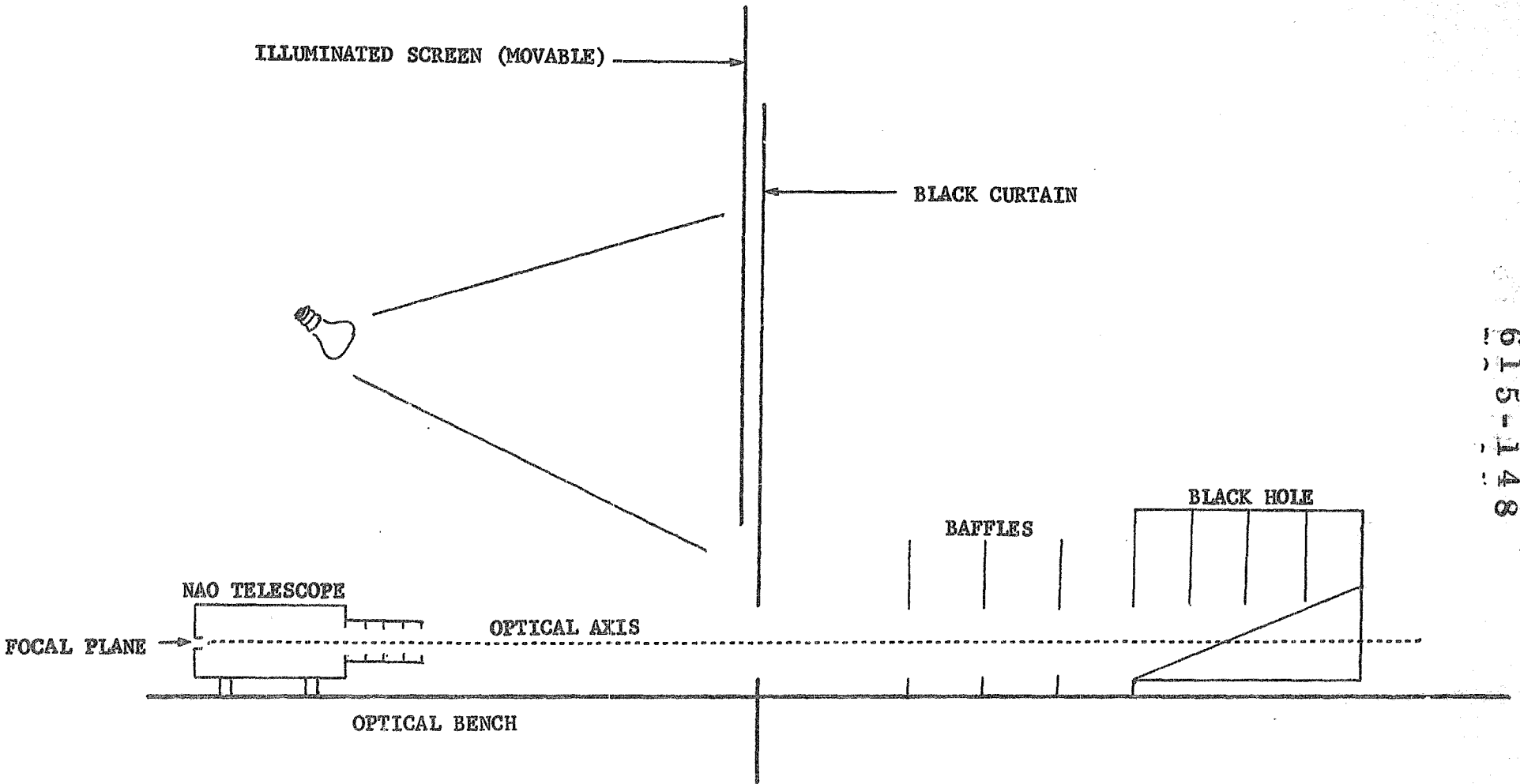


Fig. 35 VEILING GLARE TEST SETUP

TEST CONDITIONS	FIBER-OPTIC PROBE	DIRECT
Lights Off, Cap On	1.4 x .05	2.3 x .05
Lights On, Cap On	1.4 x .05	2.0 x .05
Lights On, No Screen, Black Hole	3.7 x .05	26.0 x .05
Lights On, No Screen, Styro Disc at Curtain	75.0 x 10.0	78.8 x 100
Lights On, No Screen, Styro Disc at Black Hole	4.0 x .05	31.0 x .05
Lights On, Screen Completely in FOV	63.5 x 10.0	
Lights On, Screen 345 mm Above Bench	23.7 x .05	
Lights On, Screen 437 mm Above Bench	14.9 x .05	
Lights On, Screen 502 mm Above Bench	10.1 x .05	
Lights On, Screen 890 mm Above Bench	5.0 x .05	
Lights On, Screen Completely in FOV	61.8 x 10.0	
Lights On, Screen 339 mm Above Bench		15.5 x 1.0
Lights On, Screen 390 mm Above Bench		10.0 x 1.0
Lights On, Screen 505 mm Above Bench		5.0 x 1.0
Lights On, Screen 899 mm Above Bench		38.9 x .05
Lights On, Screen to Axis w/9" Cutout		34.7 x 1.0

TABLE 10. VEILING GLARE DATA (RELATIVE UNITS)

recorded readings, and secondly by determining veiling glare as a function of off-axis angles. The latter approach was difficult, but the obtained results agreed. The veiling glare effect for the MVM '73 narrow-angle cameras can be expected to be less than 1% of flat-field illumination.

3.3 GEOMETRY

3.3.1 Optical Orientation

3.3.1.1. Narrow-Angle Optics (NAO)

The knowledge of the correct focal length is essential, as it establishes the on-axis scale factor of the object-to-image geometry. It is also the determining factor for geometric distortion measurement.

The geometric quality of a photographic system is determined by mutual relation of these four axes (Figure 36):

- (1) Optical axis - the line connecting the front and rear nodal point.
- (2) Mechanical axis - the axis of the telescope housing.
- (3) Vidicon normal - the perpendicular axis from the rear nodal point to the vidicon faceplate.
- (4) Line-of-sight (boresight axis) - the line connecting the rear nodal point and the center reseau mark.

All of these axes would be identical and perpendicular to the vidicon faceplate in an ideal system. This is a technical impossibility. However, based upon experience described in Reference 2 and Reference 3, the differences become insignificant in extremely narrow-angle photography. Best measuring accuracy determined the influence of any eventual optical distortion to be negligible.

The determination of the NAO focal length was based upon direct theodolite observations of the vidicon reseau grid through the optics. This

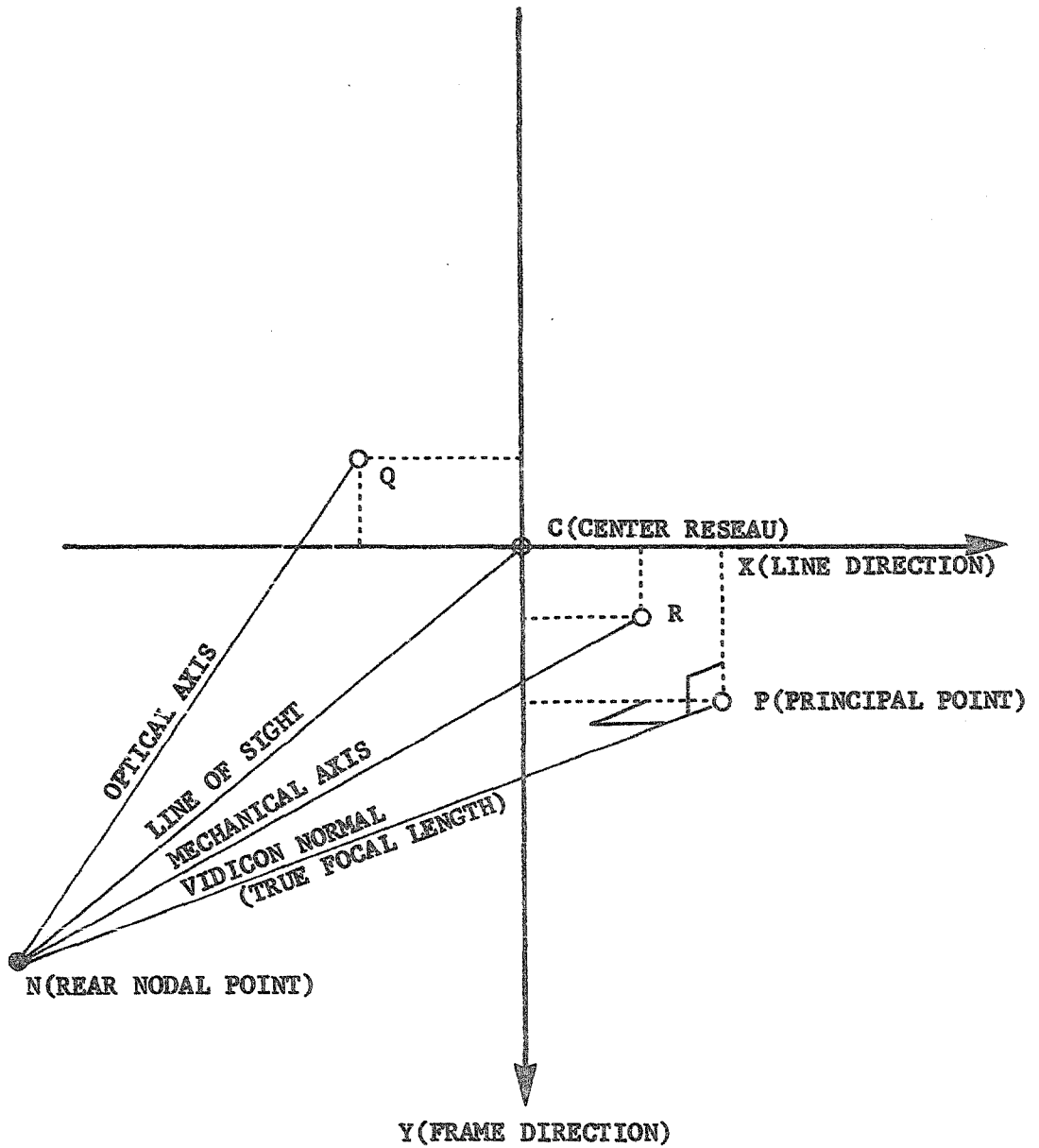


Fig. 36 GEOMETRY OF A PHOTOGRAPHIC SYSTEM

approach ensures measurement of the true subsystem focal length and is superior to any component level results. The mathematical theory of this method is given in Figure 37. The measured horizontal and vertical angles define a bundle of space vectors referring to the known reseau mark locations on the vidicon faceplate. Focal length can then be calculated as:

$$f = \frac{d}{\tan \omega}$$

The field of view is less than 0.5° , meaning that fractional observational errors in reseau mark locations or in angular measurements gain critical influence.

It was necessary, for this reason, to eliminate all reseau marks near the center reseau mark, and the remaining points were measured repeatedly and precisely, using a Wild-T3 theodolite. The obtained results based upon four independent sets of measurements of 40-80 reseau marks, are described in Table 11. The average accuracy was approximately 2 parts in 10^4 . Reference 1 requires an accuracy of 1 part in 10^4 , but this is unrealistic for a 1500 mm vidicon photographic system. Reference 2, dealing with a focal length of 500 mm, had a calibration requirement of 2 parts in 10^4 . It can thus be said that the determination of focal length was very good.

3.3.1.2 Wide Angle Optics (WAO)

The differences between the four axes of projection described in 3.3.1.1 may become very important for a wide-angle photographic system. As the WAO is only an auxiliary optical system, it was decided to consider an ideal system with one axis of projection, as the NAO had been considered.

Although the mathematical theory of the WAO focal length determination was the same as for the NAO focal length, for various technical reasons, it was not feasible to measure the reseau marks directly through the optics and a slightly modified approach was devised. A geometric grid target was inserted in a Farrand 35° collimator and the angles of its intersection

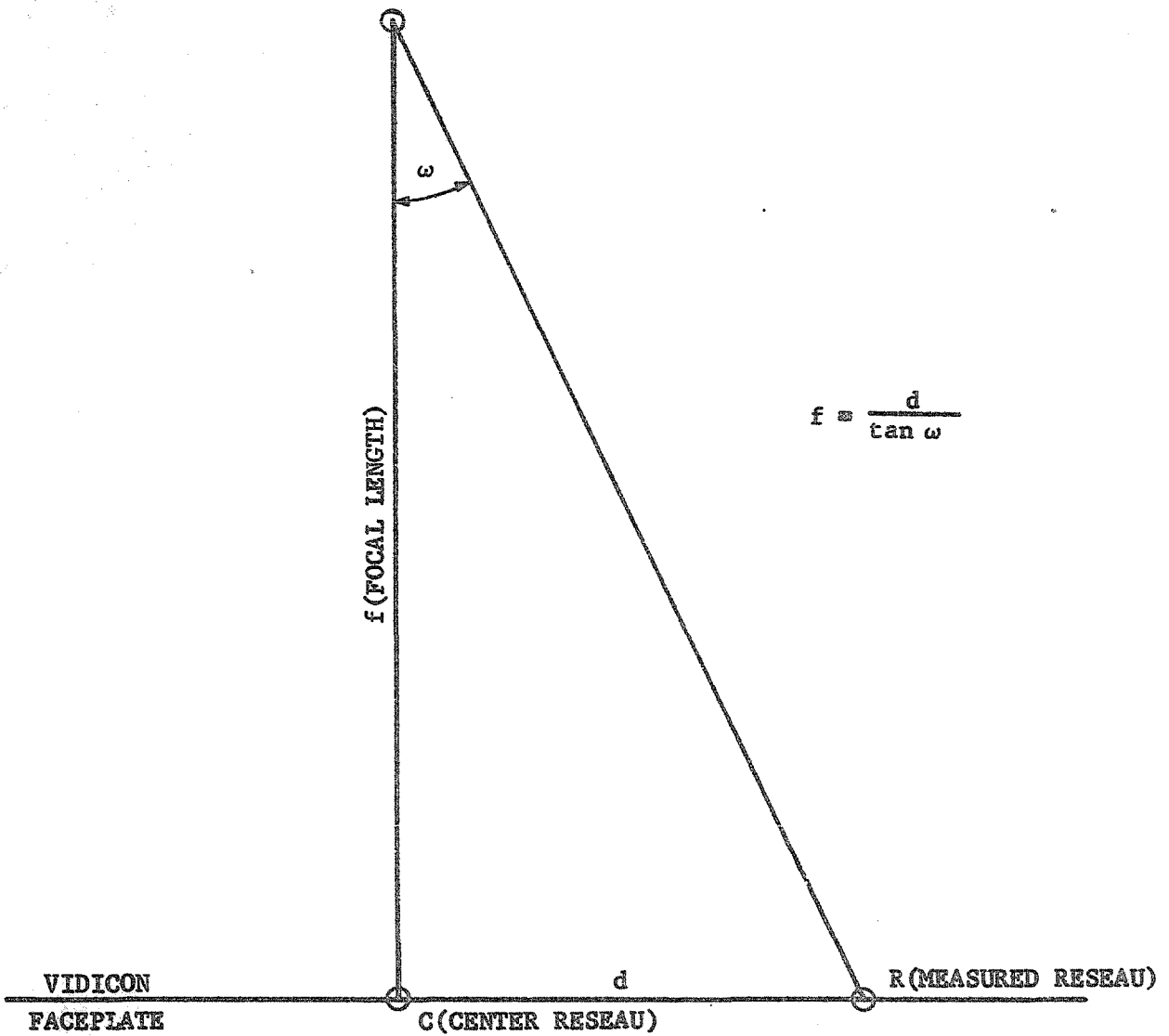


Fig. 37 NARROW-ANGLE OPTICS FOCAL LENGTH MEASUREMENT

CAMERA	FOCAL LENGTH mm	FIELD OF VIEW, DEG.		
		LINES	PIXELS	DIAGONAL
F1-A, NAO	1405.12 ± .09	0.3663	0.4730	0.5982
F1-B, NAO	1496.99 ± .33	0.3660	0.4724	0.5975
F1-A, WAO	60.52 ± .04	9.030	11.646	14.698
F1-B, WAO	62.02 ± .09	8.816	11.364	14.347
F2-A, NAO	1495.66 ± .34	0.3663	0.4729	0.5982
F2-B, NAO	1503.69 ± .34	0.3643	0.4703	0.5949
F2-A, WAO	62.02 ± .05	8.816	11.368	14.351
F2-B, WAO	62.68 ± .07	8.724	11.247	14.199

TABLE 11. MVM '73 FOCAL LENGTH AND FIELD OF VIEW

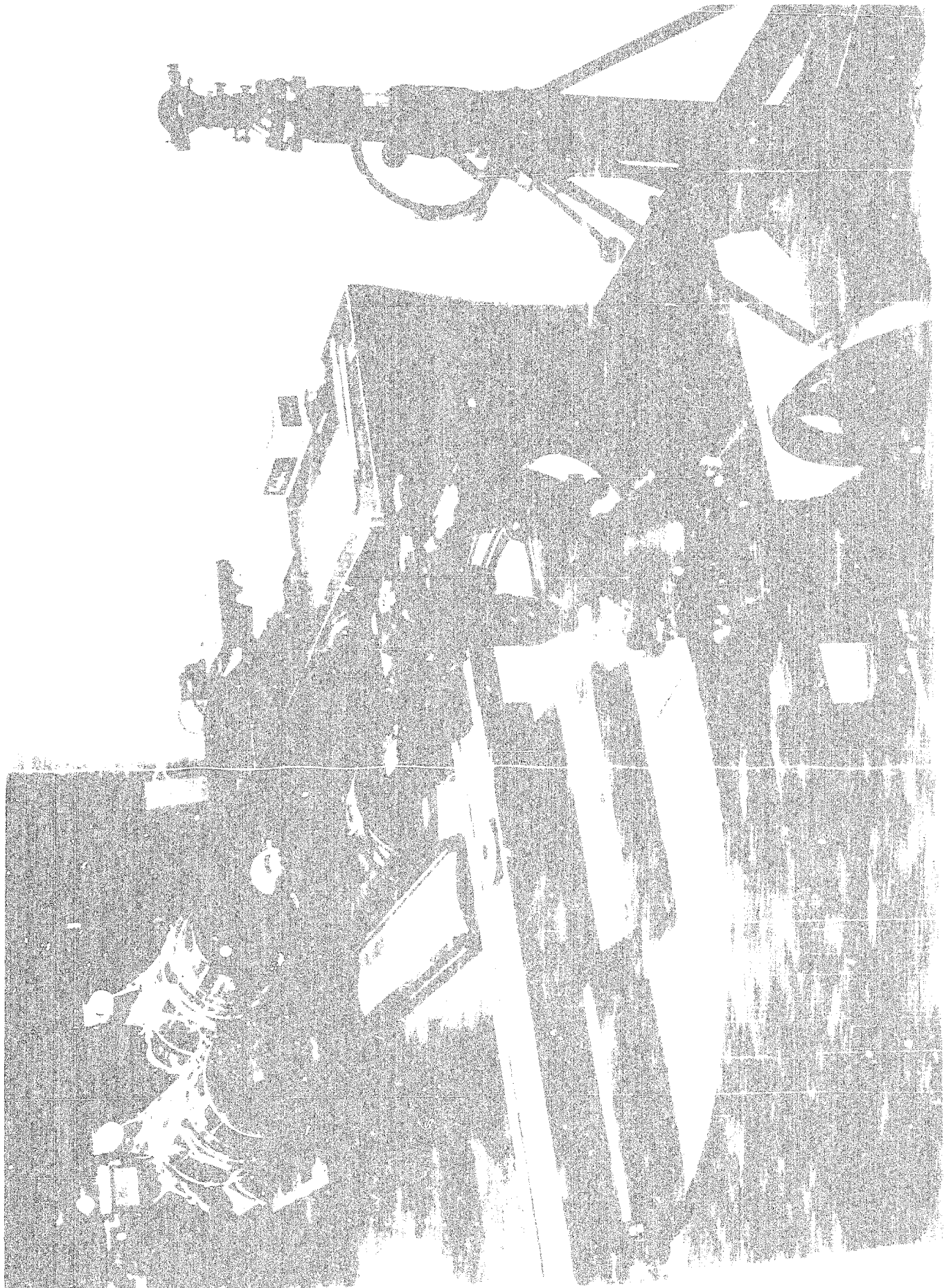
NOTE: Field of View is defined as the relation between the focal length and the extreme reseau marks

points were measured with a Wild-T2 theodolite. Coordinates of the same points were then measured in an IPL-processed photograph. After necessary geometric corrections, these data could be used for computation of the focal length using the NAO method. Results also appear in Table 11.

3.3.1.3. Opto-Mechanical Alignment

Determination of the line-of-sight (boresight axis) direction with respect to the spacecraft coordinate system was necessary for navigation and mapping purposes.

A typical optical bench setup (Fig. 38) shown schematically in Fig. 39, was used to determine the opto-mechanical alignment of each system. The mounting pins on the scan platform were chosen for the horizontal axis reference and the platform itself for the vertical reference establishing an alignment reference axis and plan common to both cameras. Using the technique outlined in Ref. 2, the horizontal and vertical components of the opto-mechanical alignment of each camera, as well as between the camera systems was determined. The obtained results, with a directional accuracy determined to be within the $\pm .0005$ radians required by Ref. 1, are presented in Figs. 40 and 41. It should be noted that the values for vertical alignment are valid when cameras are placed on the scan platform; horizontal alignment values are valid only when the mounting feet of the A camera are attached to the mounting pins, and the B camera is mounted at the specified distance from the A Camera. The mechanical accuracy of this alignment was determined to be $\pm .076$ mm, resulting in a possible accuracy loss of $\pm .60$ min/arc.



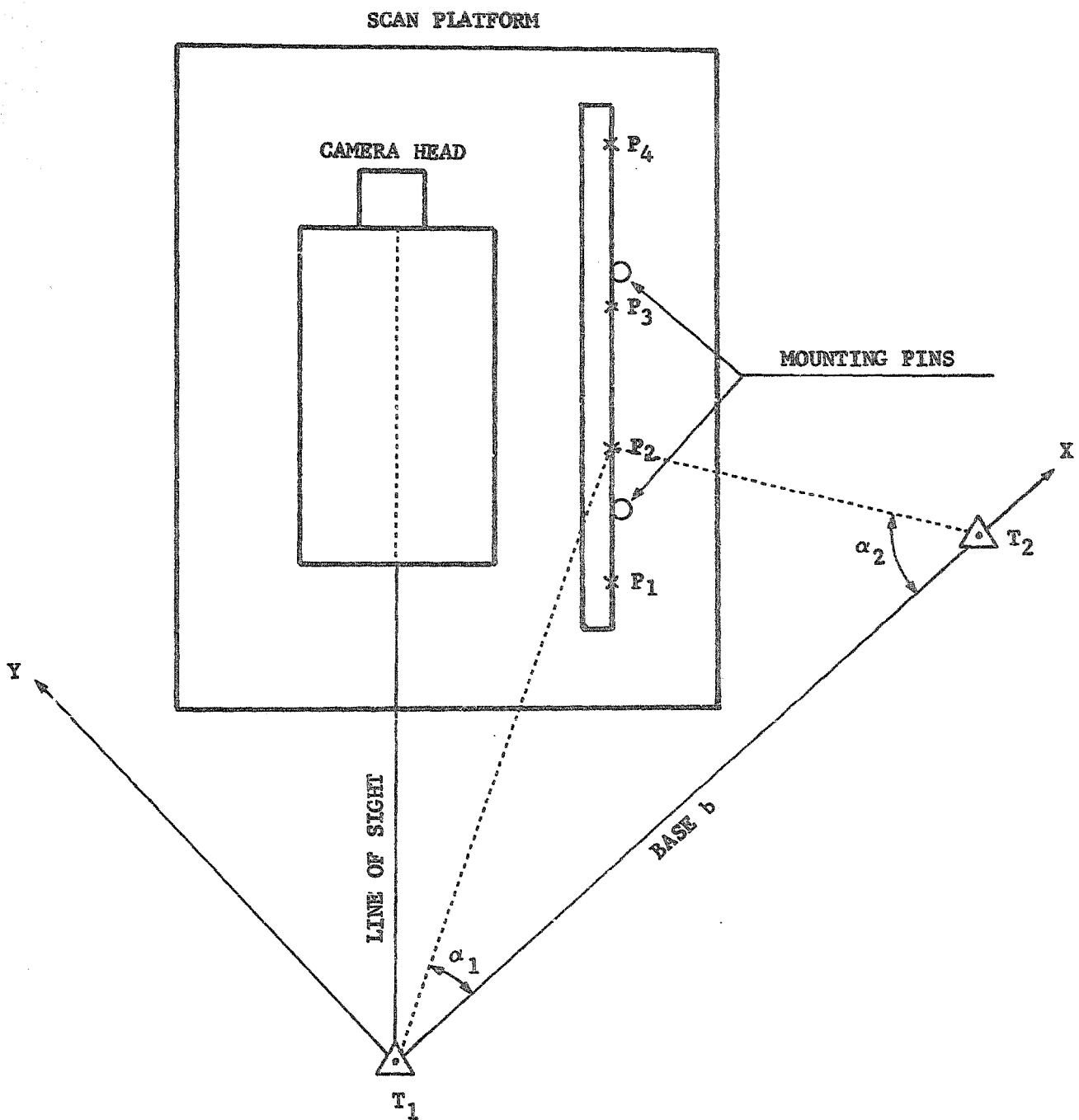


Fig. 39 GEODETIC INTERSECTION OF THE OPTO-MECHANICAL ALIGNMENT OF CAMERA B

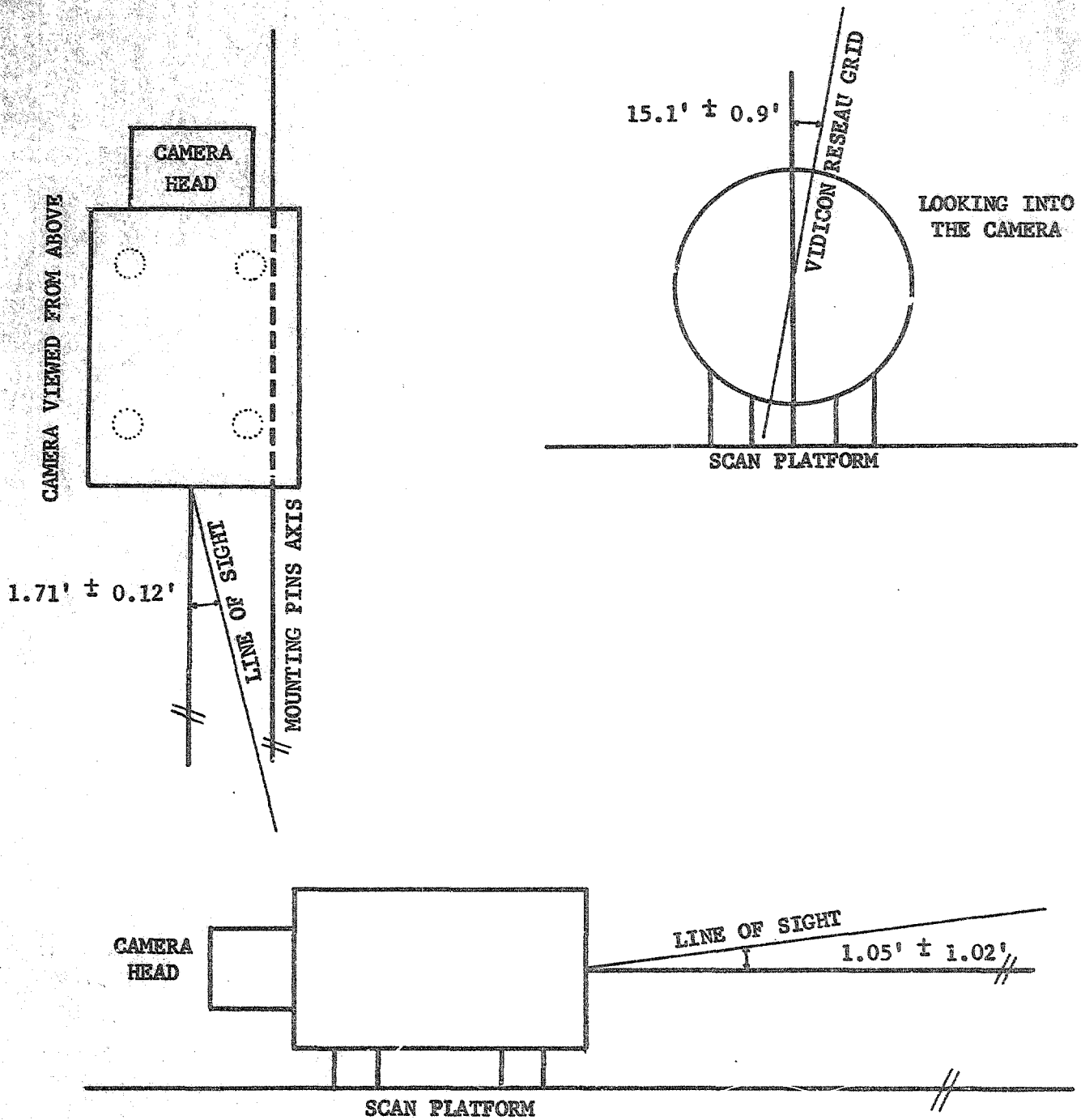


Fig. 40 FLIGHT 2-A OPTO-MECHANICAL ALIGNMENT

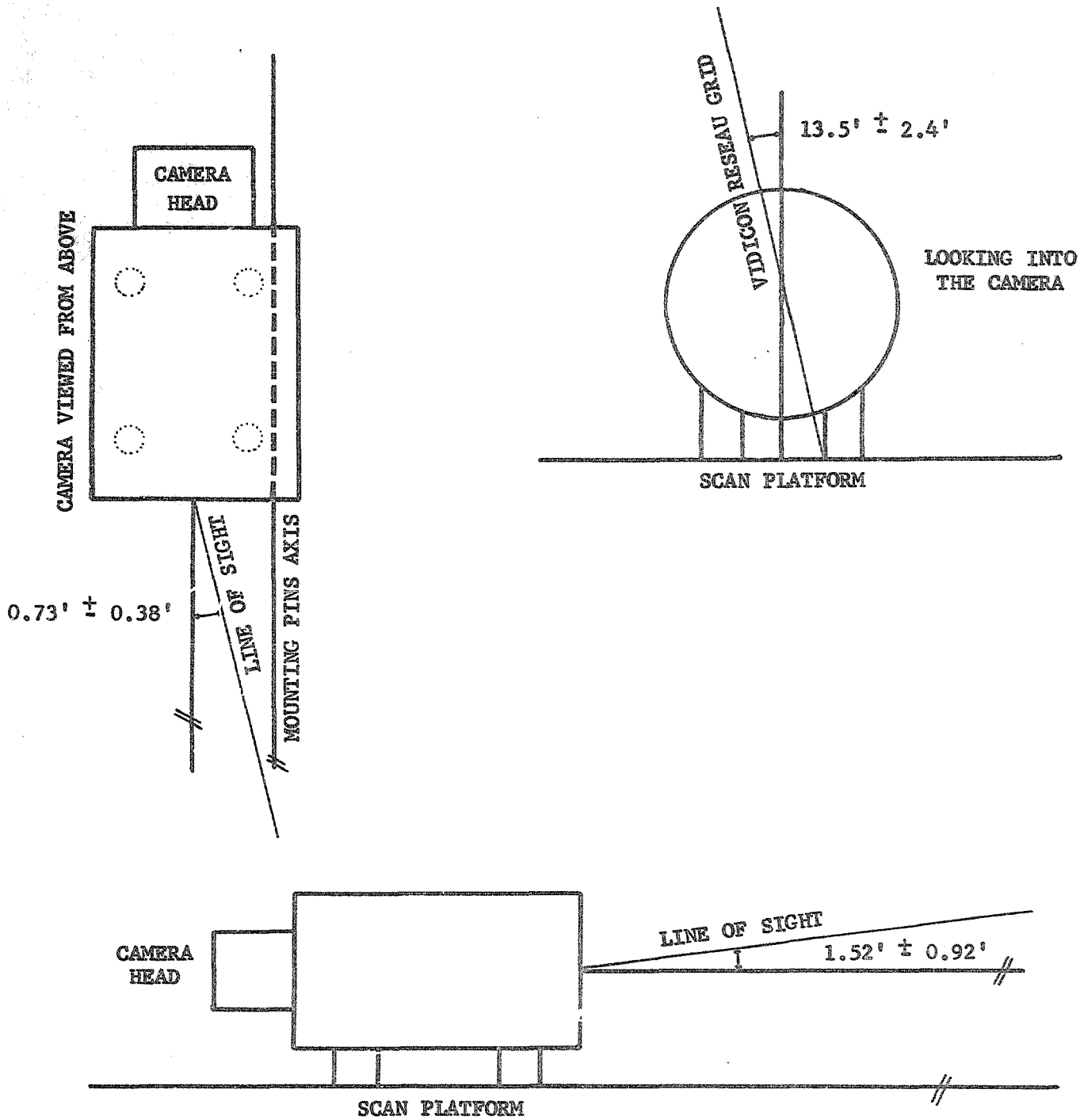


Fig. 41 FLIGHT 2-B OPTO-MECHANICAL ALIGNMENT

3.3.2. Geometric Calibration

Calibrations to enable restoration of geometric integrity to transmitted images were performed in accordance with those devised by IPL for the MM '71 vidicon and documented by J. E. Kreznar in Reference 5.

3.3.2.1. Object Space Reseau Locations

Using the techniques described in Reference 5, "nominal" reseau locations were established. Tables 12 and 13 list these values for Flight 2-a and Flight 2-B vidicons.

3.3.2.2. Apparent Aspect Ratio

The apparent aspect ratio (ratio of sampling frequency in the horizontal direction to that in the vertical direction) of the MVM '73 vidicons was determined from reseau positions in images obtained in flight. Object-space reseau locations, having various assumed aspect ratios were fit to image-space reseau locations in the frames. A least squares fit, allowing only scale, rotation, and offset variations was applied. Each assumed aspect ratio yielded a mean fit residual. When plotted against the assumed aspect ratio, this residual produced the curved shown in Figure 42. Three successive "fits" were made of areas representing 10, 40, and 80% of the frame. Those ratios which produced the minimum mean residuals were chosen as the apparent aspect ratios to be used for playback and decalibration purposes.

The apparent aspect ratios were slightly different for each camera:

$$\text{Flight 2-A A/R} = 1.069 \pm .001$$

$$\text{Flight 2-B A/R} = 1.071 \pm .001$$

The residuals from camera B were about one-half those of camera A. This was interpreted to mean that there is an intrinsic skew or deformation of the image other than rotation, translation or magnification which is greater in the A camera than in the B camera.

* 18.479, 46.145, 71.955, 44.267, 206.551, 43.969, 340.638, 43.849,
 * 474.871, 43.795, 609.446, 43.714, 744.485, 43.726, 877.665, 44.709,
 * 930.209, 46.114, 17.815, 133.032, 72.500, 133.136, 206.506, 132.729,
 * 340.793, 132.385, 475.115, 132.465, 609.459, 132.651, 743.740, 132.859,
 * 877.795, 133.061, 933.600, 132.987, 16.745, 267.705, 72.294, 266.981,
 * 206.682, 267.030, 340.500, 266.907, 475.019, 267.046, 609.777, 266.786,
 * 743.786, 267.226, 878.225, 267.139, 933.666, 267.389, 15.890, 400.112,
 * 72.507, 399.259, 206.451, 399.763, 340.756, 399.473, 475.000, 400.000,
 * 609.521, 400.079, 743.955, 400.064, 878.297, 399.926, 933.774, 399.817,
 * 16.544, 533.058, 72.389, 532.268, 206.472, 532.568, 340.789, 532.726,
 * 474.734, 533.083, 609.729, 532.595, 744.162, 532.629, 878.505, 532.391,
 * 933.124, 532.576, 16.370, 666.105, 72.720, 665.836, 206.332, 666.948,
 * 340.772, 666.880, 474.865, 667.281, 609.371, 667.351, 743.942, 666.838,
 * 878.230, 666.614, 933.556, 666.470, 16.982, 755.043, 72.807, 754.939,
 * 206.522, 755.369, 340.687, 756.062, 475.119, 756.163, 609.595, 756.354,
 * 743.753, 755.873, 877.939, 755.810, 932.451, 753.873, 18.037, 88.594,
 * 140.131, 87.005, 273.599, 86.486, 407.729, 86.414, 542.434, 86.258,
 * 676.654, 86.536, 811.012, 86.676, 932.670, 87.270, 16.932, 199.174,
 * 139.696, 198.022, 273.099, 198.611, 407.501, 198.469, 542.587, 197.925,
 * 676.816, 198.235, 811.086, 198.296, 933.580, 198.782, 16.217, 332.392,
 * 139.380, 332.315, 273.208, 332.514, 407.705, 332.526, 542.362, 332.743,
 * 677.014, 332.649, 811.293, 332.707, 933.464, 332.638, 16.467, 467.237,
 * 139.378, 466.987, 273.527, 466.958, 407.809, 467.263, 542.181, 467.296,
 * 677.092, 466.870, 811.315, 466.878, 933.405, 467.653, 16.567, 601.272,
 * 139.609, 601.163, 273.495, 600.597, 407.497, 601.943, 542.072, 601.590,
 * 676.775, 601.647, 810.938, 601.758, 933.273, 601.130, 17.058, 713.228,
 * 140.047, 712.549, 273.658, 712.968, 407.651, 713.512, 542.546, 713.074,
 * 677.020, 712.960, 811.210, 712.726, 933.799, 712.513,

TABLE 12 NOMINAL RESEAU LOCATIONS FOR FLIGHT 2-A VIDICON
 (LISTED 1-111; X COORDINATE, Y COORDINATE; UNIT OF MEASURE = PIXEL)
 MARCH 22, 1974 - OUTSIDE EARTH'S MAGNETIC FIELD

* 15.007, 41.296, 70.580, 40.348, 205.346, 40.819, 339.855, 40.689,
 * 474.796, 40.819, 610.040, 40.779, 744.852, 41.158, 879.470, 41.071,
 * 935.203, 42.596, 13.518, 130.580, 70.054, 130.577, 205.129, 130.891,
 * 339.858, 130.619, 475.165, 130.331, 610.187, 130.513, 745.193, 130.902,
 * 880.426, 131.743, 935.686, 131.736, 13.031, 266.079, 69.974, 265.997,
 * 205.066, 266.354, 339.904, 265.873, 475.055, 265.988, 610.710, 265.979,
 * 745.289, 265.898, 880.364, 266.190, 936.257, 266.038, 13.991, 399.955,
 * 69.917, 399.563, 205.095, 399.414, 340.061, 399.613, 475.000, 400.000,
 * 610.275, 399.819, 745.373, 399.688, 880.541, 399.375, 936.661, 399.630,
 * 13.911, 532.903, 70.161, 533.062, 205.124, 533.181, 340.040, 533.332,
 * 475.122, 533.223, 610.431, 533.032, 745.520, 532.728, 880.474, 532.808,
 * 936.103, 532.710, 12.634, 667.938, 70.337, 667.700, 205.392, 668.109,
 * 340.172, 668.031, 475.355, 668.082, 610.279, 668.044, 745.277, 667.791,
 * 880.271, 667.597, 936.088, 667.745, 15.321, 756.710, 70.947, 757.076,
 * 205.491, 757.697, 340.165, 757.834, 475.403, 758.018, 610.352, 757.771,
 * 745.136, 757.527, 879.777, 757.176, 934.830, 756.253, 13.808, 84.573,
 * 137.495, 83.914, 272.286, 84.053, 407.463, 84.288, 542.840, 84.093,
 * 677.917, 84.556, 813.063, 84.889, 935.759, 85.622, 13.116, 197.040,
 * 137.410, 196.832, 272.377, 196.922, 407.419, 197.020, 542.794, 196.882,
 * 677.938, 196.771, 812.686, 196.874, 936.562, 197.475, 13.886, 332.045,
 * 137.557, 331.982, 272.345, 332.042, 407.582, 331.856, 542.764, 331.968,
 * 677.947, 331.899, 813.144, 331.874, 936.110, 332.099, 13.814, 467.235,
 * 137.590, 467.164, 272.707, 467.058, 407.243, 467.544, 542.849, 467.116,
 * 678.042, 466.749, 812.623, 467.143, 936.122, 467.328, 13.679, 601.314,
 * 137.911, 602.014, 272.710, 601.834, 407.619, 602.252, 542.993, 601.778,
 * 677.973, 602.255, 813.289, 602.251, 936.367, 601.810, 13.453, 713.858,
 * 138.027, 714.429, 272.683, 714.500, 407.856, 714.361, 542.958, 714.373,
 * 678.014, 714.065, 812.609, 713.865, 935.299, 713.322/

TABLE 13 NOMINAL RESEAU LOCATIONS FOR FLIGHT 2-B VIDICON
 (LISTED 1-111; X COORDINATE, Y COORDINATE; UNIT OF MEASURE = PIXEL)
 MARCH 22, 1974 - OUTSIDE EARTH'S MAGNETIC FIELD

CAMERA	FOCAL LENGTH mm	HEIGHT	WIDTH
TVS2-A N/A	1495.66 ± .34	6393.141 ± .30491	8253.662 ± 3.491
TVS2-A WAF	62.023 ± .050	153873.463 ± .30491	198410.775 ± 3.491
TVS2-B N/A	1503.69 ± .34	6358.234 ± 3.491	8208.283 ± 3.491
TVS2-B WAF	62.685 ± .069	152255.543 ± 3.491	196293.690 ± 3.491

NOMINAL FIELD OF VIEW (MICRORADIANS)

CAMERA	IMAGE SPACE		OBJECT SPACE	
	HEIGHT	WIDTH	HEIGHT	WIDTH
TVS2-A N/A	9.435 ± .005	10.152 ± .004	8.975 ± .005	8.992 ± .004
TVS2-A WAF	227.078 ± .005	244.049 ± .004	216.003 ± .005	216.161 ± .004
TVS2-B N/A	9.427 ± .005	10.163 ± .004	8.865 ± .005	8.896 ± .004
TVS2-B WAF	225.744 ± .005	243.043 ± .004	212.292 ± .005	212.745 ± .004

NOMINAL FIELD OF VIEW (PIXELS)

CAMERA	IMAGE SPACE		OBJECT SPACE	
	HEIGHT	WIDTH	HEIGHT	WIDTH
TVS2-A N/A	677.623 ± .001	812.997 ± .001	712.368 ± .001	917.884 ± .001
TVS2-B N/A	674.460 ± .001	807.651 ± .001	717.199 ± .001	922.670 ± .001

ANGULAR SUBTENSE (MICRORADIANS/PIXEL)

TABLE 14. DIMENSIONS OF IMAGES

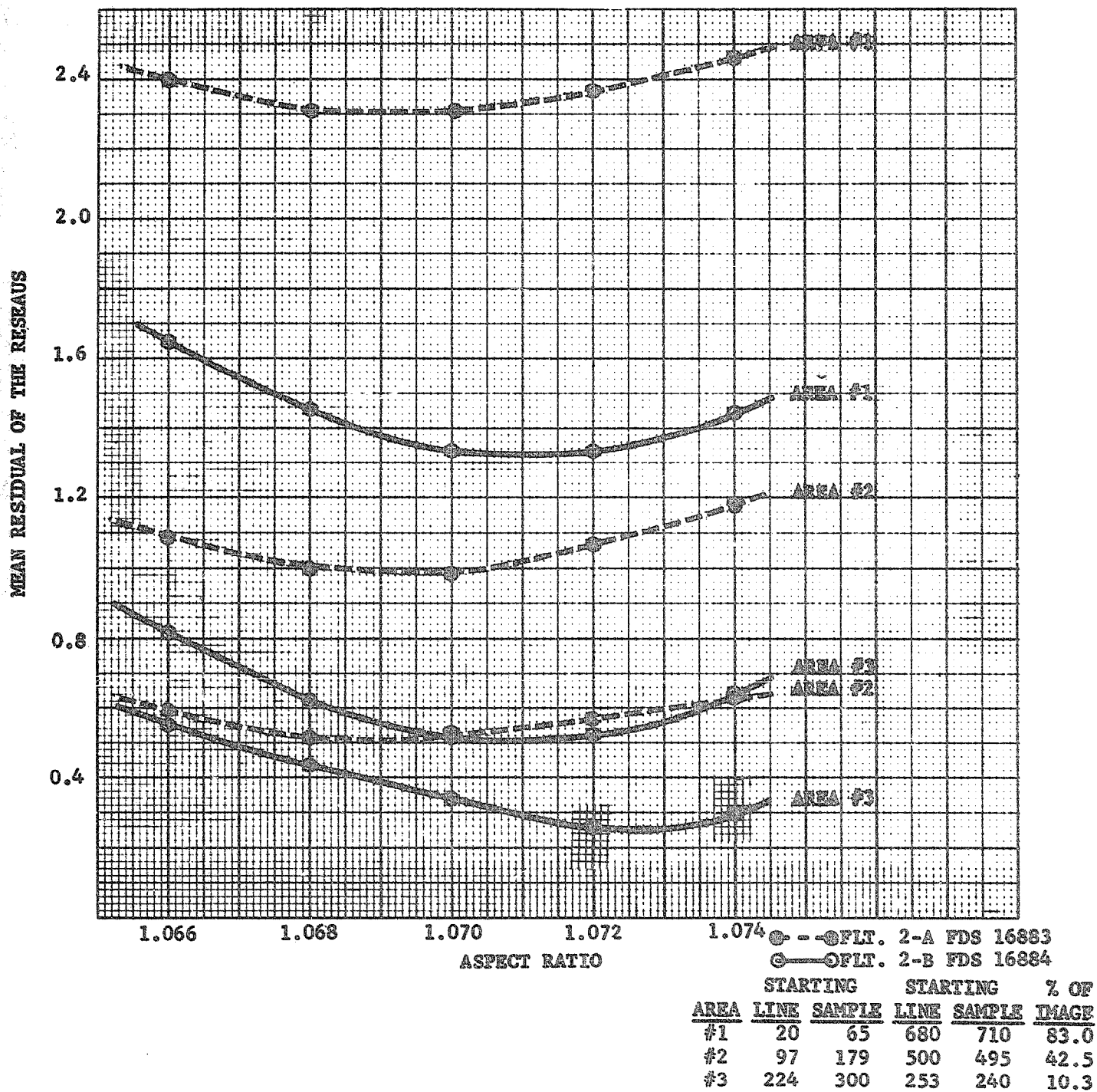
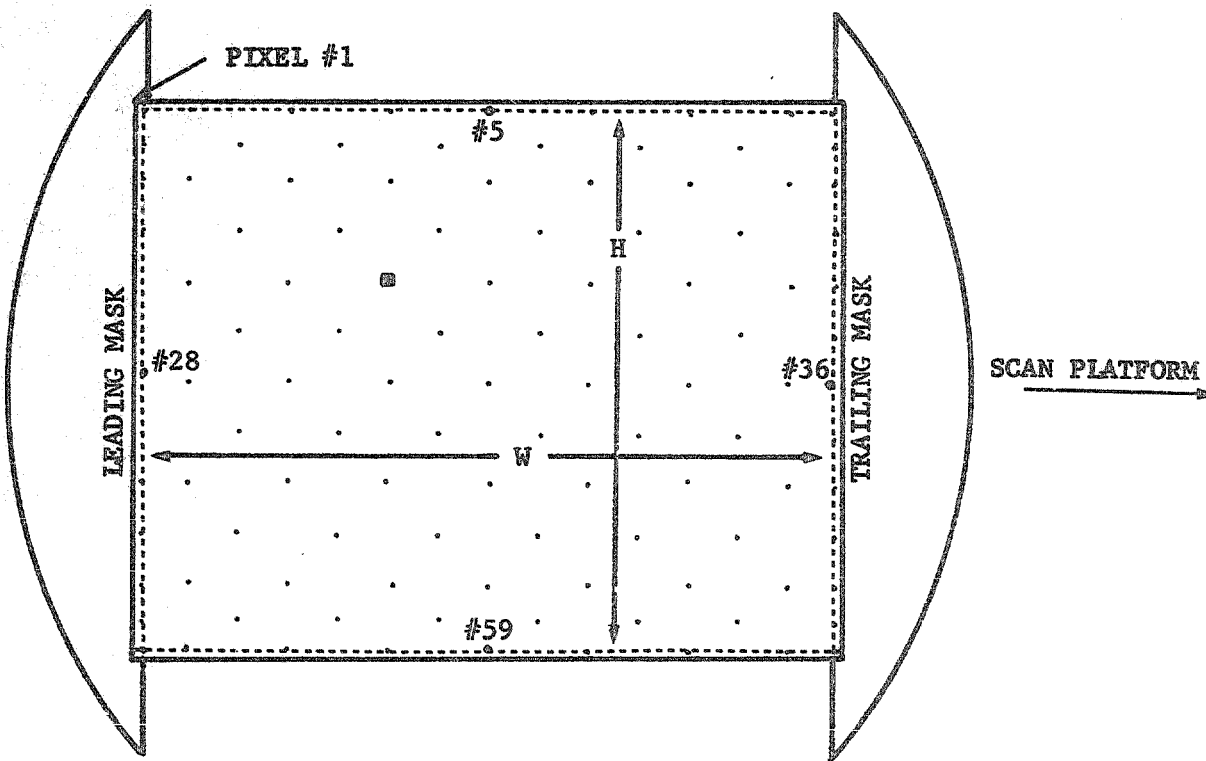


Fig. 42 MEAN ASPECT RATIO VS PICTURE AREA, FLIGHT 2



NOTE: H AND W MEASURED TO CENTER OF RESEAS

Fig. 43 FORMAT DIMENSIONS

3.3.2.3. Nominal Field of View

The nominal field of view was measured for all flight cameras between reseaus 5 and 59, and reseaus 28 and 36 as shown in Figure 43. Table 14 gives the average angle subtended per pixel for each camera through each of the optical systems. Values given for Image Space (raw image) are usable only for center-of-frame calculations of scale distances due to the distortions near the frame edges. Object Space (geometrically corrected image) values are not similarly limited.

3.4. MODULATION TRANSFER FUNCTION

The Modulation Transfer Function (MTF) is an analytical description in frequency space of the entire system response which eventually limits the highest resolution discriminable in the output data. The system calibration tests incorporated sine wave targets to verify system function.

In order to graphically display this, MTFs were defined as follows:

$$MTF(f) = \frac{A_i(f)}{A_i(f_0)} \cdot K(f)$$

where A_i is the amplitude in DN of the image at spatial frequency f ;

$A_i(f_0)$ is the amplitude of the lowest spatial frequency, and $K(f)$ is a correction factor which accounts for unequal amplitudes in the target.

$$K(f) = \frac{A_o(f_0)}{A_o(f)}$$

This definition is equivalent to the classical one on the condition that the lowest spatial frequency is not degraded.

The amplitudes $A_i(f)$ were determined from line plots taken through computer averaged lines in the images. The correction factors $K(f)$ were determined from densitometer traces through the original targets. Plots were similar for the four vidicons. Figure 44 shows the results obtained for the Flight 2-A and 2-B cameras.

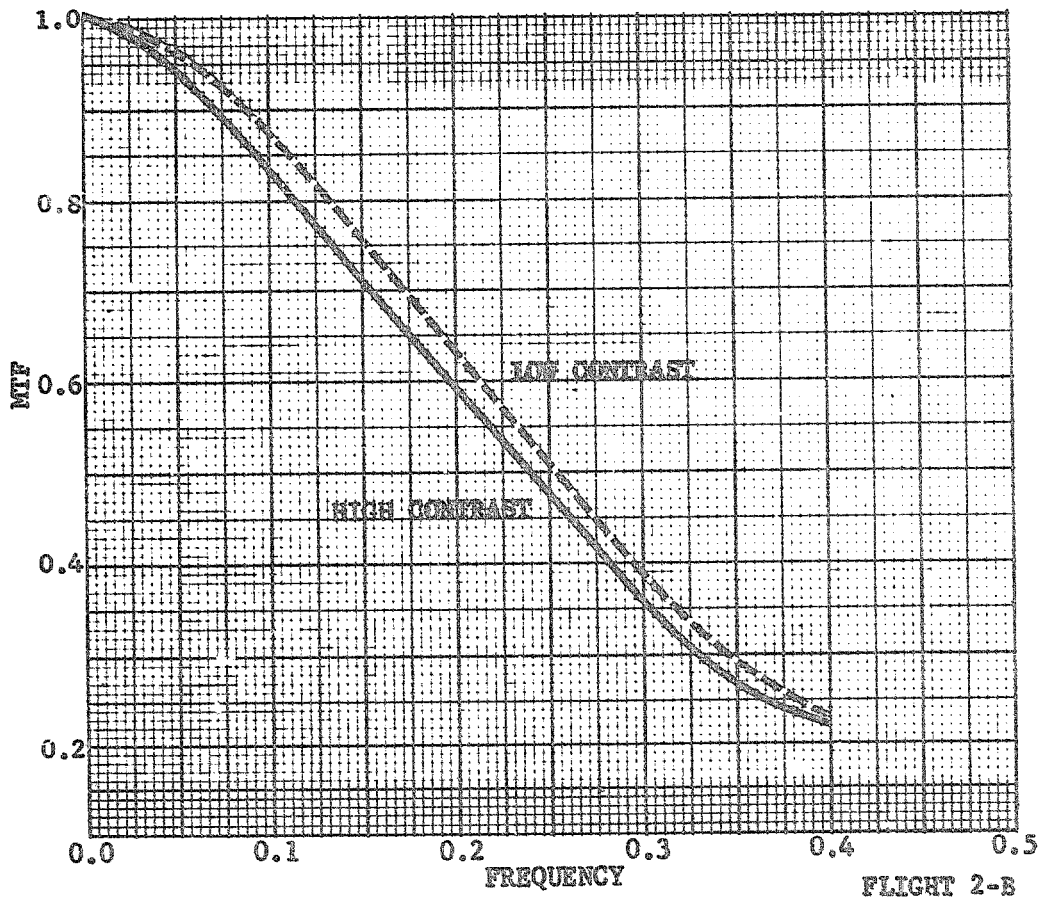
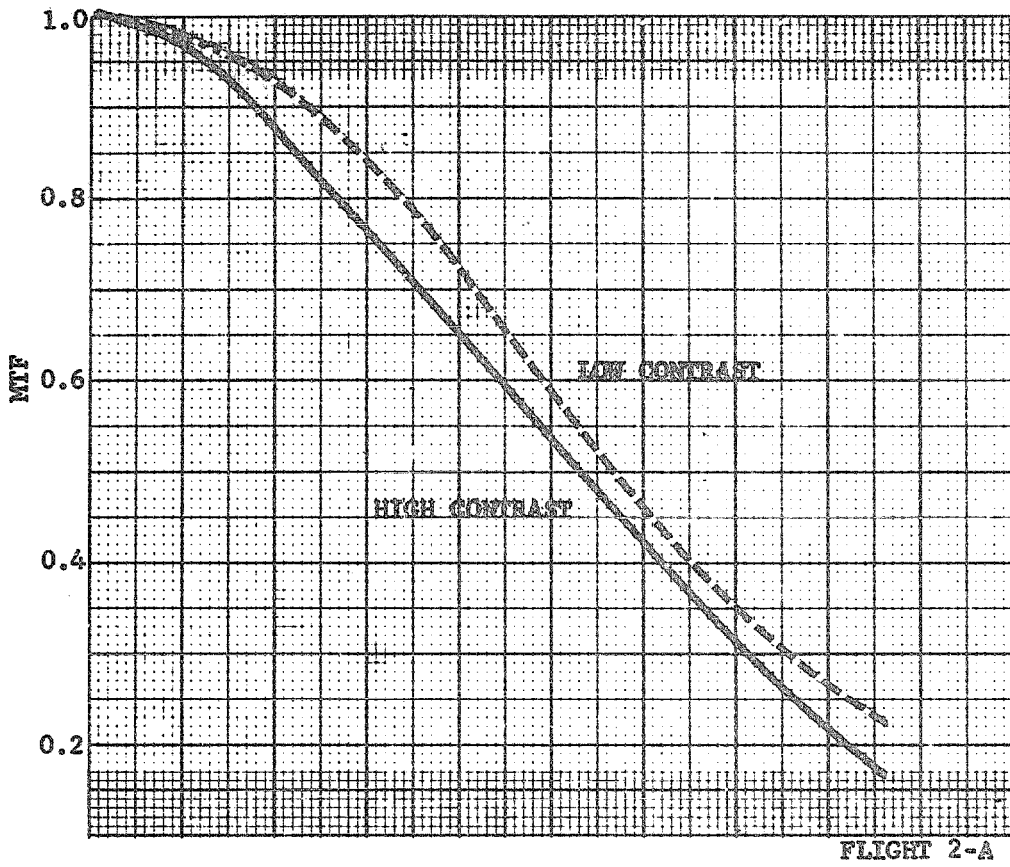


Fig. 44 MTF, MTF TARGET

3.5. NOISE ANALYSIS

3.5.1. Power Spectra

In order to identify the magnitude and frequency of possible coherent noise, power (Fourier amplitude) spectra were generated for a number of flat field images for the four areas illustrated in Figure 45. Figure 46 shows a power spectrum plot typical of those observed during bench test. The spectra showed no significant noise during testing.

3.5.2. Coherent vs. Random Noise

A quantitative assessment of the relative DN levels of coherent and random noise in flat-field images was performed for all vidicons. A selected flat-field image was processed to remove reseaus and blemishes. The image was then two-dimensionally high-pass filtered to minimize the effects of vidicon shading. The Fourier transform of a 256 x 256 pixel square area at the image center was analyzed and displayed. The standard deviation of this spectrum yielded a measure of the total noise in the test area. Further computer processing was utilized to remove the coherent noise. (Contrast enhancement by a factor of ten was necessary to obtain any measurable value for the coherent noise in these images). Figure 47 illustrates values of total, random, and coherent noise observed for the Flight cameras.

Coherent noise levels observed in bench tests were much less than one DN. Random noise levels were of the order of one DN.

4. SYSTEM LEVEL CALIBRATIONS

4.1. THERMAL VACUUM TESTING

To simulate flight conditions, both flight systems were operated in the 10 foot Ion Chamber (Figure 48) at various temperatures (F.A. cold -15°C ; F.A. room $+23^{\circ}\text{C}$; F.A. hot $+35^{\circ}\text{C}$) and high vacuum conditions (2.5×10^{-8} torr). Due to post-launch heater failure on the spacecraft, data was processed for Flight 2 cameras. The major goals were to test the effects of temperature on light transfer characteristics and on modulation transfer function.

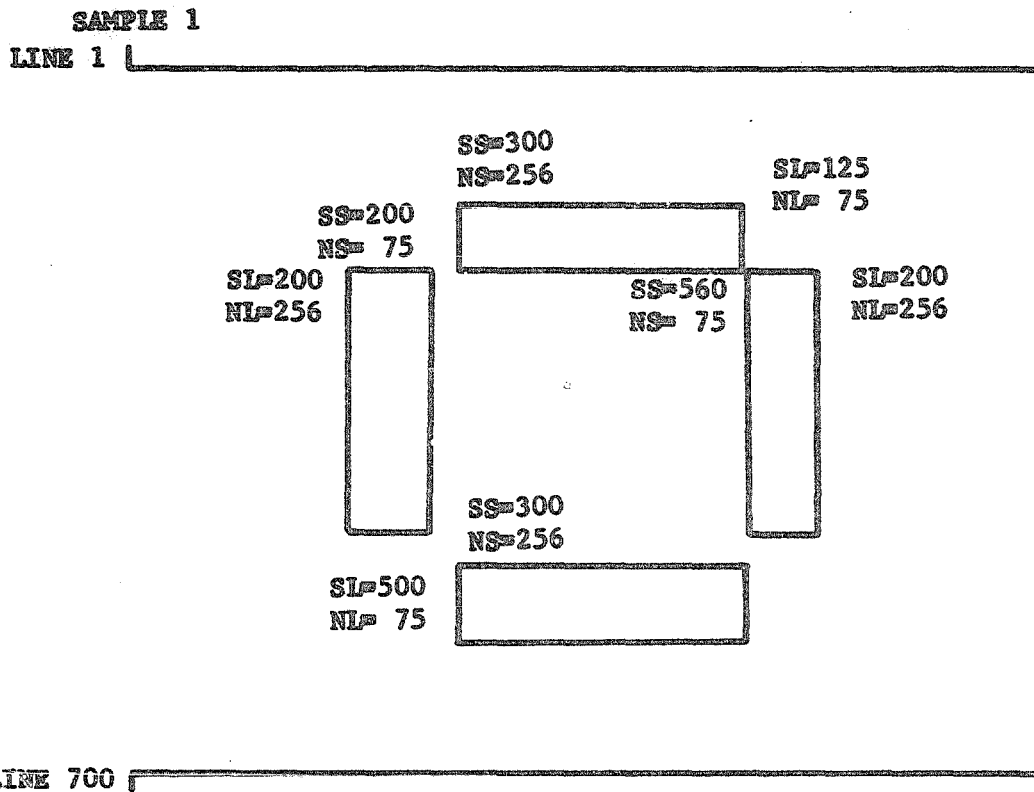


Fig. 45 POWER SPECTRA SAMPLE AREAS

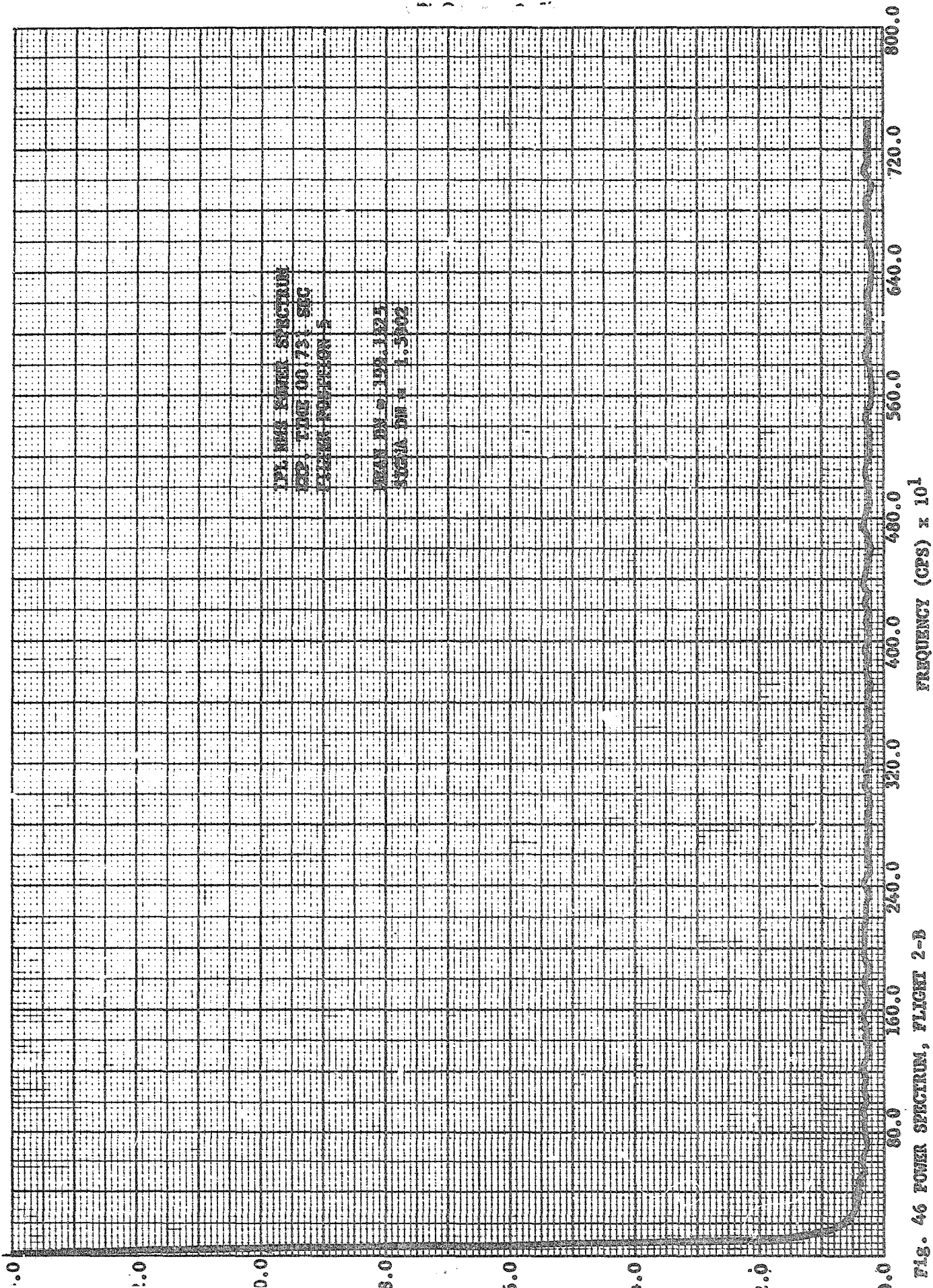
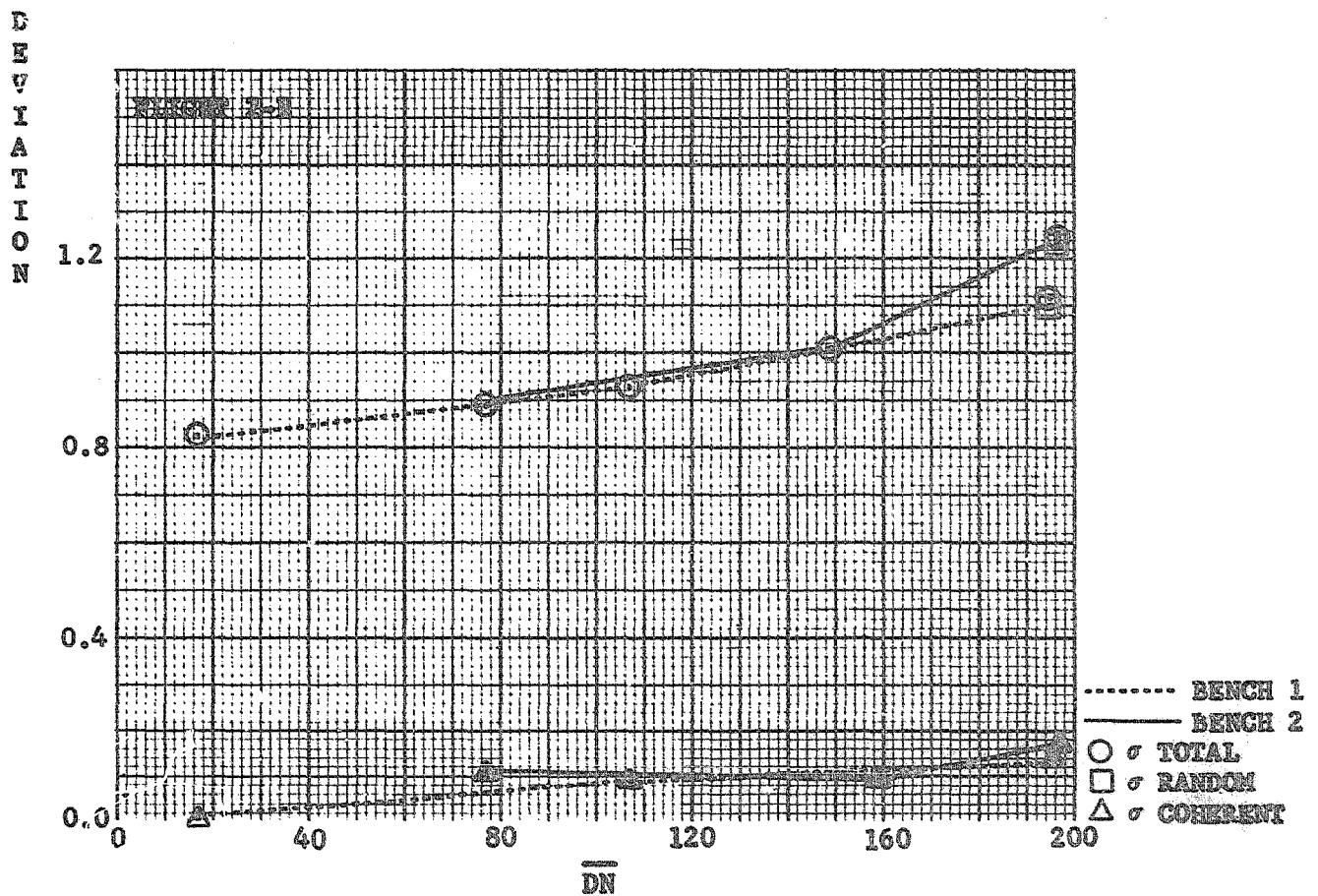
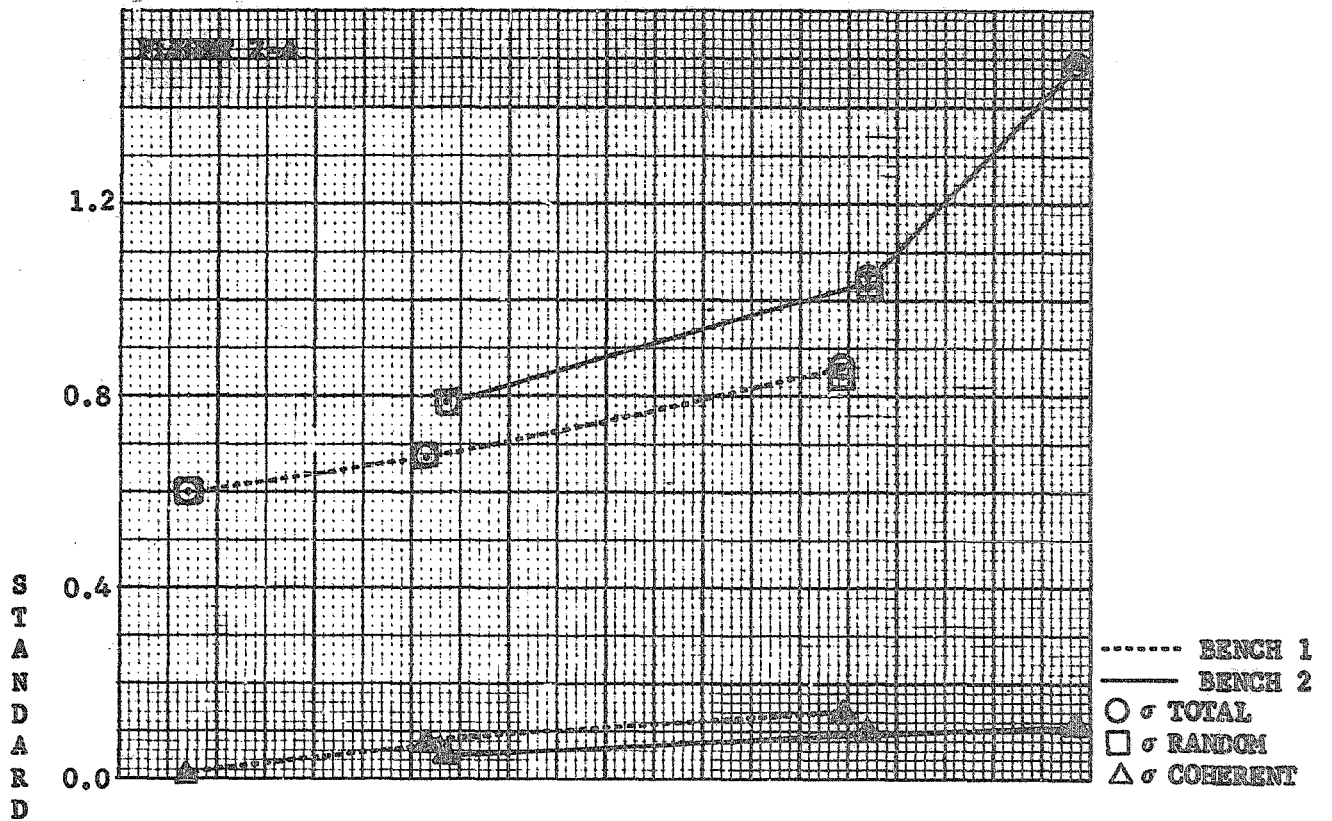


FIG. 46 POWER SPECTRUM, FLIGHT 2-B

Fig. 47 TYPICAL NOISE LEVELS, FLIGHT 2



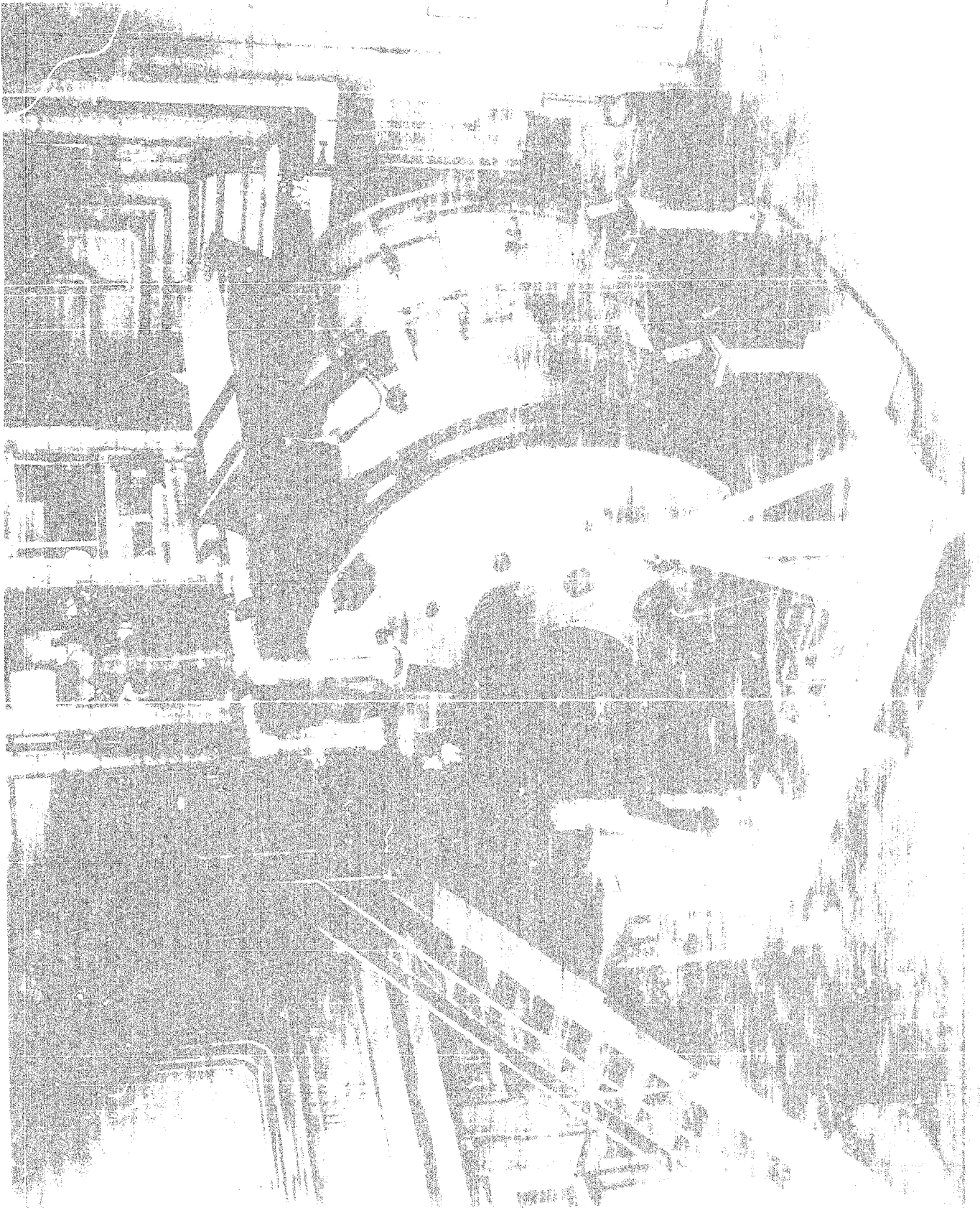
4.4.1. Light Transfer

Light transfer test were conducted through an optosil quartz window in the vacuum chamber (Figures 48 - 49) and illuminated by the 12" light cannon. Bench 3 and F.A. room temperature light transfer curves for Flight 2-A were analyzed and an effective transmission factor of 0.8426 was determined (cross-checked by Figure 50 giving 0.877 without allowances for window reflection losses. To compare radiometric response at the various temperatures, illumination levels were corrected for window losses and shutter offset and plotted against DN with dark current removed (Figures 51 - 52). A rough prediction of camera performance as it relates to vidicon temperature can be derived by curves of DN (with dark current removed) as a function of varying temperature (Figures 53 -54).

The effect of temperature on vidicon shading can be seen by comparing Figures 55 and 56 with Figures 30 and 31. This comparison shows the Flight 2-A vidicon to have a much flatter shading profile when cold while the Flight 2-B vidicon seems to be relatively unaffected by temperature variation.

4.1.2 Modulation Transfer Function

Television frames were taken at F.A. temperatures using bar targets imaged by the Celestron collimators. There was no apparent change from bench test MTF data. Slight microphonics of less than .5 DN were believed to be due to vibrations caused by shutter and filter wheel motion in one camera while the other was reading out. Similar effects were later noted during spacecraft systems testing.



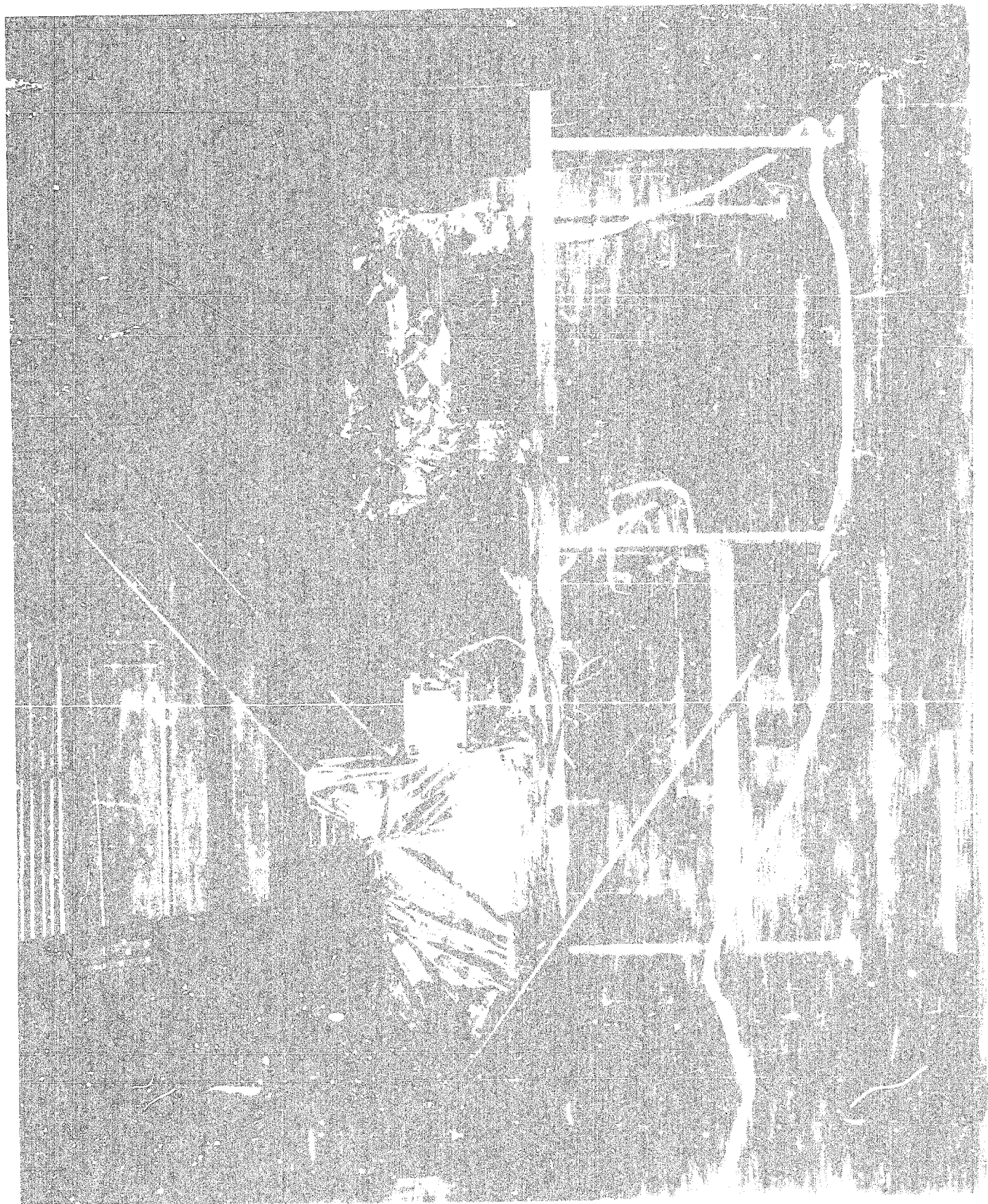


Fig. 49

Optical Transmission

Measurements made through 10mm thickness

FIG. 3

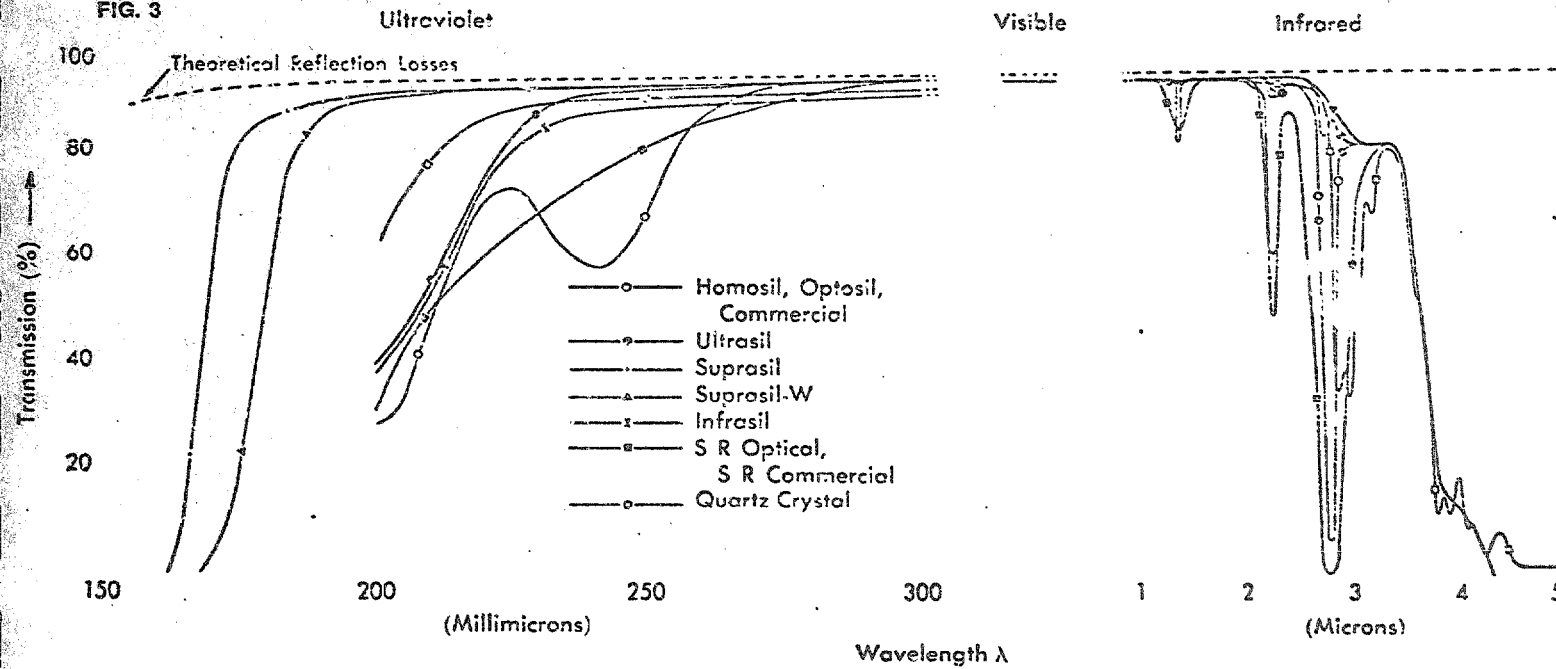


Fig. 50 OPTICAL TRANSMISSION

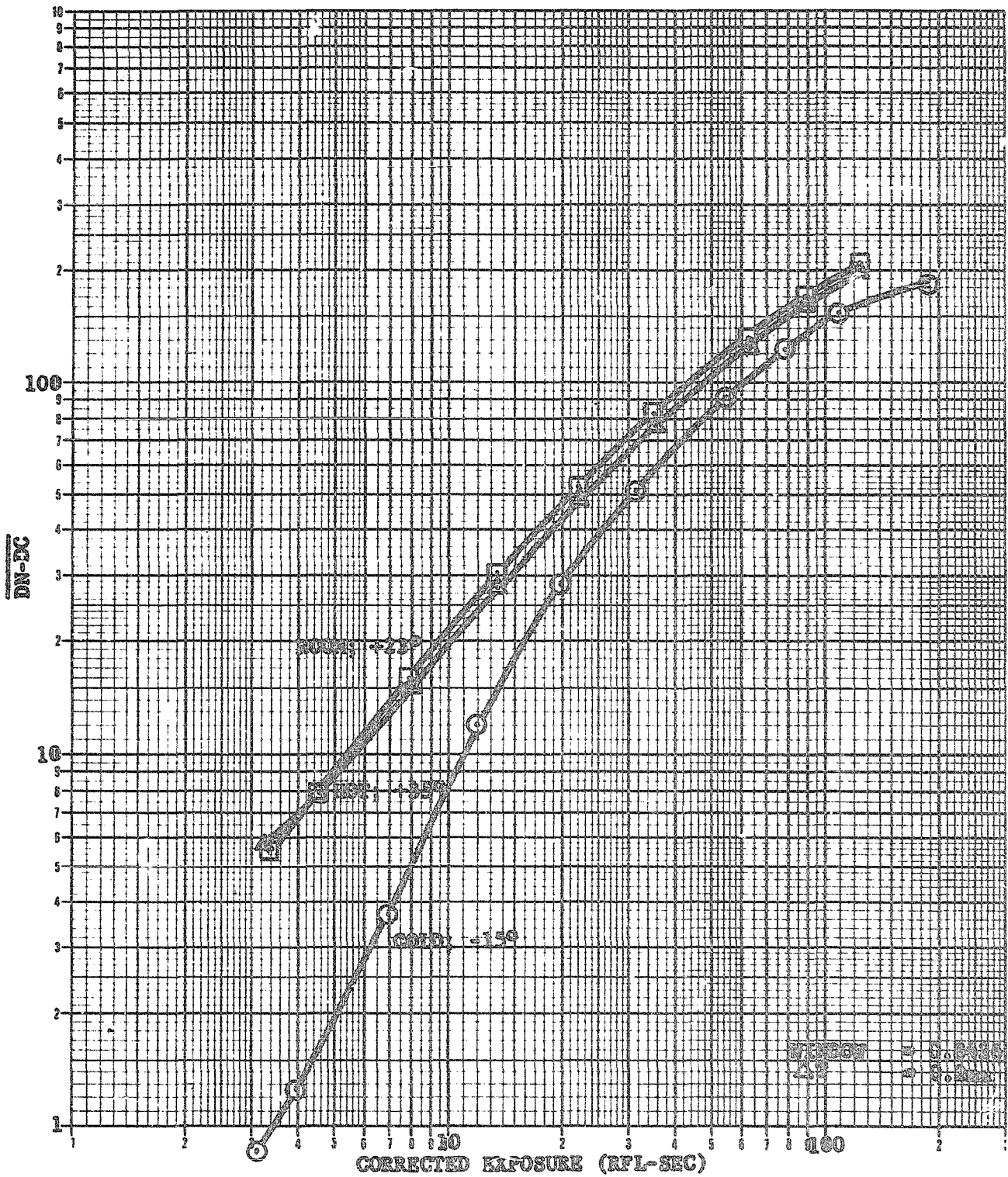


Fig. 51 FLAT FIELD L/T CORRECTED FOR WINDOW LOSSES AND SHUTTER OFFSET, FLIGHT 2-A

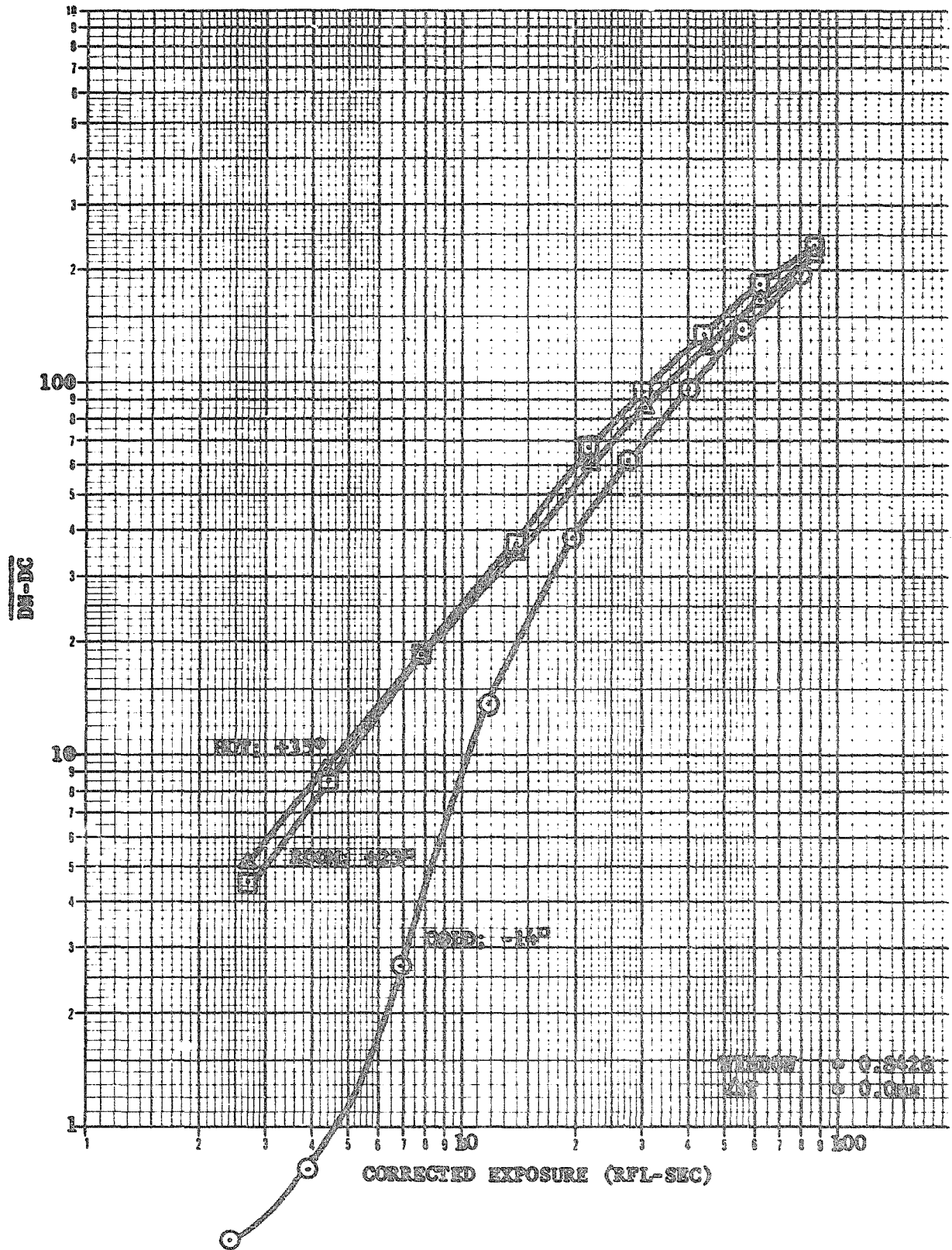


Fig. 52 FLAT FIELD L/T CORRECTED FOR WINDOW LOSSES AND SHUTTER OFFSET, FLIGHT 2-3

AD-0837-01

3 CYCLES X 70 DIVISIONS

SEMI-LOGARITHMIC

Buffalo, New York

GRAPHIC CONTROLS CORPORATION

Printed in U.S.A.

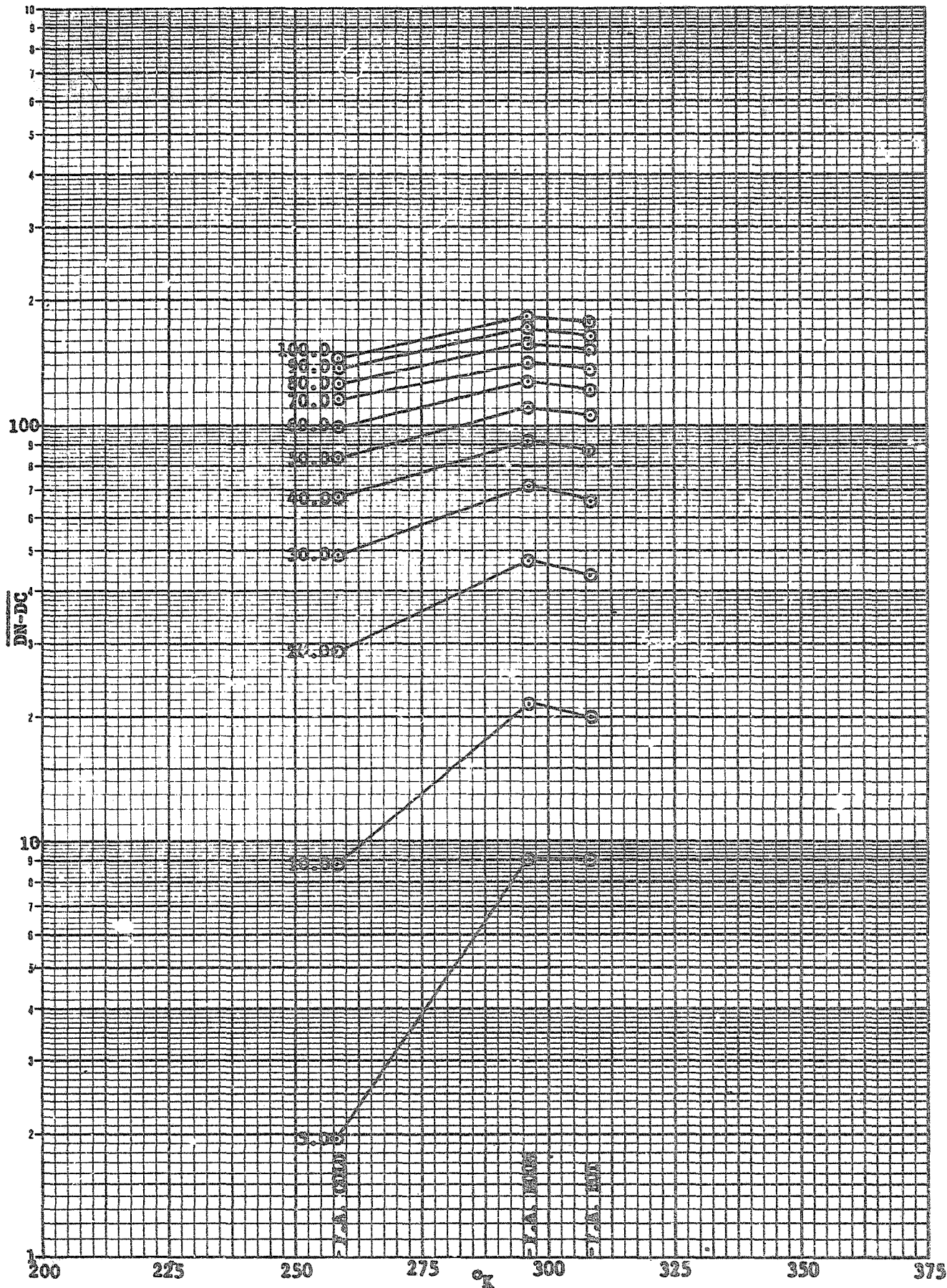


Fig. 53 RESPONSE AS A FUNCTION OF TEMPERATURE AT CONSTANT EXPOSURES, FLIGHT 2-A

SEMI-LOGARITHMIC 3 CYCLES X 70 DIVISIONS AD-0837-01

GRAPH-PAPER GRAPHIC CONTROLS CORPORATION Buffalo, New York
Printed in U.S.A.

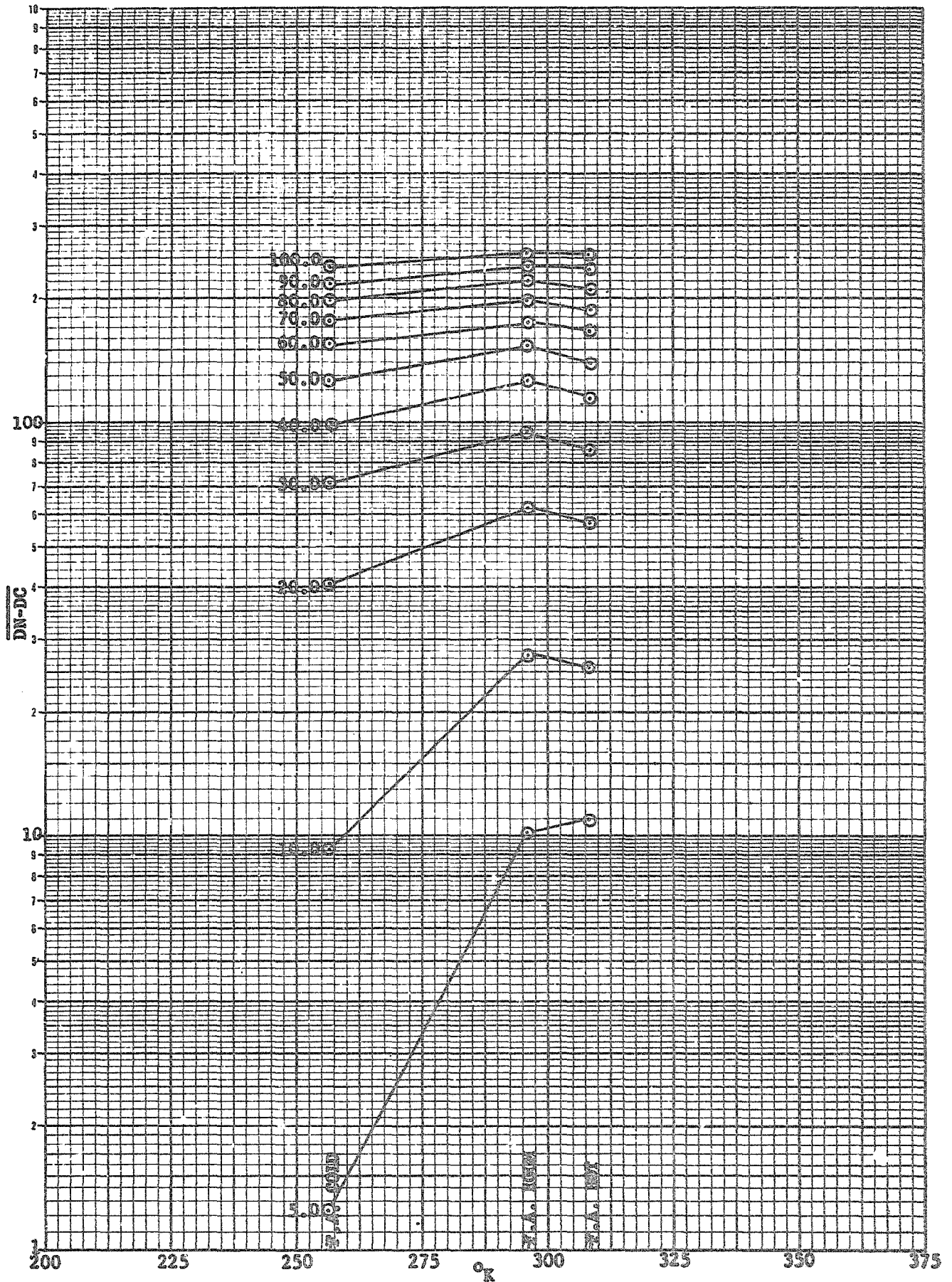


Fig. 54 RESPONSE AS A FUNCTION OF TEMPERATURE AT CONSTANT EXPOSURE, FLIGHT 2-B

615-148

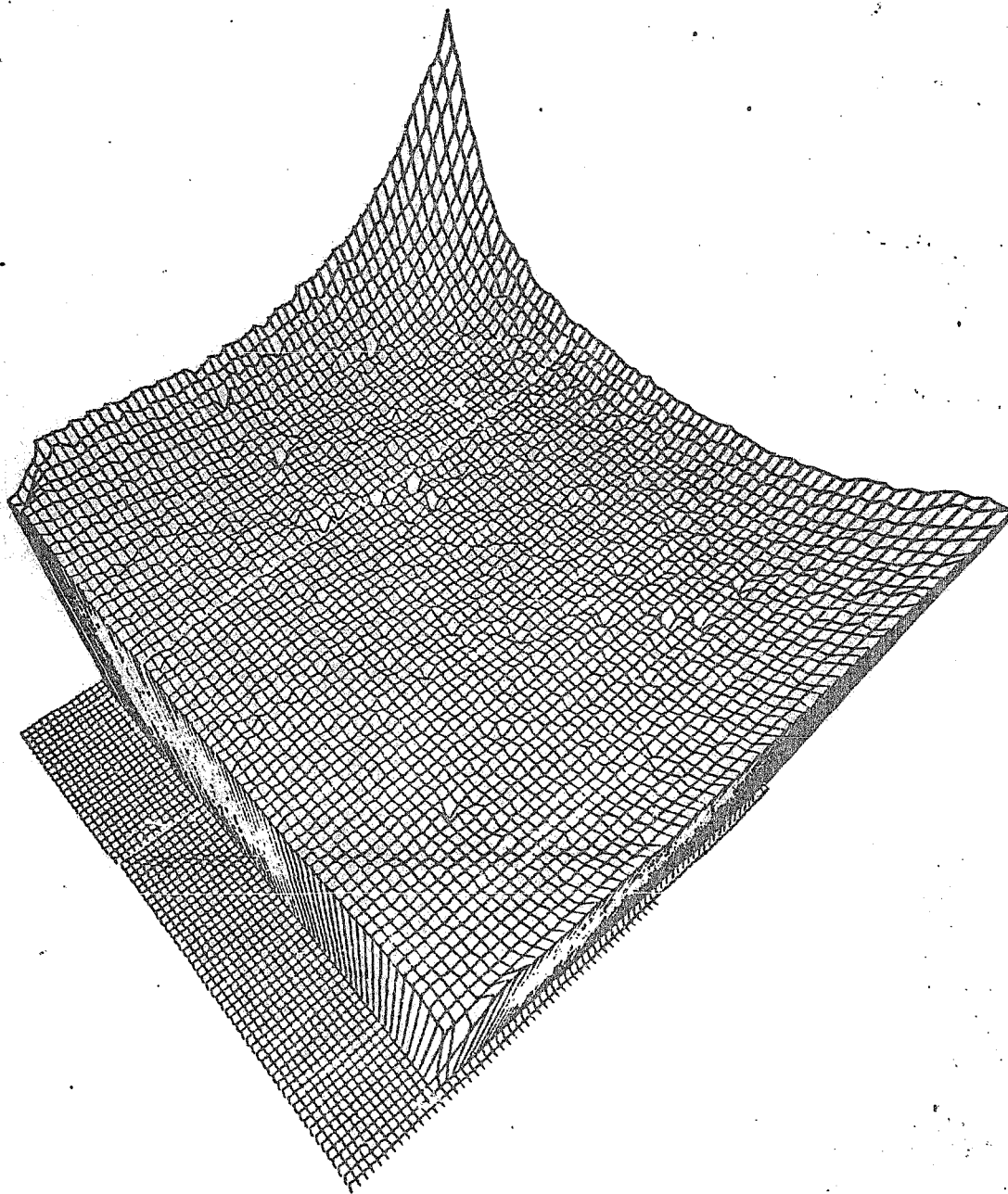


Fig. 55 FLAT FIELD L/T WITH VIDICON SHADING, FLIGHT 2-B (COLD)

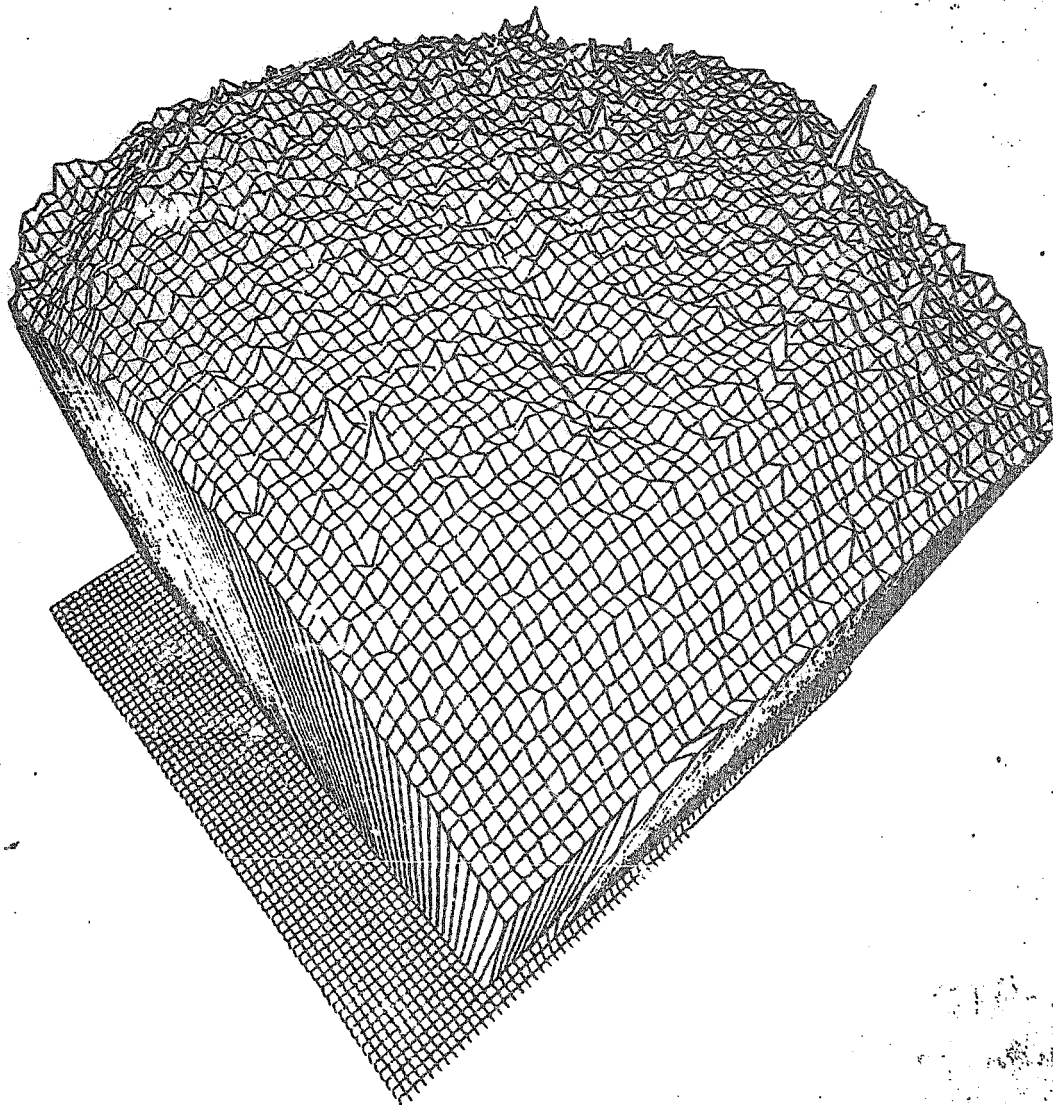


Fig. 56 FLAT FIELD L/T WITH VIDICON SHADING, FLIGHT 2-A (COLD)

REFERENCES

1. Mariner Venus-Mercury 1973 Television Subsystem, Calibration Plan and Requirements Document, JPL 615-50, 1 January 1972.
2. Snyder, L. M., Mariner 9 TV Subsystem Calibration Report, JPL 610-202, 15 November 1971.
3. Benesh, M., Extraterrestrial Convergent Photogrammetric Mapping System - An Error Analysis, JPL Technical Memorandum 33-455, 1 December 1970.
4. Danielson, G. E., La Baw, C. C., et al, Mariner Mars 1969 Television Experiment Science Calibration Report, JPL 605-149, 1 February 1970.
5. Kreznar, J. E., User and Programmer Guide to the MM '71 Geometric Calibration and Decalibration Programs, JPL 900-575, 1 March 1973.